SCIENCE APPLICATIONS, INC.

12

SPATIAL DISTRIBUTION OF VERTICAL SHEAR

SAI-82-294-WA

ATLANTA • ANN ARBOR • BOSTON • CHICAGO • CLEVELAND • DENVER • HUNTSVILLE • LA JOLLA
LITTLE ROCK • LOS ANGELES • SAN FRANCISCO • SANTA BARBARA • TUCSON • WASHINGTON

SPATIAL DISTRIBUTION OF VERTICAL SHEAR

SAI-82-294-WA

OPD-TR-81-201-02

March 1981

Prepared by:
S. L. Patterson
F. C. Newman
D. M. Rubenstein
R. B. Lambert, Jr.
Science Applications, Inc.
McLean, Virginia 22102

Prepared for:
Dr. E. M. Stanley
NORDA Code 540
Ocean Measurements Program
NSTL Station
Bay St. Louis, MS 39529

Contract No. N00014-79-C-0652

SCIENCE APPLICATIONS, INCORPORATED
1710 Goodridge Drive, P.O. Box 1303
McLean, Virginia 22102
(703) 821-4300

SECURITY CLASSIFICATION OF THIS PAGE (When Data Entered)

REPORT DOCUMENTATION PAGE

READ INSTRUCTIONS BEFORE COMPLETING FORM

1. REPORT NUMBER: SAI-82-294-WA (OPD-TR-81-201-02) — 2. GOVT ACCESSION NO.: AD-A098150 — 3. RECIPIENT'S CATALOG NUMBER:

4. TITLE (and Subtitle): SPATIAL DISTRIBUTION OF VERTICAL SHEAR

5. TYPE OF REPORT & PERIOD COVERED: Technical Report 9/1/80 through 2/28/81

6. PERFORMING ORG. REPORT NUMBER: SAI-82-294-WA

7. AUTHOR(s): S. L. Patterson, F. C. Newman, D. M. Rubenstein and R. B. Lambert, Jr.

8. CONTRACT OR GRANT NUMBER(s): N00014-79-C-0652

9. PERFORMING ORGANIZATION NAME AND ADDRESS:
Science Applications, Inc.
1710 Goodridge Drive
McLean, VA 22102

10. PROGRAM ELEMENT, PROJECT, TASK AREA & WORK UNIT NUMBERS: P.E. 63704 Project 520 118

11. CONTROLLING OFFICE NAME AND ADDRESS:
NORDA Code 540
Ocean Measurements Program
NSTL Station, Bay St. Louis, MS 39529

12. REPORT DATE: March 1981

13. NUMBER OF PAGES: 137

14. MONITORING AGENCY NAME & ADDRESS(if different from Controlling Office): Same

15. SECURITY CLASS. (of this report): Unclassified

15a. DECLASSIFICATION/DOWNGRADING SCHEDULE

16. DISTRIBUTION STATEMENT (of this Report)

Approved for public release; distribution unlimited.

Technical rept. 1 Sep 80-28 Feb 81

17. DISTRIBUTION STATEMENT (of the abstract entered in Block 20, if different from Report)

Approved for public release; distribution unlimited.

18. SUPPLEMENTARY NOTES

19. KEY WORDS (Continue on reverse side if necessary and identify by block number)

Vertical Shear	Brunt-Väisälä Frequency
Shear	Ocean Vertical Profiles
Velocity Finestructure	Richardson Number
Density Stratification	YVETTE

20. ABSTRACT (Continue on reverse side if necessary and identify by block number)

Spatial variations in small scale vertical shear in the upper ocean are described, relationships between small scale vertical shear and density stratification are investigated, and the potential for predicting mean vertical shear from measurements of the density field is assessed. Fifteen vertical profiles of density and horizontal velocity are used. These were obtained in several dynamically different ocean areas with a sensor package known as YVETTE. It is concluded that a reasonable first approximation to a climatology of small scale shear (at least, in the North Atlantic) might

DD FORM 1 JAN 73 1473 EDITION OF 1 NOV 65 IS OBSOLETE S/N 0102-LF-014-6601

404 464

SECURITY CLASSIFICATION OF THIS PAGE (When Data Entered)

be derived from a characterization of the large scale density stratification. Contributions by factors other than density stratification to the observed levels of small scale vertical shear in the upper ocean are also considered. We recommend that additional measurements be made with an YVETTE-type profiler in a wide variety of ocean areas. This work was supported through contract N00014-79-C-0652 from the Naval Oceanographic Research and Development Activity.

TABLE OF CONTENTS

LIST OF FIGURES

LIST OF FIGURES (Continued)

LIST OF FIGURES

LIST OF FIGURES (Continued)

LIST OF FIGURES (Continued)

LIST OF FIGURES (Continued)

LIST OF FIGURES (Continued)

LIST OF FIGURES (Continued)

LIST OF FIGURES (Continued)

ABSTRACT

Spatial variations in small scale vertical shear in the upper ocean are described, relationships between small scale vertical shear and density stratification are investigated, and the potential for predicting mean vertical shear from measurements of the density field is assessed. Fifteen vertical profiles of density and horizontal velocity are used. These were obtained in several dynamically different ocean areas with a sensor package known as YVETTE. It is concluded that a reasonable first approximation to a climatology of small scale shear (at least, in the North Atlantic) might be derived from a characterization of the large scale density stratification. Contributions by factors other than density stratification to the observed levels of small scale vertical shear in the upper ocean are also considered. We recommend that additional measurements be made with an YVETTE-type profiler in a wide variety of ocean areas. This work was supported through contract N00014-79-C-0652 from the Naval Oceanographic Research and Development Activity.

Section 1
INTRODUCTION

1.1 BACKGROUND

Vertical shear is a parameter derived from the vertical distribution of horizontal velocity, and its importance to Navy programs has been described in a number of documents. These are cited and summarized in an SAI report to NORDA by Lambert and Patterson (1980), in which the current status of measurements of vertical shear in the upper ocean was reviewed. As a result of that report, it was decided to focus attention on shear over the scale range between 1 meter and a few tens of meters. Two free-fall profiling instruments capable of resolving the velocity field in this range, were identified in that report. These are YVETTE and SCIMP. Two subsequent SAI reports to NORDA have compared the response of these two instrument systems (Rubenstein et al., 1980) and presented profiles of data obtained by them (Lambert et al., 1980). Because of the availability of the YVETTE data and the wide variety of ocean areas in which it had been deployed, it was decided to focus on the YVETTE data in order to investigate the spatial and oceangraphic variability of upper ocean vertical shear.

1.2 OBJECTIVES

This report focuses on fifteen vertical profiles of density and horizontal velocity obtained with YVETTE in several dynamically different ocean areas. The objectives of the report are:

- to describe the observed spatial variations in small scale vertical shear in the upper ocean, and

- to investigate the possible occurrence of systematic relationships between small scale vertical shear and density stratification.

1.3 APPROACH

The first step is to become familiar with the vertical distribution of the various observed and derived parameters. Section 2 contains a brief discussion of the profiles from a single sample station, while profiles from the other stations are presented in Appendix A. It is shown that the magnitudes of gradient quantities (particularly vertical shear) in the ocean are naturally arranged into distinct stratification regimes. Profiles from dynamically different ocean areas are compared and contrasted in terms of these stratification regimes.

In Section 3 the magnitudes of gradient quantities within each stratification regime of the sample station are examined with the use of histograms. Histograms for the remaining stations are presented in Appendix B. The distributions revealed by the histograms for the different stratification regimes are contrasted and discussed. Since the gradient quantities are computed by taking simple vertical differences, the effects of changing the vertical differencing interval are illustrated and explained. The histograms from various ocean areas are compared and the variation of mean Brunt-Väisälä frequency squared ($\overline{N^2}$) and mean vertical shear squared ($\overline{S^2}$) from one ocean area to another is illustrated and discussed.

Relationships between N^2 and S^2 are examined in Section 4. This includes an examination of the effects of varying the vertical differencing interval and the vertical smoothing interval (filter length) on the correlation between N^2 and S^2. The potential for predicting $\overline{S^2}$ from measurements of N^2 is discussed.

1.4 YVETTE

At the time these profiles were obtained (1973-79), YVETTE consisted of a four-meter-long tube equipped with Neil Brown conductivity, temperature, and depth (CTD) sensors as well as an orthogonal pair of acoustic current meters (Figure 1.1). A detailed description of YVETTE is provided by Evans et al. (1979). When deployed, the probe falls freely through the water column at a rate of 20 to 25 cm s^{-1}. The water temperature, conductivity, two orthogonal components of horizontal velocity relative to the probe housing, and the orientation of the instrument relative to the earth's magnetic field are internally recorded in digital form on magnetic cassette tape. The environment is sampled at a rate of 2.5 times per second to yield a vertical sampling interval of 8 to 10 cm. The CTD data have a least bit resolution of 0.001 mmho cm^{-1}, 0.0005°C, and 0.05 dbar, respectively. The acoustic current meters have a least bit resolution in speed of 0.05 cm s^{-1} and the compass can resolve orientation to within 3°. Noise levels in all sensors are dominated by least bit resolution.

The data set provided to us by David Evans (University of Rhode Island) has been filtered to remove variations on vertical scales less than 2m. The velocity

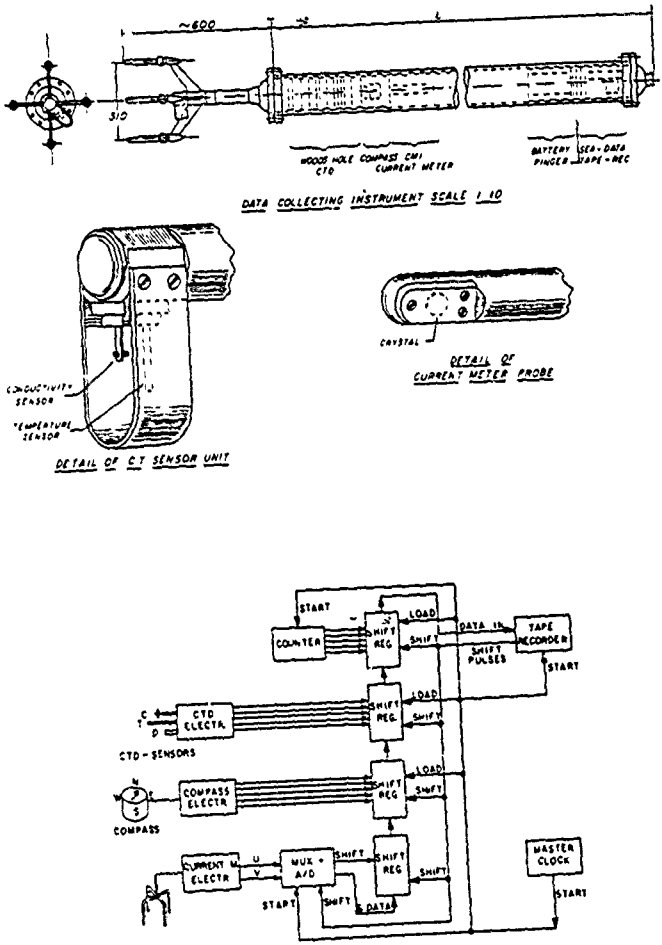

Figure 1.1 Schematic diagram of YVETTE and a block diagram of the electronics and recording system (from Evans et al., 1979).

profiles have also been corrected for horizontal drag effects imposed on the housing of YVETTE by the large scale vertical shear. A description of this processing is contained in the SAI report to NORDA by Lambert et al. (1980). The resulting data set can resolve horizontal velocity structure with vertical scales between 2m and 100m. The instrument response to larger scale shear cannot be estimated.

1.5 DISTRIBUTION OF PROFILES

The position, date, and other relevant information about the individual YVETTE stations are presented in Table 1.1. The various ocean areas sampled by YVETTE are also indicated on the map shown in Figure 1.2.

Table 1.1
YVETTE STATIONS[1]

Station Number	Time (GMT)	Date	Latitude (N)	Longitude (W)	Comment
5	1942	5 Nov. 75	32°19'	64°34'	Near Bermuda
8	0225	8 Nov. 75	35°00'	66°30'	Sargasso Sea
9	1219	"	"	"	"
10	1814	9 Nov. 75	38°09'	69°06'	Gulf Stream
11	0036	10 Nov. 75	38°05'	69°03'	"
12	1312	"	38°15'	69°07'	"
18	—	7 May 77	22°47'	70°43'	Edge of thermocline eddy
21	—	9 May 77	22°27'	70°57'	Center of thermocline eddy
23	—	16 May 77	36°24'	67°36'	Outer part of GSR[2]
24	—	"	36°20'	67°44'	Midway along radius of GSR
25	—	17 May 77	36°09'	67°53'	Near center of GSR
NOR 1	--	1973	—	--	Norwegian Fjord
NOR 4	—	"	—	—	"
NOR 6	—	"	—	—	Norwegian Coastal Current
EPOCS[3]6	—	July 79	0°03'	109°57'	Data start just below EUC[4]

1 Adapted from Lambert et al. (1980)
2 Gulf Stream Ring
3 Equatorial Pacific Ocean Climate Study
4 Equatorial Undercurrent

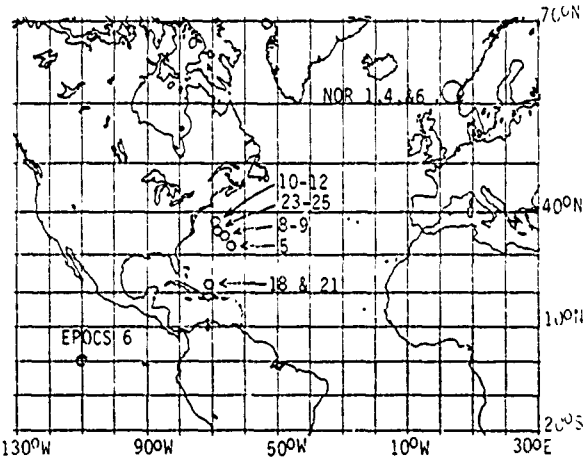

Figure 1.2 Positions of YVETTE stations

Section 2
VERTICAL PROFILES

2.1 TYPES OF PROFILES

The types of vertical profiles constructed for each YVETTE station are illustrated in Figures 2.1, 2.2, and 2.3, using YVETTE station 8 as an example. These figures exhibit various aspects of the vertical distribution of density, horizontal velocity, and Richardson number, respectively. Profiles from the other YVETTE stations are shown in Appendix A. The presentation here differs from that in Lambert et al. (1980) in that all profiles are presented on a uniform set of coordinate scales to facilitate comparison between stations.

The vertical distribution of temperature, salinity, density (sigma-t), Brunt-Väisälä (B.V.) frequency, and the vertical gradient of temperature are shown in Figure 2.1. Sigma-t (σ_t) is related to density (ρ) by

$$\sigma_t = (\rho - 1) \times 10^3 \ .$$

B.V. frequency (N) is related to the vertical gradient of density by

$$N = \left(\frac{g}{\rho} \frac{\partial \rho}{\partial z} \right)^{1/2}$$

where g is gravitational acceleration and z increases downward. The vertical gradients were computed by taking simple differences along the filtered profiles over a vertical

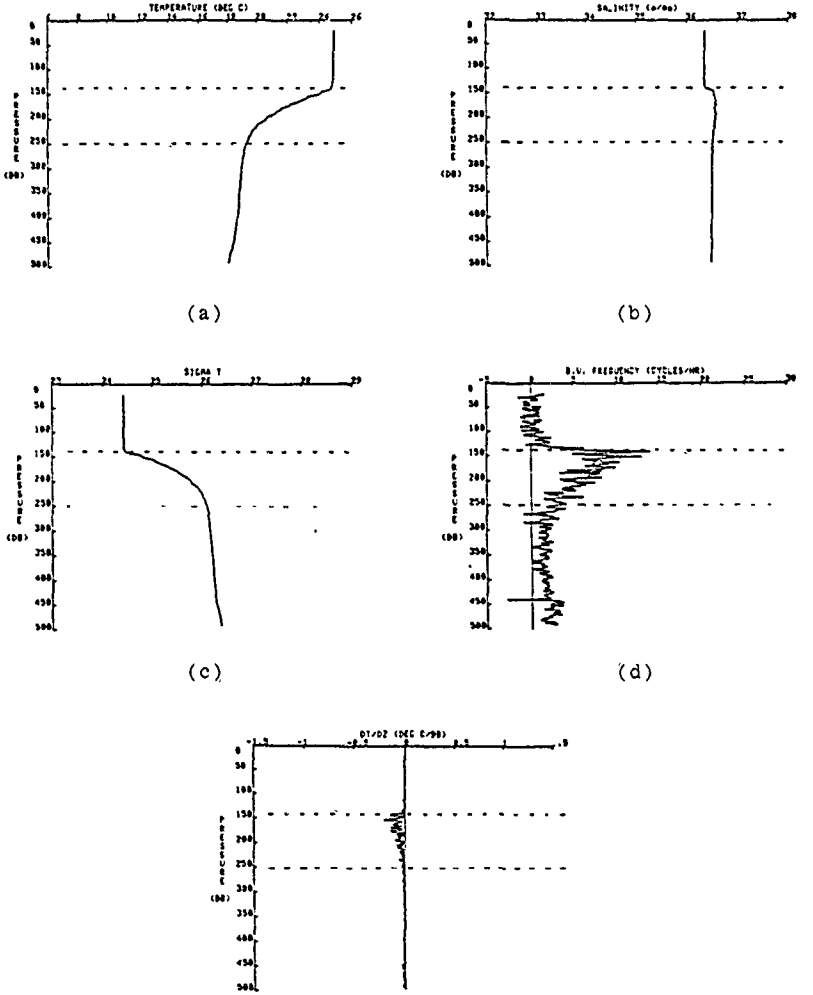

Figure 2.1 Profiles of (a) temperature, (b) salinity, (c) density (σ_t), (d) Brunt-Väisälä frequency, and (e) vertical gradient of temperature for YVETTE station 8 occupied on 8 November 1975 at 35°00'N, 66°30'W (Sargasso Sea). The profiles can be divided into stratification regimes as indicated by the dotted lines at 135 and 250 dbars.

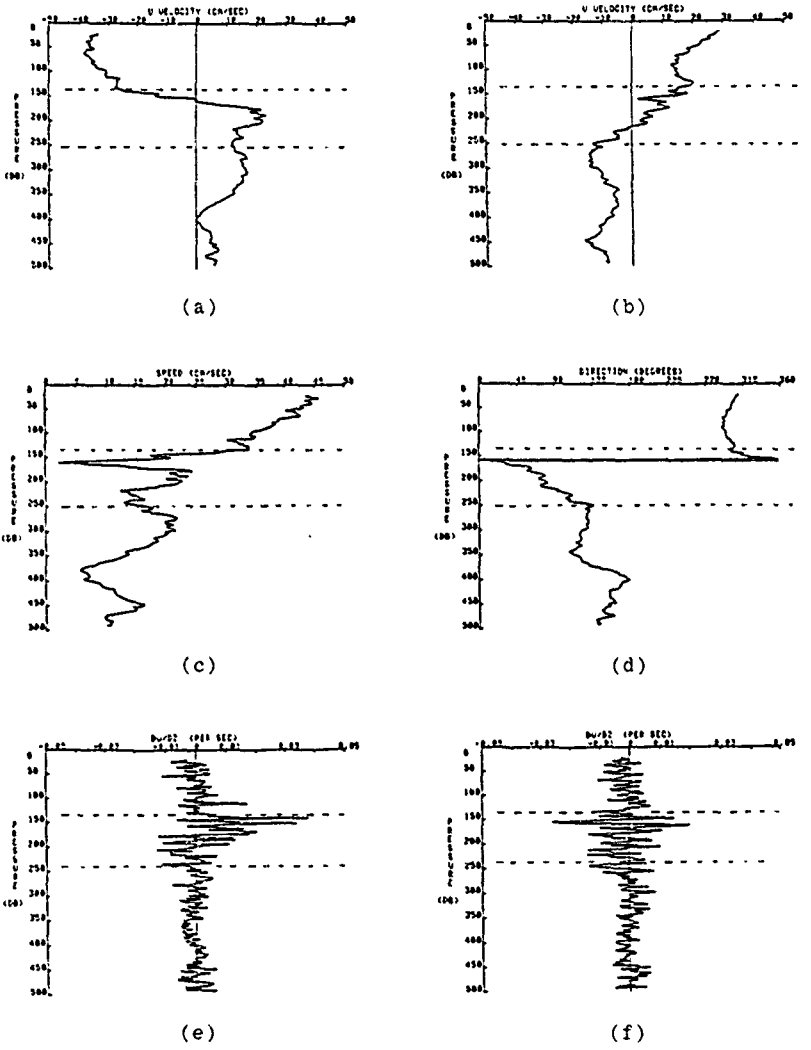

Figure 2.2 Profiles of the (a) east and (b) north component of velocity, the (c) magnitude and (d) direction of the horizontal velocity vector, and the vertical gradient of the (e) east and (f) north component of velocity for YVETTE station 8 in the Sargasso Sea. The dotted lines are at 135 and 250 dbars.

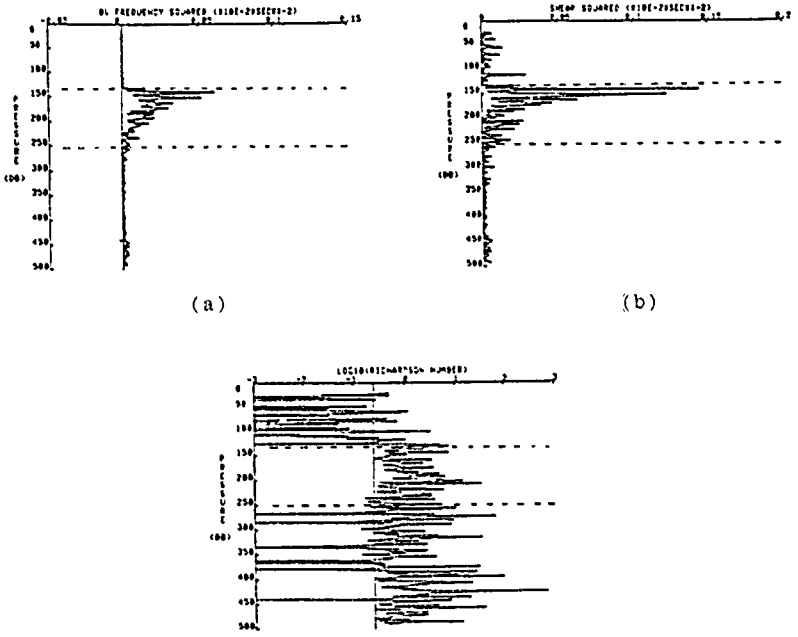

(a)

(b)

(c)

Figure 2.3 Profiles of (a) Brunt-Väisälä frequency squared, N^2, (b) vertical shear squared, S^2, and (c) Log_{10} (Ri), where $Ri = N^2/S^2$, for YVETTE station 8 in the Sargasso Sea. The vertical line in (c) is at $Ri = 0.25$. The dotted lines are at 135 and 250 dbars.

interval of approximately 2 dbars. For the purposes of this paper, 1 dbar is considered to be equal to 1 meter. In regions of near neutral stability, such as within the surface mixed layer, noise in the temperature and/or salinity profile can produce apparent inversions in the density profile. These apparent inversions result in imaginary B.V. frequencies. As a matter of convenience in constructing the B.V. profiles, the imaginary B.V. frequencies have been plotted as negative real quantities.

The water column sampled at station 8 can be divided into three stratification regimes on the basis of the vertical gradient of either temperature or density. This division is indicated in Figures 2.1, 2.2, and 2.3 by dashed lines at 135 dbars and 250 dbars. The placement of the boundaries between regimes is somewhat subjective. Above 135 dbars is the surface mixed layer (ML), characterized by nearly constant temperature, salinity, and density. Between 135 dbars and 250 dbars is the near-surface thermocline (ST) characterized by a relatively large mean vertical gradient in temperature and density. Below the thermocline is a regime (henceforth abbreviated as BST) of significantly smaller mean vertical gradients in temperature and density. We note that in the case of YVETTE 8, the BST regime could be further divided. Between approximately 300 and 400m there is a nearly homogeneous layer (18°C water) which is characterized by uniformly low B.V. frequency. Below this layer is the top of the main thermocline where the temperature begins to decrease and the B.V. frequency begins to increase. The profiles from the other YVETTE stations can be similarly divided into stratification regimes on the basis of the relative magnitudes of vertical gradients, however, the depth and thickness of the regimes vary from

station to station (see Appendix A). Since the profile data begin at various distances below the sea surface, in many of the profiles no surface mixed layer is observed.

Various aspects of the vertical distribution of horizontal velocity are shown in Figure 2.2. Profiles of the east (u) and north (v) components of horizontal velocity are shown in panels (a) and (b), respectively. Profiles of the magnitude (speed) and direction of the horizontal velocity vector are shown in panels (c) and (d). In the direction plot, north corresponds to 0°, east corresponds to 90°, etc. The vertical gradient of the east and north components of velocity are shown in panels (e) and (f). It is evident that these velocity gradients exhibit a broader range of values within the ST regime than elsewhere. This means that there are sharper or more abrupt variations (along the vertical axis) of the horizontal velocity vector within the thermocline than elsewhere. These variations can be due to changes in either the magnitude or the direction of the vector, or both.

The variations in du/dz and dv/dz are combined and made non-negative by computing shear squared (S^2), where

$$S^2 = \left(\frac{du}{dz}\right)^2 + \left(\frac{dv}{dz}\right)^2 .$$

The gross similarity between the profile of B.V. frequency squared (N^2) and that of S^2 is seen by comparing panels

(a) and (b) of Figure 2.3. Both profiles exhibit relatively small values within the ML and BST regimes, but relatively large peaks within the ST regime. This suggests that some relationship may exist between N^2 and S^2. However, the profile of the logarithm of Richardson number (Ri), where $Ri = N^2/S^2$, exhibits a broad range of values in panel (c) of Figure 2.3. Hence a linear relationship between N^2 and S^2 that is suggested by comparing whole profiles (that is, 500 m profiles) does not hold when comparing individual points. The vertical line in panel (c) at Log_{10} (Ri) = -0.602 corresponds to Ri = 0.25. Simple linear theory predicts that Ri must be less than this critical value for the existence of shear-induced instabilities. Figure 2.3 suggests that most of the very low values of Ri occur in portions of the water column where N^2 is low rather than in portions where S^2 is high. This same tendency is evident in all YVETTE profiles (see Appendix A).

In regions of very low N^2 or S^2, the noise level inherent with the sensor package causes the relative error in the calculated values of N^2 and S^2 to become large. Therefore, in such regions the relative error in Ri is also quite large. From the precision of the various sensors we have estimated (Molinelli et al., 1981) that the signal-to-noise ratio in the N^2 profile is greater than unity when $N^2 > 1.8 \times 10^{-6}$ s^{-2}, and that in the S^2 profile is greater than unity when $S^2 > 3.3 \times 10^{-8}$ s^{-2}. Outside the surface mixed layer, the values of N^2 and S^2 are only rarely below the estimated noise level. A more detailed

discussion of the effects of noise level in YVETTE data on calculations of R_1 is presented in Newman et al. (1981). While YVETTE is descending through the water column, various dynamic responses of the system may increase the noise level above that estimated here. This issue remains to be resolved. In any case, the actual noise level is not expected to have any appreciable impact on the gross characterizations presented herein.

2.2 COMPARISONS BETWEEN STATIONS

Representative profiles from each ocean area sampled by YVETTE are presented in Figure 2.4 to contrast the different oceanic conditions encountered. It can be seen that a fairly broad range of oceanic conditions, from the cold, fresh waters off the coast of Norway to the warm, salty waters of the Sargasso Sea, are represented by the data set. Waters in the equatorial Pacific are colder and fresher than most of the waters of the North Atlantic. Although the temperature and salinity profile from the Gulf Stream (station 10) exhibits substantial interleaving, the sigma-t profile shows that these fluctuations are essentially density-compensating. The amplitude of the temperature and salinity interleaving increases from southeast to northwest across the Gulf Stream. (Compare stations 11, 10, and 12, in sequence, in Appendix A.) We note from the sigma-t profiles in Figure 2.4 that below 50 meters density increases along constant pressure surfaces radially outward from a point in the central Sargasso Sea (station 8) toward Bermuda (station 5), the Bahamas (station 18), and the Gulf Stream (station 10). This is due to the large scale anticyclonic circulation in the Sargasso Sea.

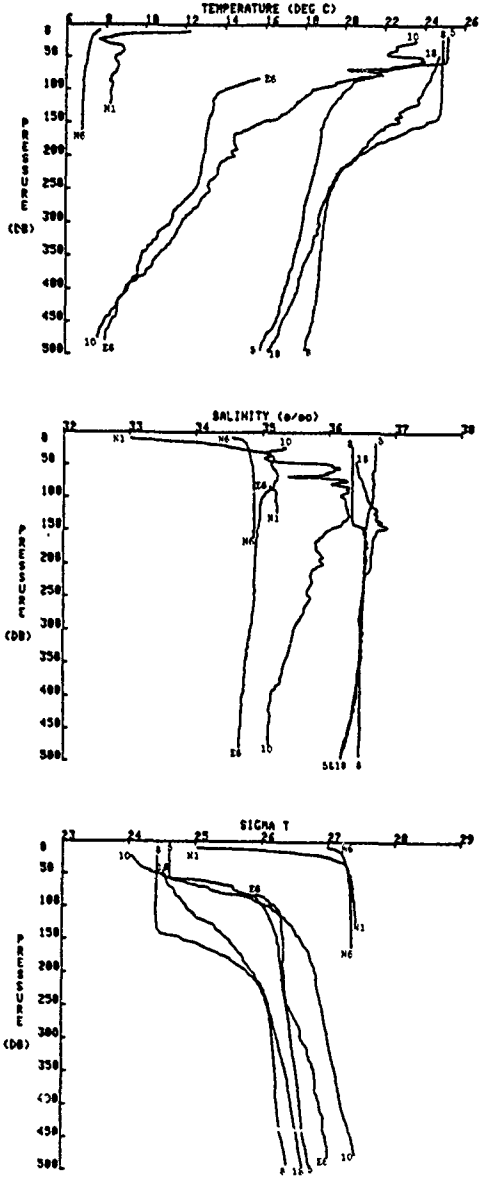

Station Number	Ocean Area
5	Bermuda
8	Sargasso Sea
10	Gulf Stream
18	Bahamas
N1	Norwegian Fjord
N6	Norwegian Coastal Current
E6	Equatorial Pacific

Figure 2.4 Representative profiles of temperature, salinity, and density (sigma-t) for various ocean areas. Station times, dates, and positions are listed in Table 1.1.

A profile of shear squared for YVETTE station 8 is shown in Figure 2.3. Profiles of shear squared for the other representative stations are shown in Figure 2.5. It is evident that the vertical distribution of shear squared is just as diverse as any of the other parameters.

The contrasts from one stratification regime to another and from one ocean area to another will be further illustrated and discussed in Sections 3 and 4.

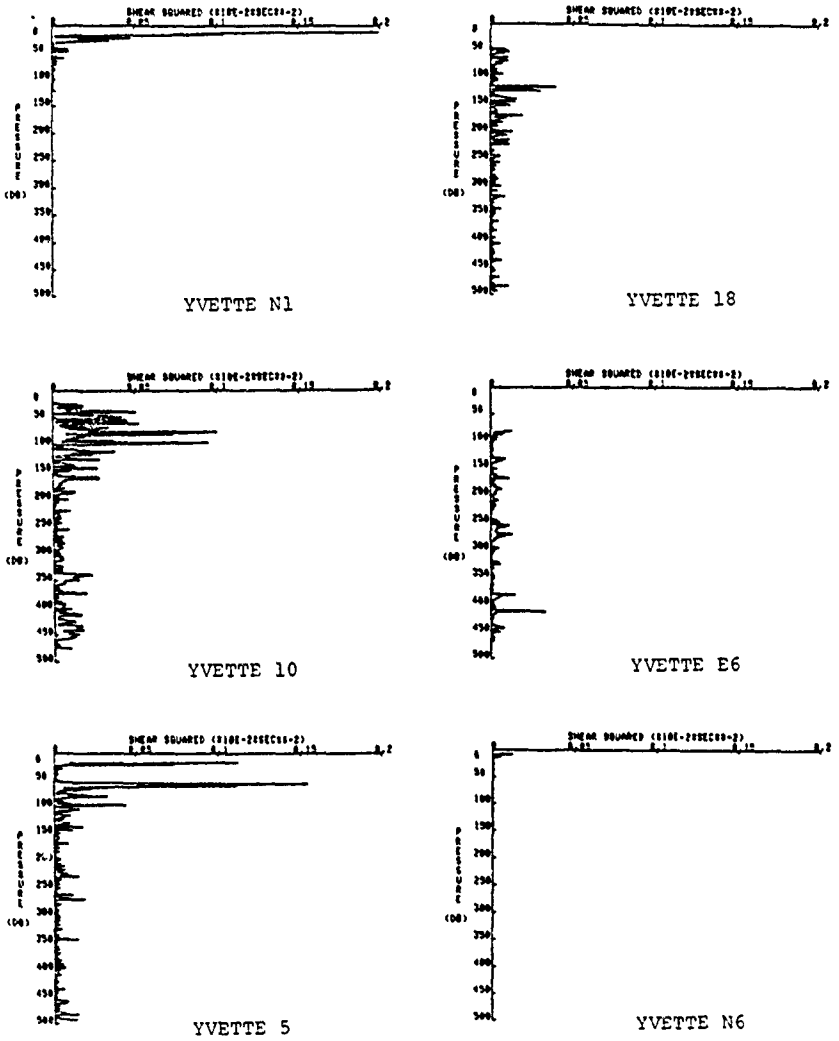

Figure 2.5 Vertical profiles of shear squared for the YVETTE stations shown in Figure 2.4

Section 3
HISTOGRAMS

3.1 INTRODUCTION

The YVETTE profiles presented in the preceeding section showed the distribution of various parameters with depth. It was noted that, for each station, the profiles of the gradient quantities can be divided along the depth axis into two or more distinctly different regimes which correspond to regimes of different mean density stratification. In order to further examine the differences between these stratification regimes and the differences between ocean areas, histograms of the gradient quantities were constructed for each regime and each different ocean area.

The data points in the processed YVETTE profiles are equally spaced in time. Due to variations in the descent rate of the instrument, the points are not always equally spaced in depth, although the nominal spacing is 1m. The gradient value at each observed depth was computed by differencing the values above and below the specified depth and dividing by the differencing interval, Δz. Since the gradients are computed in this way, the effects of changing the vertical differencing interval are illustrated and explained.

3.2 TYPES OF HISTOGRAMS

As in Section 2, YVETTE 8 is used to illustrate the types of histograms constructed (Figures 3.1, 3.2, 3.4, and 3.7). Histograms of B.V. frequency squared (N^2), shear squared (S^2), and Richardson number (Ri) for the other YVETTE stations are presented in Appendix B.

Note that the vertical axis of these histograms is in units of observed probability or fractional frequency of occurrence. When the observed probability exceeds 0.35, the histogram bar is truncated and the observed probability is enclosed in parentheses above the appropriate bar. For example, in Figure 3.1 (a), 0.7 of the observed values occur in the interval between 0.0 and 0.05 x 10^{-4} rad^2 s^{-2}. While the observed range of values for each parameter is quite large, in many of the distributions the majority of the values are contained within a relatively narrow range. We note that the shape of a histogram can be quite sensitive to bin width. Hence, the range and bin widths were selected to accommodate most of the values observed in the entire data set (i.e., 15 stations) and at the same time provide a reasonably smooth distribution in the vicinity of the mode (i.e. the peak or most probable value). Once selected, the range and bin width for each parameter are held constant so that the histograms can be easily compared. Values that exceed the bounds of the horizontal axis are accumulated in the last bin on the extreme left or right, whichever is appropriate. For example, in Figure 3.1 (b), 0.42 of all values are greater than 1.3 x 10^{-4} rad^2 s^{-2}.

The mean, median, and variance of each distribution are indicated in the legend on each histogram. The depth range and number of observations within each stratification regime are indicated in the legends of the histograms on the left side of each figure. Since a gradient value is computed at each observed depth, the number of observations is approximately one per meter. In the histograms of Ri (e.g. Figure 3.7) the legend includes a line indicating the observed probability of Ri less than the critical Richardson number, 0.25.

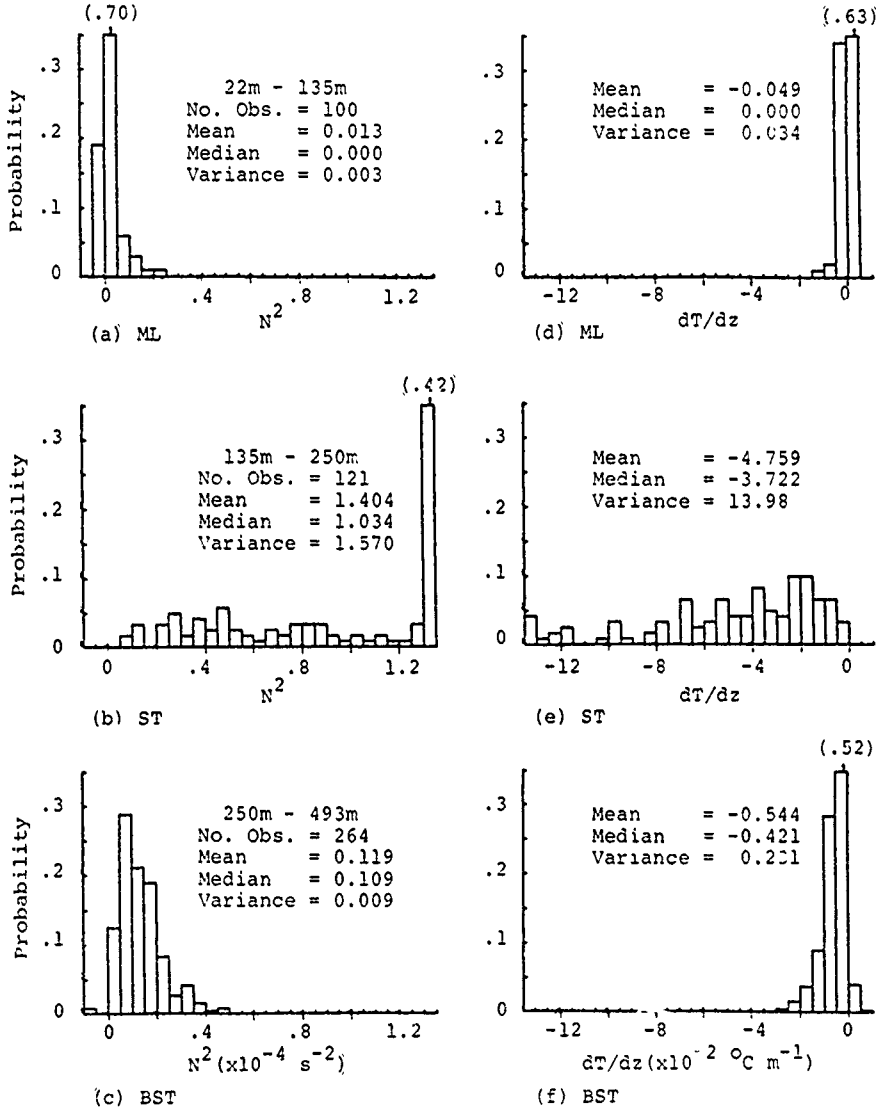

Figure 3.1 Histograms of Brunt-Väisälä frequency squared (N^2) for the (a) surface mixed layer (ML), (b) the near-surface thermocline (ST), and (c) the regime below the thermocline (BST) at YVETTE station 8. Histograms of the vertical gradient of temperature for (d) the ML, (e) the ST, and (f) the BST regime.

Recall that at station 8 the water column has been divided into three regimes: the mixed layer (22 to 135 dbars), the near-surface thermocline (135 to 250 dbars), and the region below the thermocline (250 to 493 dbars). The observed distributions of density gradient and temperature gradient values in these three regimes are shown in Figure 3.1. Panels (a), (b), and (c) show histograms of N^2 for the ML, ST, and BST regimes, respectively. (Compare with panel (a) in Figure 2.3.) Panels (d), (e), and (f) show the corresponding histograms of dT/dz. (Compare with panel (e) in Figure 2.1).

Since temperature typically decreases with depth and density increases with depth, the majority of the values of dT/dz are opposite in sign to those of B.V. frequency squared. To the extent that density variations are dominated by variations in temperature rather than salinity, the histograms of dT/dz should be the mirror image of those for B.V. frequency squared. The contrast between the three stratification regimes is clearly illustrated by the histograms. The majority of the values within the ML are near zero. Within the BST regime, the water column is more stably stratified and the variance of the distribution is somewhat larger. Within the ST the stratification is much more stable and the variance of the distribution is quite large. This same pattern is evident in the histograms of N^2 for the other YVETTE stations shown in Appendix B. Hayes et al. (1975) have noted that a Poisson distribution function provides a reasonably good visual fit to a similar set of histograms of dT/dz.

Histograms of du/dz are presented in Figure 3.2. Once again the contrast between the three stratification regimes is clearly illustrated by the histograms. (Compare with panel (e) in Figure 2.2.) The variance is significantly greater within the ST than within the ML or BST regimes. Panels (a), (b), and (c) show distributions of du/dz computed by differencing over a vertical interval of 2m. Panels (d), (e), and (f) were computed by differencing over 8m. Increasing the vertical differencing interval, Δz, effectively subsamples the velocity profile provided by YVETTE. This is analogous to measuring the velocity profile with a lower resolution discrete technique such as a vertical array of current meters. Of course, such discrete data are aliased to some extent by small scale structure. A lower resolution profiling instrument would not be sensitive to the small scale structure. Such profiler data could be simulated by low-pass filtering the YVETTE profiles to remove the high wavenumber structure.

Although the du/dz histogram shapes resemble a Gaussian probability distribution function, similar histograms (Figure 3.3) statistically tested by Simpson (1975) proved to be non-Gaussian to a high level of confidence. It is seen in Figure 3.2 that the shape of the distributions of du/dz is sensitive to changes in the vertical differencing interval. For example, in all regimes the variance of the distributions decreases as Δz increases. This is because the contributions to the "tails" of the du/dz histograms come chiefly from the small scale structure in the velocity profile. When Δz increases, the ability to

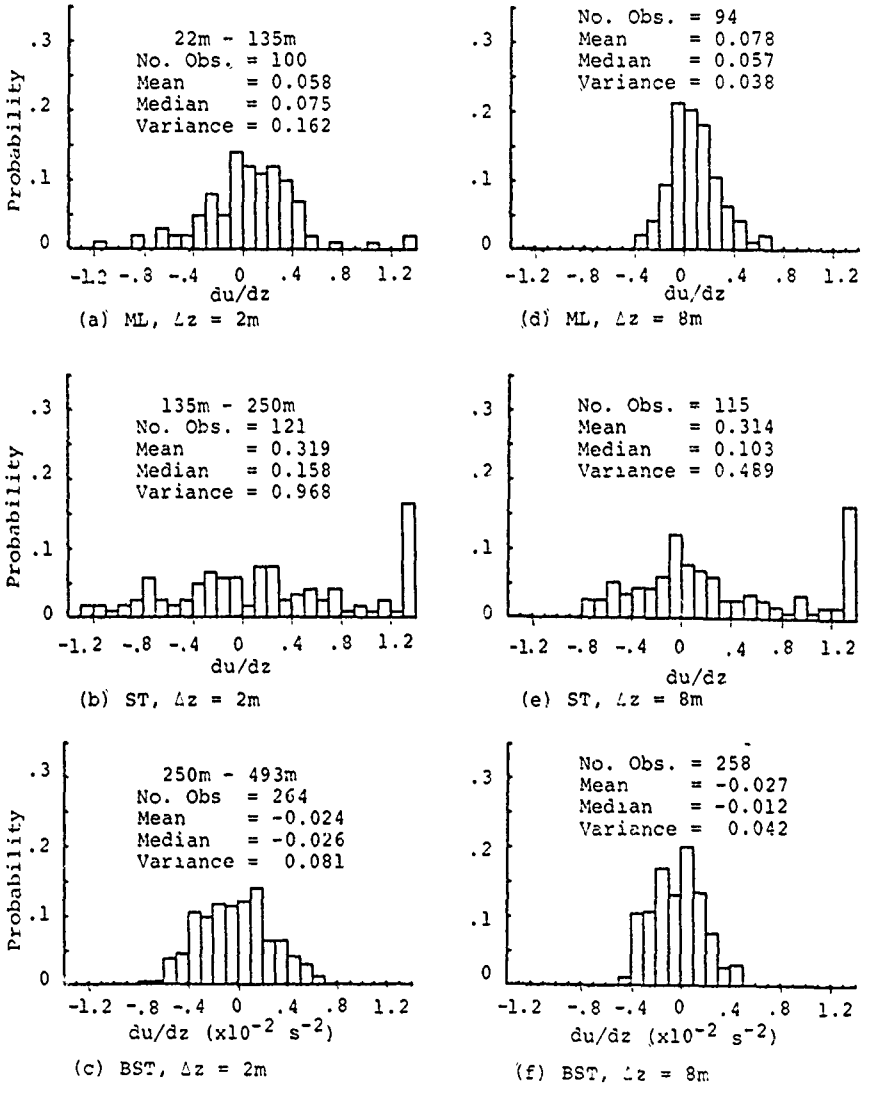

Figure 3.2 Histograms of du/dz computed by differencing over a vertical interval of 2 m for (a) the ML, (b) the ST, and (c) the BST regime. Histograms of du/dz computed by differencing over an interval of 8 m for (d) the ML, (e) the ST, and (f) the BST regime.

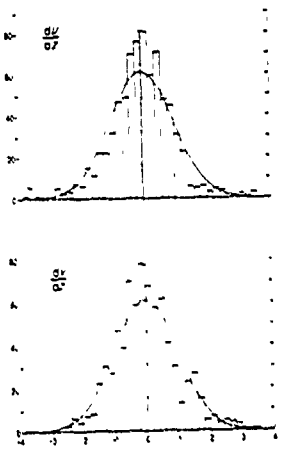

Figure 3.3 Histograms of the velocity shear components for the depth range 668-806 m at 52° 23.2' N, 16° 18.0'W (near Rockall Trough). The continuous curve represents the normal distribution. Each histogram contains 770 data points and the abscissa is in units of one standard deviation (from Simpson, 1975)

resolve this structure is lost, and hence variance decreases. Lower vertical resolution within a single profile also implies a smaller number of statistically independent observations, which reduces the confidence in any statistical tests imposed. Therefore, the details of the distribution shape, such as whether or not it fits a Gaussian probability curve, may depend as much on the vertical resolution of the velocity profile as on the ocean environment itself. The results of statistical tests of the YVETTE data are presented by Hebenstreit and Grabowski (1981).

Histograms of vertical shear squared (S^2) are presented in Figure 3.4. As with the du/dz histograms, distributions of shear squared computed using a vertical differencing interval of 2m are presented in panels (a), (b), and (c) and those computed using an interval of 8m are presented in panels (d), (e), and (f). The difference between stratification regimes is as expected from panel (b) Figure 2.3. That is, small values of S^2 are more common in the ML and BST regimes than within the ST regime. This is a general result as illustrated by the S^2 histograms (computed using a vertical differencing interval of 2m only) from the other YVETTE stations presented in Appendix B. The S^2 histograms resemble Chi-square probability distribution functions. If the shear components do follow Gaussian distributions, then this observation is not surprising. (The distribution of the sum of the squares of two normally distributed random variables is the Chi-square distribution.) Furthermore, this suggests that Chi-square distributions might serve as suitable models of S^2 distributions. This line of inquiry is addressed by Hebenstreit and Grabowski (1981).

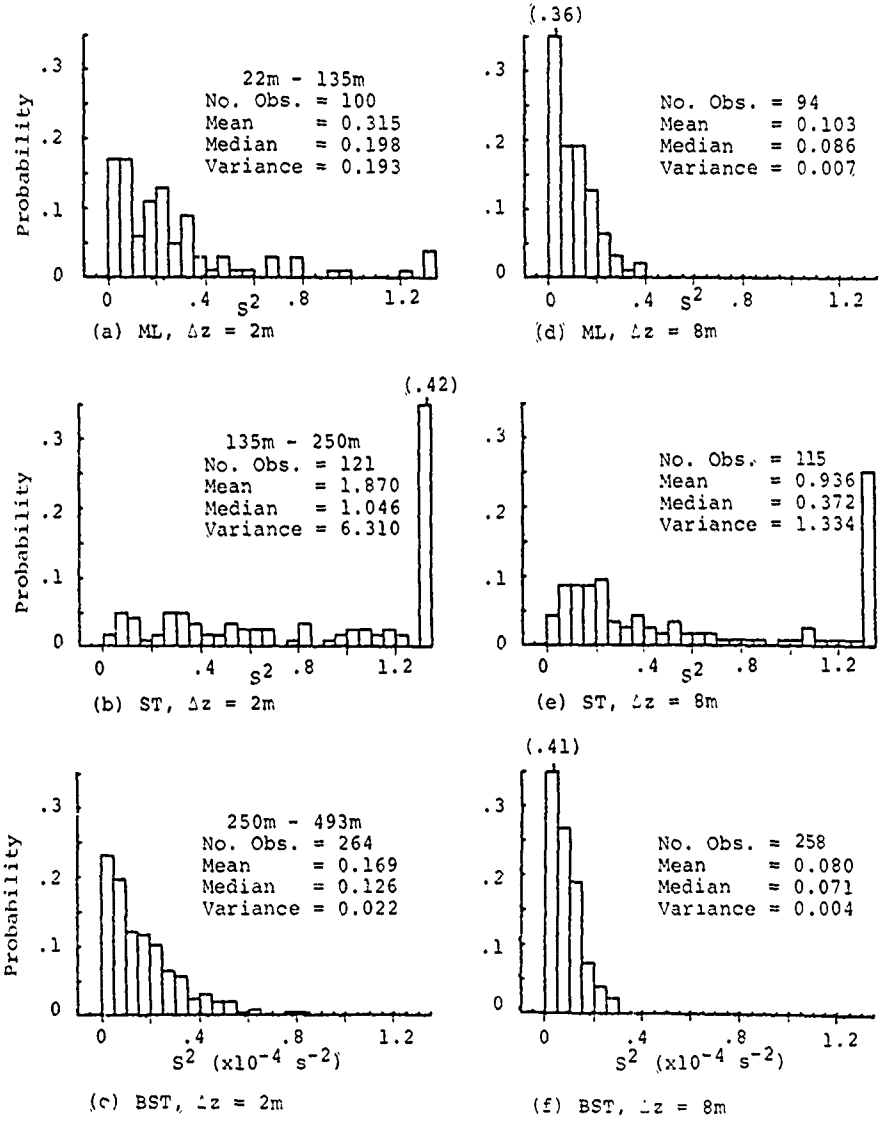

Figure 3.4 Histograms of vertical shear squared (S^2) computed by differencing over a vertical interval of 2 m for (a) the ML, (b) the ST, and (c) the BST regime. Histograms of S^2 computed by differencing over an interval of 8 m for (d) the ML, (e) the ST, and (f) the BST regime.

Since the shape of the du/dz histogram is sensitive to the vertical differencing interval, the same is necessarily true for histograms of S^2. It is seen in Figure 3.4 that in all regimes, both the mean and the variance of the distributions decrease as Δz increases. The variation of mean S^2 with stratification regime and with Δz is further illustrated in Figure 3.5. The effect of increasing Δz on the mean value of S^2 distributions is a general result which is illustrated in Figure 3.6. This effect has been modeled by Grabowski (1980). These relations suggest that it may be possible to use some of the lower resolution velocity profilers, such as the EMVP (Sanford et al., 1978), the XCP (Sippican Corp., 1979), or even vertical arrays of current meters (Pollard, 1980), to provide at least rough estimates of the mean S^2 that would have been observed by a high resolution profiler like YVETTE. This might allow data sets obtained with different resolution instruments to be compared. A discussion of many of the existing velocity profilers is presented in Lambert and Patterson (1980).

As noted earlier the ratio of N^2 to S^2 is the Richardson number (Ri). Histograms of Ri are presented in Figure 3.7. The format is the same as for Figure 3.2 and 3.4 except that the observed probability of subcritical Ri (i.e., $Ri < 0.25$) is indicated in the legend. It was noted in Section 2.1 that when considering the profiles as a whole, N^2 and S^2 appear to be related to each other. However, the profile of Log_{10} (Ri) presented in Figure 2.3, rather than being nearly constant, exhibited a broad range of values. From examination of the histograms (Figures 3.1

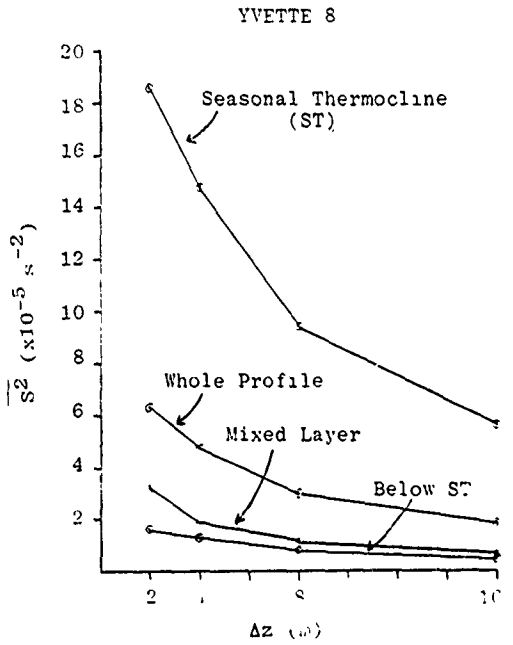

Figure 3.5 Mean vertical shear squared, $\overline{S^2}$, for different stratification regimes at YVETTE station 8 versus differencing interval, Δz.

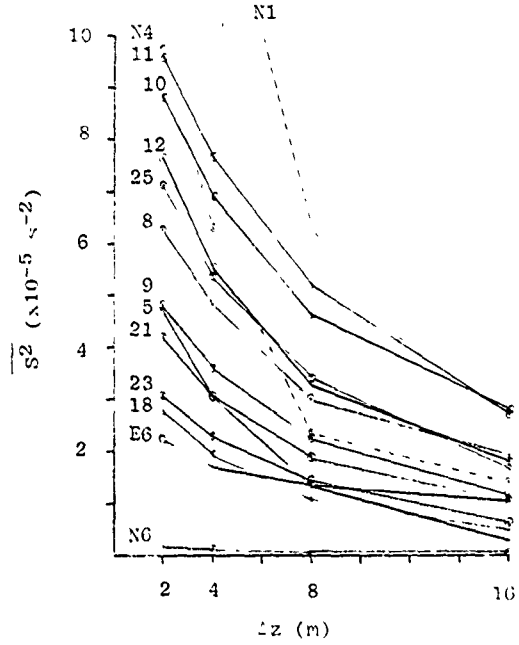

Figure 3.6 Mean vertical shear squared ($\overline{S^2}$) versus differencing interval (z) for all YVETTE stations except 24 which is a very short profile. Here the mean in each case is computed using data from the entire profile.

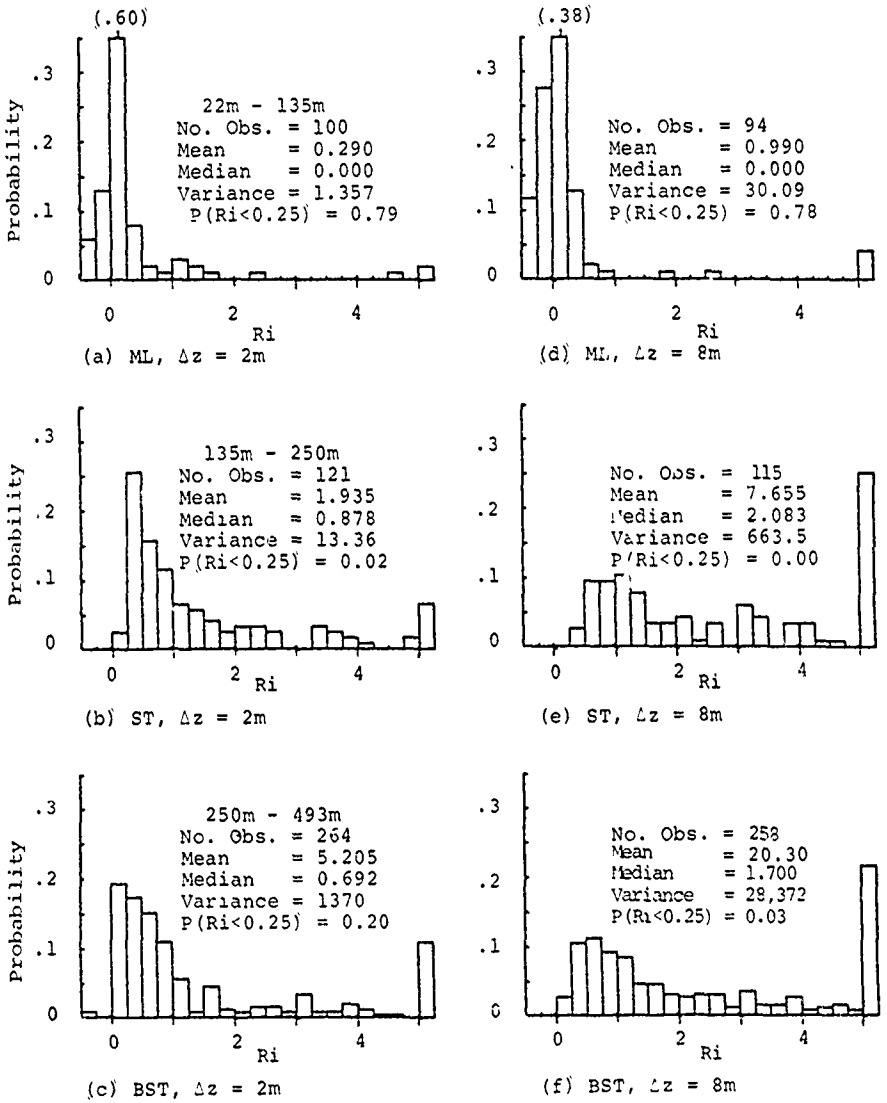

Figure 3.7 Histograms of Richardson number (Ri) computed by differencing over a vertical interval of 2 m for (a) the ML, (b) the ST, and (c) the BST regime. Histograms of Ri computed over an interval of 8 m for (d) the ML, (e) the ST, and (f) the BST regime.

and 3.4), we once again observe than N^2 and S^2 exhibit qualitatively similar behavior, namely, a predominance of low values within the BST regime and a broad range of values within the ST regime. In the case of Ri, however, the histrograms for the ST and BST regimes are remarkably similar. This is as one might expect from the profiles shown in Figure 2.3. Hence, while the distributions of N^2 and S^2 within the ST regime are markedly different than those below, the distribution of their ratio remains relatively constant. This situation does not hold, however, within the ML regime. Under conditions of extremely weak density stratification, the presence of any significant shear will result in very low values of Ri. As seen in Figure 3.4, the values of S^2 within the ML are significant and are comparable to those within the BST regime, whereas the values of N^2 (Figure 3.1) in these regimes are significantly different. Hence, while it seems quite appropriate on the basis of N^2 or S^2 to divide the water column into three regimes, it seems on the basis of Ri that the column should be divided into only two regimes, namely, the surface mixed layer and the region below the mixed layer. This same behavior is observed in the histograms for the other YVETTE stations shown in Appendix B.

Since histograms of S^2 are sensitive to changes in the vertical differencing interval (histograms of N^2 are relatively insensitive), it is not surprising that histograms of Ri are also sensitive. In Figure 3.7 we observe that as Δz increases from 2m to 8m, the Richardson number distribution shifts to higher values. This is consistent with the shift of the S^2 distribution toward

lower values (Figure 3.4). We also note that the change in histogram shape induced by differencing over different vertical intervals is substantially greater than the slight contrast observed between the ST and the BST regimes. This strongly suggests that the vertical resolution of the profile of velocity is a more important factor in determining the shape of the Ri distribution than the variations in the ocean environment itself. This conclusion should be borne in mind when attempting to generalize from a single data set or when attempting to compare results obtained with different sensors. Earlier, we alluded to the potential for using S^2 values obtained with one resolution to estimate the mean S^2 value that would have been observed with an instrument with a different resolution. Such an exercise might allow one to compare Ri distributions obtained with different instruments. The effects of vertical resolution on calculated values of Ri is illustrated and discussed in more detail in Newman et al. (1981).

3.3 COMPARISONS BETWEEN STATIONS

Histograms for YVETTE 8 were presented in the preceeding section. Histograms of B.V. frequency squared, vertical shear squared, and Richardson number for the remaining YVETTE stations are presented in Appendix B. The effect of variations in the vertical differencing interval, Δz, on histogram shape has been illustrated. Since this effect is consistent, the histograms presented in Appendix B are all constructed using a vertical differencing interval of 2m. Clearly, to compare histograms from different stations, it is necessary to hold Δz constant. The differencing interval of 2m was selected to take advantage of the finest resolution afforded by the filtered YVETTE profiles.

While details of the histogram shapes (Appendix B) change from station to station, the tendencies noted for station 8 seem to prevail throughout the data set. In some cases (e.g. YVETTE 24, Figure B.9) the histogram shapes in each stratification regime are poorly resolved because the profile is short and there are consequently only a small number of observations. At YVETTE stations N1 and N4 (Figures B.11 and B.12) the observed mean stratification and vertical shear squared within the upper regime are so great ($>5X10^{-4}$ s^{-2}) that the values are off scale. Surprisingly the Richardson number histograms conform well to those of the other stations. In one case, the ST regime at YVETTE station E6 (Figure B.14), the Richardson number histogram is somewhat anomalous. Here the broad range of values of B.V. frequency squared are accompanied by predominantly small values of shear squared. This results in unusually high values (mode > 2) of Richardson number. It is noted, however, that this histogram is one of those whose shape is poorly resolved because of the small number of observations.

Rather than comparing histograms, the variations from one station to another can be more concisely shown by a plot of a single parameter of the histogram, such as the mean, versus station number. Therefore, the variations from station to station of the mean value of N^2 and S^2 ($\overline{N^2}$ and $\overline{S^2}$) within each stratification regime are shown in Figure 3.8. In this figure the stations are arranged in descending order with respect to the mean value of S^2 (computed at each station with values from the whole profile). Since some of the profiles are relatively short

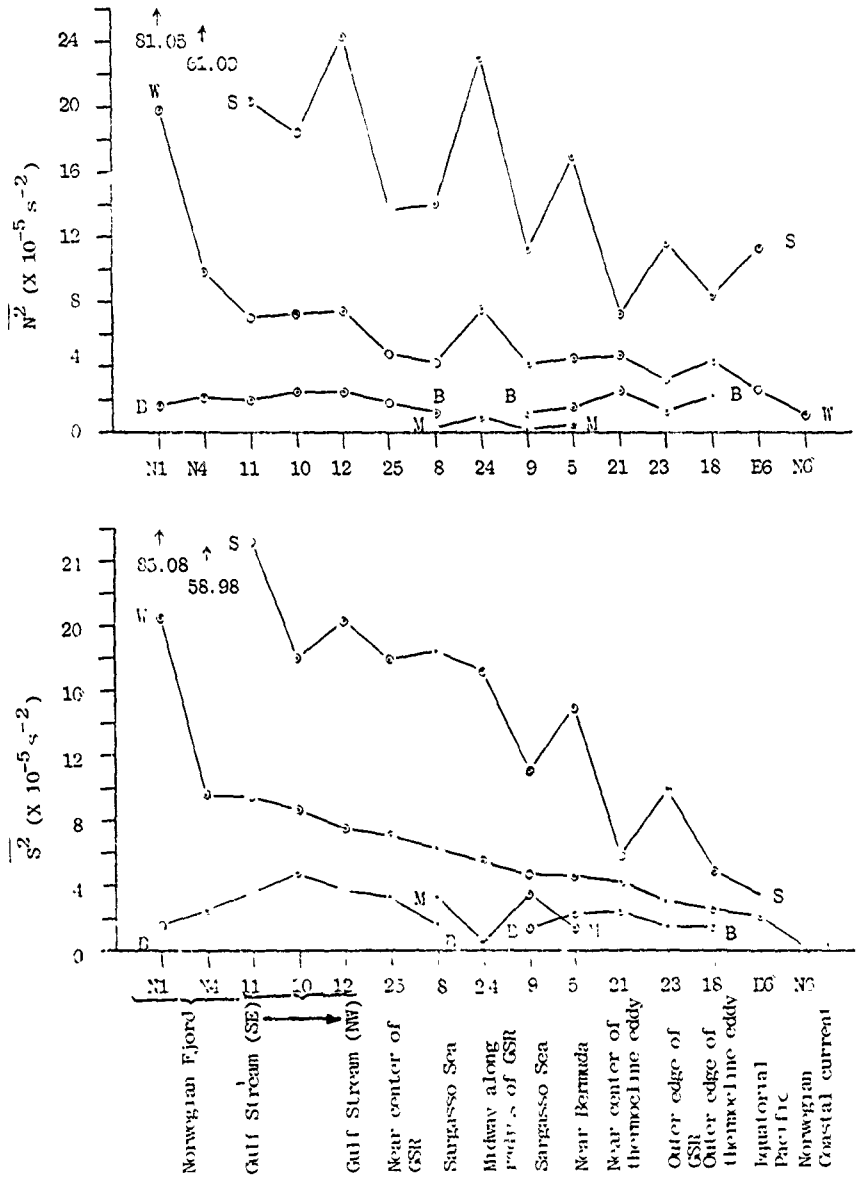

Figure 3 8 Mean N^2 (top) and mean S^2 (bottom) of the surface mixed layer (M), the near-surface thermocline (S) the regime below the thermocline (B), and the whole profile (W) versus station number

(YVETTE 24, N1, N4, and N6), the mean values for these profiles are not strictly comparable to the others. Bearing this in mind, they are included anyway for the sake of completeness.

The high mean values at YVETTE stations N1 and N4 are due to the extremely high values in the upper regime (i.e., the upper 34m) and are not truly representative of the bulk of the water column, which is more appropriately represented by the lower regime. (See profiles in Figures A.33 and A.36, respectively.) Except for YVETTE statons N1 and N4, there is a tendency in the North Atlantic profiles for $\overline{S^2}$ levels to decrease with distance from the Gulf Stream, that is, to decrease from the Gulf Stream to the Gulf Stream ring, the Sargasso Sea, Bermuda, the Bahamas, and finally the Norwegian Coastal Current. Possibly the same trend would be observed in the North Pacific with distance from the Kuroshio. With existing data, we can only observe that in the equatorial Pacific, the $\overline{S^2}$ levels are relatively low.

Examination of Figure 3.8 reveals that, to a first approximation, $\overline{N^2}$ levels computed over whole profiles decrease with the corresponding $\overline{S^2}$ levels. The anomalously high $\overline{N^2}$ levels at YVETTE station 24 are due to the very high values within the thermocline which are probably an artifact of poor resolution due to the abrupt termination of the profile (Figure A.28). The $\overline{N^2}$ and $\overline{S^2}$ levels within different stratification regimes rank themselves as expected. Note that the $\overline{S^2}$ levels within the surface mixed layer sometimes exceed those below the

thermocline (e.g. YVETTE stations 8 and 9). Note also that within each stratification regime there is a tendency for the $\overline{N^2}$ and $\overline{S^2}$ levels to vary up and down in parallel fashion. This tendency will be examined further in Section 4.

From the temperature profiles shown in Figures A.22, A.25, and A.28, it is evident that the Gulf Stream ring sampled by YVETTE stations 23, 24, and 25 is a cold core, cyclonic ring. While it is not possible with only three profiles to know the precise location of the center of the ring, we note in Figure 3.8 the trend of increasing $\overline{N^2}$ and $\overline{S^2}$ toward the center of this mesoscale feature. (Recall that the $\overline{N^2}$ levels at YVETTE 24 are suspect.) The same trend is evident in the thermocline eddy (a mesoscale feature confined in vertical extent to the thermocline portion of the water column) observed near the Bahamas by YVETTE stations 18 and 21. The mesoscale feature is most clearly revealed by the lens of relatively high salinity water observed at station 21 between 100 and 250 dbars. (cf. Figures A.16 and A.19.)

The tendency for $\overline{N^2}$ to increase toward the center of a cyclonic eddy may be due to the convergence (in the vertical) of surfaces of constant density toward the center of such features. This phenomenon is observed in the vertical sections across Gulf Stream rings shown in Figure 3.9. (We note that in the region of the Gulf Stream, surfaces of constant density are almost parallel to surfaces of constant temperature.) The accompanying increase in $\overline{S^2}$ toward the center of such features is not yet explained,

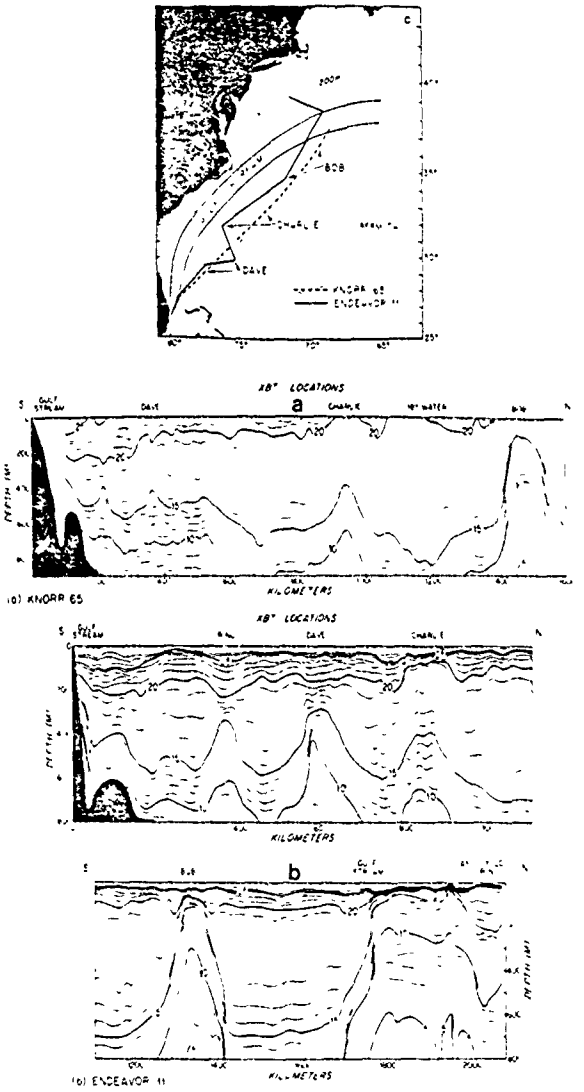

Figure 3.9 Temperature sections between (a) Florida and 38°N, 68°W (KNORR 65 9-14 April 1977) and (b) Florida and New England (ENDEAVOR 11, 26 July-18 August 1977) Several Gulf Stream cyclonic rings (as confirmed by short XBT surveys or by drifter trajectories) were crossed including those called Bob, Charlie, and Dave. Also an anticyclonic ring was observed northwest of the Gulf Stream (from Richardson, 1980)

but it is consistent with the observed tendency for $\overline{S^2}$ to vary with $\overline{N^2}$. From the above discussion we would expect both $\overline{N^2}$ and $\overline{S^2}$ to decrease toward the center of an anticyclonic ring. Since we have no data from an anticyclonic ring, this remains as an hypothesis to be tested during future field work.

Section 4

RELATIONSHIPS BETWEEEN VERTICAL SHEAR AND DENSITY STRATIFICATION

4.1 INTRODUCTION

In Figure 2.3, we noted that a visual comparison of the profiles of N^2 and S^2 suggests that some relationship exists between these two parameters. In this figure, individual values were obtained by differencing over a vertical interval of 2m. However, individual values of Ri, the ratio of N^2 to S^2, fluctuate over several orders of magnitude, and no relationship is evident when individual values of N^2 and S^2 are compared. Yet, in spite of the broad range of values of Ri, there is a tendency (below the surface mixed layer) for values of Log_{10} (Ri) to remain in the neighborhood of zero (i.e. values of Ri are of order 1). This tendency is also illustrated by the histograms of Ri shown in Figure 3.7. Hence, some relationship between the 2m values of N^2 and S^2 appears to hold in a statistical sense. In Figure 3.8 we noted that N^2 and S^2 values averaged over stratification regimes exhibited qualitatively similar behavior. This reinforces the notion that the two parameters are statistically related. In this section we display the relationship between N^2 and S^2 in various ways, attempt to explain the observed relationships, and assess the potential for predicting $\overline{S^2}$ from measurements of $\overline{N^2}$.

4.2 PROPORTIONALITY OF $\overline{N^2}$ AND $\overline{S^2}$

Figure 4.1 is a plot of $Log_{10}(N^2)$ versus $Log_{10}(S^2)$. To the extent that density stratification and vertical shear are related by some power law, the points on a log-log plot should tend to lie along a straight line. For example, if $\overline{S^2}$ varies as $\overline{N^3}$ as suggested by WKB scaling arguments (Grabowski, 1980), then the line will have a slope of 2/3. If S^2 varies as N^2, then the line will have a slope of one, implying that N^2 and S^2 are directly proportional and the proportionality constant is the Richardson number. On the log-log plot, variations in this proportionality constant correspond to variations in the y-intercept of the line with unit slope. In Figure 4.1 diagonal lines with slopes equal to one indicate the various values of Ri. Note that zero values of N^2 or S^2 (and negative values of N^2) are undefined on this type of plot. The horizontal and vertical lines on the plot represent the value of N^2 and S^2, respectively, below which the signal-to-noise ratio (see Section 2.1) becomes less than one.

The distribution of points in Figure 4.1 does not clearly indicate any particular power law relationship. For any given value of N^2 there is a broad range of observed values of S^2. To compare the power law relations suggested above, cross-correlation coefficients were computed between N^P and S^2, where P=1,2, and 3. This was done for several YVETTE stations including station 8. The cross-correlation coefficients were computed for different stratification regimes and for a range of values of Δz. The

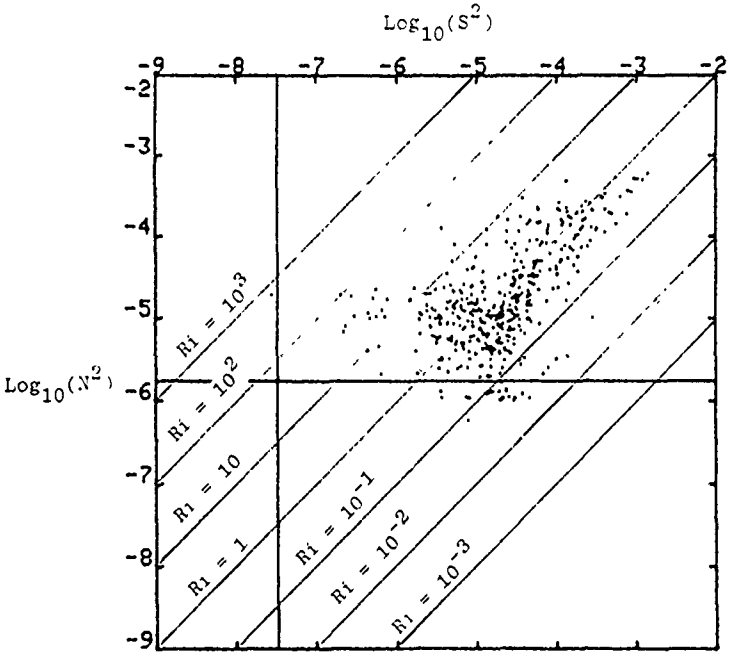

Figure 4.1 $Log_{10}(N^2)$ versus $Log_{10}(S^2)$ for YVETTE station 8 Each point is derived from differences over a vertical interval of 2m (cf Figure 2 3). Points to the left of the vertical line or below the horizontal line are below the noise level (see Section 2.1).

results did not indicate a preferred power law relationship, a conclusion consistent with Figure 4.1. It is noted that the points in Figure 4.1 do tend to cluster around a line for which the value of Ri is of order one. The distribution shown here is consistent with that shown in panel (c) of Figure 2.3, except for the absence of the lowest values of Ri which are associated with zero or negative values of N^2.

We now compute, for every station, the mean of the 2m values of N^2 and the mean of the corresponding values of S^2 within each stratification regime. These mean values, displayed on a log-log plot in Figure 4.2, suggest that $\overline{N^2}$ and $\overline{S^2}$ are approximately proportional with a proportionality constant of Ri=1. The points in Figure 4.2 are grouped in two clusters. The cluster with higher values of $\overline{N^2}$ and $\overline{S^2}$ is from the ST regime, and the cluster with lower values is from the BST regime. Though all points from the ML regime have low values of $\overline{N^2}$, they are not clustered because of the wide variations in $\overline{S^2}$.

To check our visual perception that $\overline{N^2}$ is approximately equal to $\overline{S^2}$, for each YVETTE station we averaged the 2m N^2 values and the corresponding S^2 values over non-overlapping 30m intervals. The averaging used a triangular weighting scheme. A composite of the resulting $\overline{N^2}$ and $\overline{S^2}$ values is presented in Figure 4.3. The best straight-line fit to these points was determined, using least squares regression, to have a slope of 1.02 ± 0.06 which is not significantly different than 1.0. Hence, our visual perception seems to be correct.

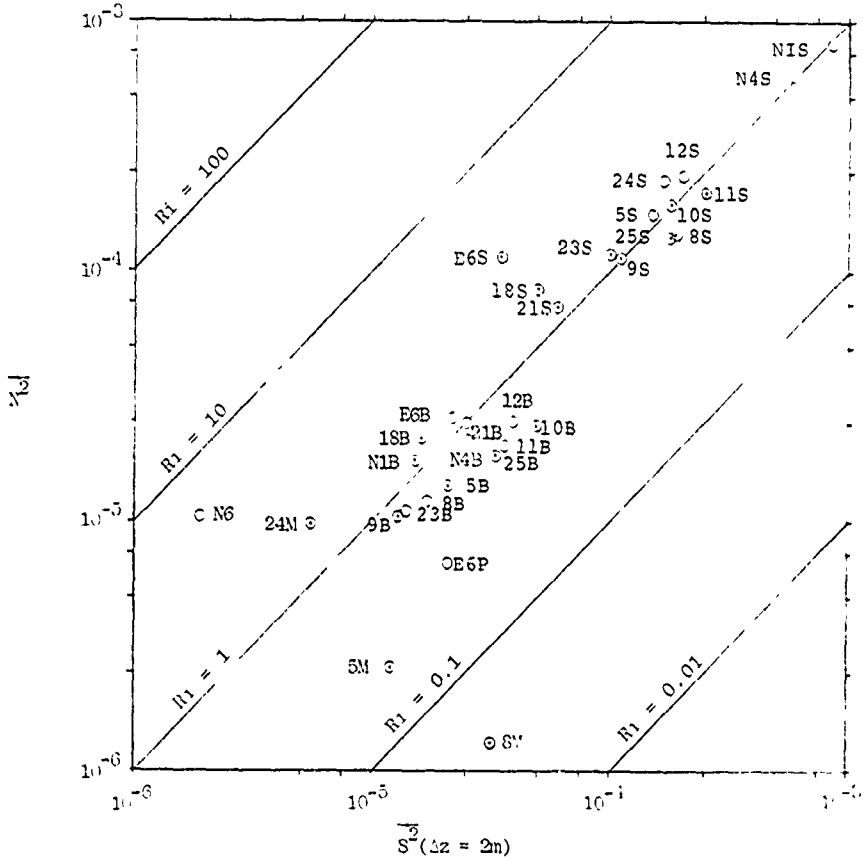

Figure 4.2 $\overline{N^2}$ versus $\overline{S^2}$ for a vertical differencing interval of 2m The point labels consist of the appropriate station number followed by a letter to indicate the stratification regime

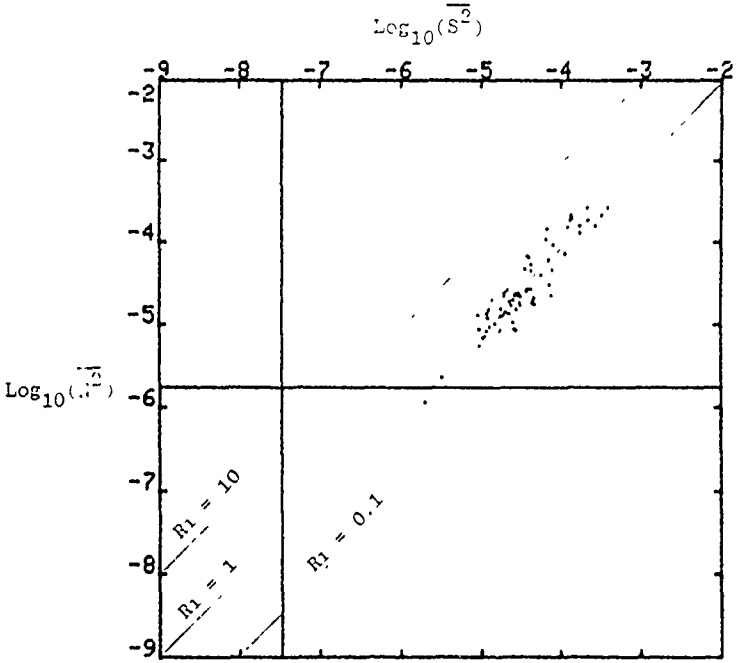

Figure 4.3 $\text{Log}_{10}(\overline{N^2})$ versus $\text{Log}_{10}(\overline{S^2})$ for 19 MILTY stations in the western North Atlantic. Each point is derived by averaging the 2m values of N^2 and S^2 over a vertical interval of 30m as described in the text. The best straight-line fit to these points has a slope of 1.02 ± 0.06.

4.3 CORRELATION BETWEEN N^2 AND S^2

We have shown that the individual 2m values of N^2 and S^2 exhibit no obvious relationship, but that vertically averaged values or points in smoothed profiles appear to be better correlated and, moreover, directly proportional with a proportionality constant of one. To quantify the correlation between N^2 and S^2 and the effects that data processing has on this correlation, we will now examine the linear cross-correlation coefficient between N^2 and S^2 and the way in which it varies with vertical differencing interval and with vertical smoothing length.

We estimate the linear correlation between two parent populations x and y by evaluating the following expression for a sample of observed pairs (x_i, y_i), $i=1,2,\ldots M$,

$$r = (1/M) \sum (x_i-\bar{x})(y_i-\bar{y})/\sigma_x \sigma_y ,$$

where $\bar{x}$ and $\bar{y}$ are sample averages. The terms σ_x and σ_y denote sample standard deviations. The sample correlation coefficient r may have values in the range between -1 and +1. Values close to zero indicate no correlation, while the values $\pm$ 1 indicate perfect correlation.

In order to evaluate the accuracy of a correlation coefficient estimate, we must first evaluate the number of statistically independent sample points, F. Each profile contains a different number of statistically independent sample points which depends on the profile depth D and the

total effective correlation length τ;

$$F = D/\tau \ .$$

Since N^2 and S^2 may have different correlation lengths, we take τ to be the geometric mean of the correlation lengths of N^2 and S^2;

$$\tau = \sqrt{\tau_{N^2} \tau_{S^2}}$$

Here we define τ_X as the integral of the auto-covariance function,

$$\tau_X = \int_0^{\tau_0} R_X(\tau) d\tau \ .$$

The upper limit of this integral, τ_0, is defined such that $R_X(\tau_0) = 0.1$, which allows us to make consistent estimates of τ_X.

We can assess the accuracy of correlation coefficient estimates by computing confidence levels at the 68% (one standard deviation) level of significance. We expand upon the procedure outlined by Bendat and Piersol (1971). Let us define a random variable

$$w = 1/2 \ln \left(\frac{1 + r}{1 - r} \right) .$$

From Brownlee (1965), w has an approximately normal distribution with a mean and standard deviation of

$$\bar{w} = 1/2 \ln \left(\frac{1 + r'}{1 - r'} \right),$$

$$\sigma = (F-2)^{-1/2} \ ,$$

where r' is the correlation coefficient of the parent population, and F is the number of independent observations.

We solve for r in terms of w,

$$r = \frac{e^{2w} - 1}{e^{2w} + 1} \quad .$$

The standard deviation confidence limits r_+ and r_- are given by substituting $w \pm \sigma$ for w;

$$r_{\pm} = \frac{e^{2(w \pm \sigma)} - 1}{e^{2(w \pm \sigma)} + 1}$$

Linear correlation coefficients were computed for several YVETTE profiles. The results for YVETTE station 8 are presented in Figure 4.4. Correlations for the near-surface thermocline (135 to 250 m), the regime below the thermocline (250 to 473m), and the combination of the two regimes (135 to 473m) are presented. The N^2 and S^2 values were computed using differencing intervals of 2m and 8m. The resulting profiles of N^2 and S^2 were filtered using triangular weighting functions with half-widths of 5m and 20m. Such a weighting function is computationally simple and it has a well understood response function. By filtering N^2 and S^2 we increase the effective correlation lengths of the profiles. This tends to reduce the number of independent observations and to degrade the confidence in the correlation coefficient estimates.

We see that the correlation in the combined regime is better than either of the separate regimes. This result

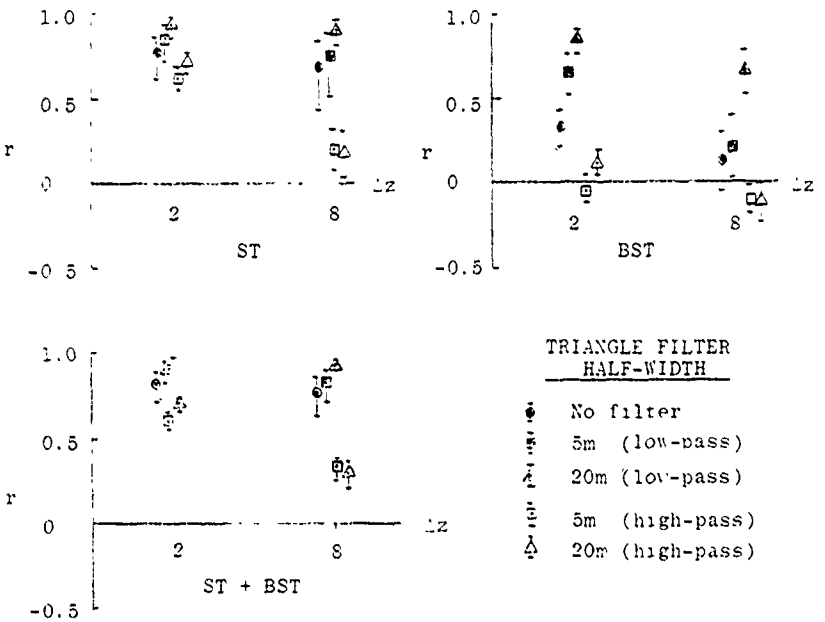

Figure 4.4 Linear correlation coefficient between N^2 and S^2 for the ST regime, the BST regime, and the combination of the two regimes at YVETTE station 8. Correlation is plotted versus vertical differencing interval for different triangle filter widths. Confidence limits are indicated by the vertical bars

applies to all of the profiles. This is due to the fact that in the near-surface thermocline, N^2 and S^2 are much greater than in the regime below. Therefore the combined regime contains a wider range of values than either of the separate regimes, and the resulting correlation is stronger. However, no general statement can be made about the relative magnitude of the correlation coefficients for the near-surface thermocline and for the regime below.

Smoothing N^2 and S^2 generally improves correlations. In fact, correlation increases as the smoothing length increases. This implies that long wavelength components of the N^2 and S^2 profiles correlate better than short wavelength components. We reach the same conclusion by applying a high pass filter to N^2 and S^2. The high pass filtered profiles are computed by subtracting the low pass filtered profiles from the original profiles. The resulting frequency response is the complement of the original frequency response of the triangular weighting function. We see that the correlation coefficients for the high-pass filtered profiles are consistently lower than those for the low-pass filtered profiles.

Although in Figure 4.4 the correlation coefficient tends to decrease with increasing vertical differencing interval, this is not a general result. There appears to be no consistent relationship between the magnitude of the correlation coefficient and the magnitude of the vertical differencing interval.

4.4 PREDICTION OF $\overline{S^2}$ FROM $\overline{N^2}$

While Figure 4.1 shows that it would not be possible to predict S^2 over a given 2m interval from the corresponding observed value of N^2, Figures 4.2 and 4.3 suggest that below the surface mixed layer one can predict with some confidence the vertical average of several S^2 values by assuming it is equal to the vertically averaged N^2. Fortunately obtaining a vertically averaged value of N^2 does not require a high resolution density profile as provided by a CTD. It can be obtained by simply differencing over a large (i.e. much greater than 2m) vertical interval as would be possible with Nansen cast data. In fact, a first cut at the climatology of small scale (2m) vertical shear for the North Atlantic might be derived from the historical observations of the density field contained in the data archives. While the simple relationship described above is probably equally valid in other oceans, this remains to be demonstrated. In any case, a relationship such as this can, at best, provide only a first approximation to the mean 2m vertical shear that would actually be observed in any given profile. This fact is demonstrated in Figure 4.5 which shows profiles of $\overline{N^2}$ (solid lines) and $\overline{S^2}$ (+ marks) for several of the YVETTE stations. The points in the profiles represent non-overlapping 50 m block averages of the individual N^2 and S^2 values which were derived using a Δz of 2m. This approach is similar to that used by Simpson (1975). While the profiles of vertically averaged values are qualitatively similar, occasionally the agreement at specific depths is

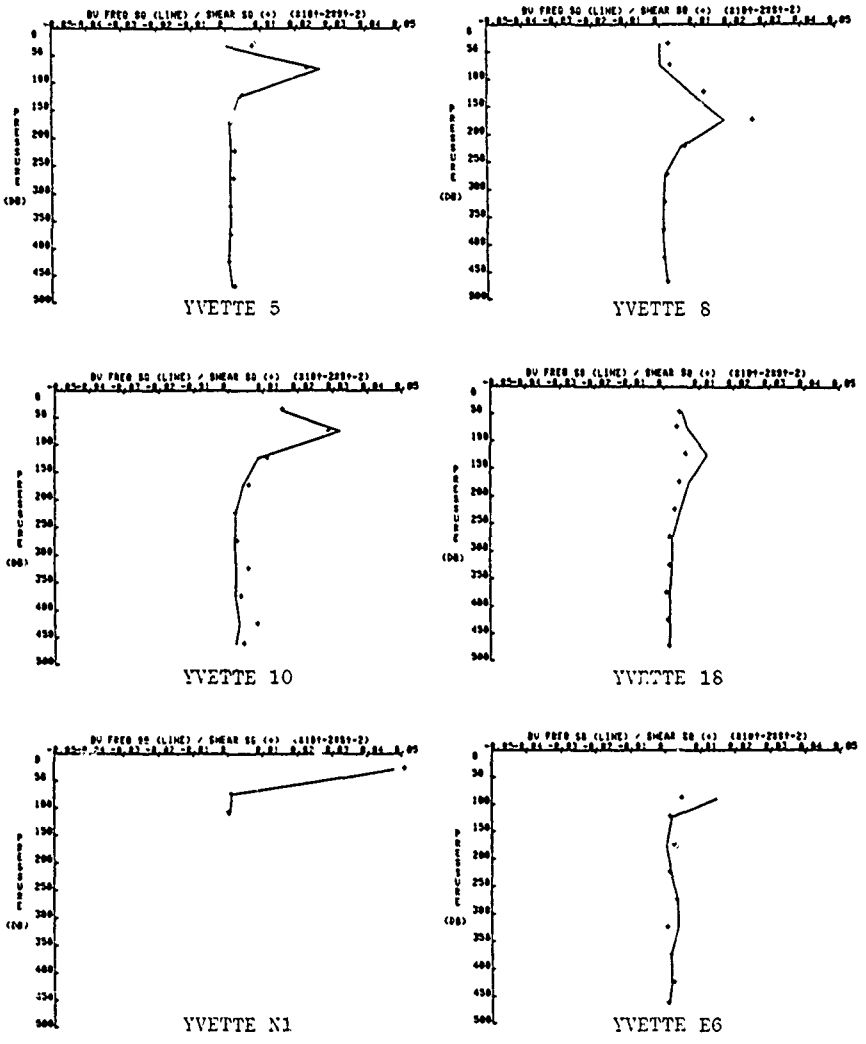

Figure 4.5 Vertical profiles of mean N^2 (solid line) and mean S^2 (+ marks) for selected YVETTE stations. The individual points represent non-overlapping 50m vertical averages of the 2m values of N^2 and S^2. The presentation is similar to that used by Simpson (1975)

not very good. It may be that a temporally averaged value of S^2 (Δz = 2m) at a specific depth would be more in agreement with the local mean N^2. A single YVETTE profile is, after all, only one realization of a temporally varying ocean, and as such, it may not be realistic to expect better agreement than that shown in Figure 4.5. Whether temporally averaged values would in fact exhibit better agreement remains to be demonstrated with a time series of velocity profiles.

In Figures 3.5 and 3.6 we showed the effect on $\overline{S^2}$ of increasing the vertical differencing interval. This effect is shown again in the sequence of $\overline{N^2}$ versus $\overline{S^2}$ plots presented in Figure 4.6. As expected from the previous discussions, $\overline{S^2}$ decreases and the ratio of $\overline{N^2}$ to $\overline{S^2}$ increases as Δz increases (i.e. the relationship between $\overline{N^2}$ and $\overline{S^2}$ changes as Δz changes). However, Figure 4.6 also reveals that the scatter of the points in each cluster increases as Δz increases. Hence, for a given value of $\overline{N^2}$ we observe an increasing percentage variation of $\overline{S^2}$. This suggests that we can predict a mean value of $\overline{S^2}$ over a 2m vertical scale with a smaller percent uncertainty that we can predict a mean value over a larger vertical scale. The reason for this is not yet clear. Nonetheless, the empirical relationship between $\overline{N^2}$ and $\overline{S^2}$ is sensitive to the magnitude of Δz and we have more confidence in the relationship if Δz is small. However, we noted in Figure 4.5 that even for Δz = 2m, the relationship is only approximate.

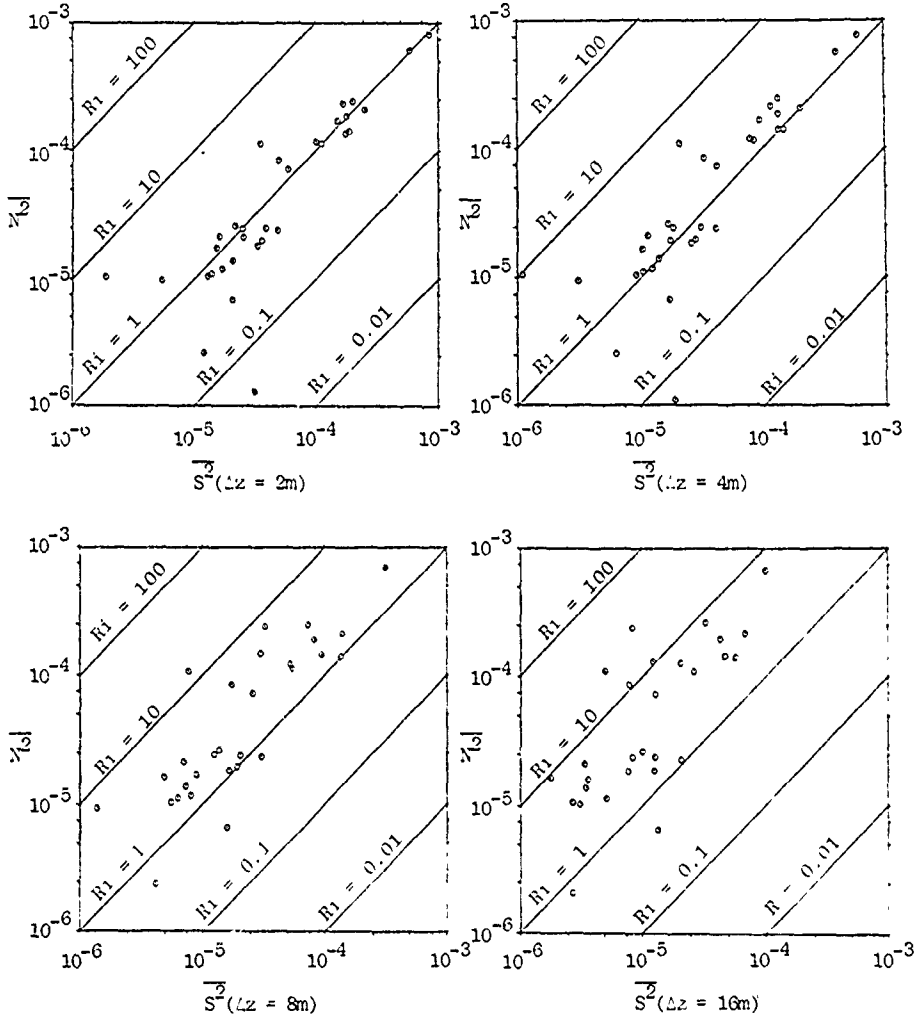

Figure 4.6 Plots of $\overline{N^2}$ versus $\overline{S^2}$ showing the effect of varying the vertical differencing interval employed in computing the vertical gradients. The case of Δz = 2m was originally shown in Figure 4.2

In Figure 3.8 we showed that $\overline{S^2}$ for each stratification regime varied in almost parallel fashion with $\overline{N^2}$. If $\overline{N^2}$ were exactly proportional to $\overline{S^2}$, then their ratio would be constant. In Figure 4.7 we present a plot of the ratio of $\overline{N^2}$ to $\overline{S^2}$ versus station number. The stations are arranged according to decreasing $\overline{S^2}$ as in Figure 3.8. The ratio for each stratification regime is plotted as well as the ratio for the whole profile. To the extent that the ratio is not constant, the proportionality relationship fails. We note that while the ratio below the surface mixed layer is usually of order one, the actual value varies from station to station. The high ratio observed at stations E6 and N6 results from anomalously low values of $\overline{S^2}$. The significance of this is not yet clear, but it suggests that the relationship between $\overline{N^2}$ and $\overline{S^2}$ which holds in the western North Atlantic may not be universal. There is a tendency seen in Figure 4.7 for different stratification regimes to vary in parallel fashion, that is, if the ratio is relatively high in the ST regime, it is usually high in the BST regime also. Hence, whatever it is that causes the ratio to vary from one station to another, it tends to affect the whole profile in the same way. As noted earlier a temporally averaged S^2 at each station might exhibit better agreement with the local $\overline{N^2}$.

The ratio of $\overline{N^2}$ to $\overline{S^2}$ in Figure 4.7 is almost always higher in the ST regime than below. This might possibly be explained in terms of the natural variation in vertical scales that occurs in the stratified ocean. An

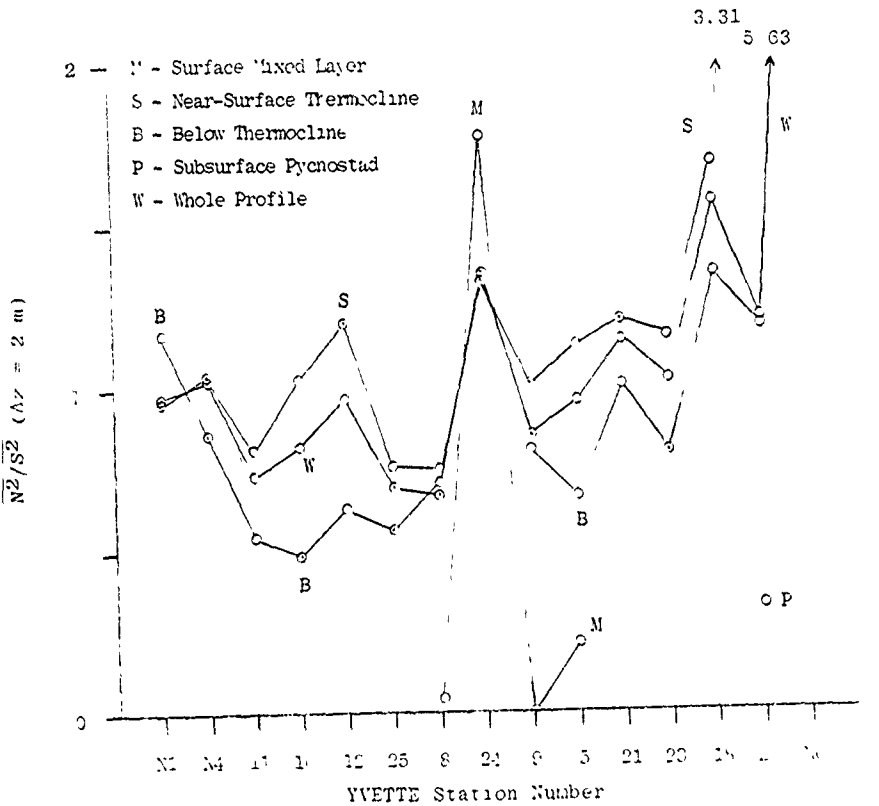

Figure 4.7 Ratio of $\overline{N^2}$ to $\overline{S^2}$ versus station number for the different stratification regimes.

internal wave propagating vertically through the water column decreases its vertical wavelength as N^2 increases. Also the Osmidov scale of turbulent overturning decreases as N^2 increases. Hence, within the ST regime, variations in horizontal velocity tend to occur over smaller vertical scales than in the BST regime. With any fixed vertical differencing interval, such as $\Delta z = 2m$, we are not able to resolve variations that occur over smaller vertical scales. Hence, our estimate of $\overline{S^2}$ will always be somewhat too low, but it will be proportionately lower within the ST regime than below. This is consistent with the observation that the ratio of $\overline{N^2}$ to $\overline{S^2}$ is usually higher within the ST regime.

In Figure 4.7 there appears to be a slight trend of increasing ratio from left to right across the figure. Recall that both $\overline{N^2}$ and $\overline{S^2}$ are generally decreasing in this direction, and hence the increasing ratio suggests that $\overline{S^2}$ must be decreasing faster than $\overline{N^2}$. To the extent that the perceived trend is significant, the simple proportionality relationship between $\overline{N^2}$ and $\overline{S^2}$ fails again.

Intuitively it is perhaps more surprising that $\overline{N^2}$ and $\overline{S^2}$ are as consistently related to each other from station to station as the observations indicate, than the fact that the relationship is not perfect. This is because it seems reasonable to expect that the $\overline{S^2}$ level within any given profile is dependent to some extent on the variable influence of present and past forcing events. In other words, two stations with the same $\overline{N^2}$ levels might have different $\overline{S^2}$ levels because of a difference in recent

or local forcing conditions. As the kinetic energy is being put into the water column, it will tend to arrange itself in accordance with the local density profile, e.g. vertical shear will be greatest in regions of high density gradient. In the case of YVETTE stations 8 and 9, we note that they were occupied at the same location and were separated in time by approximately 10 hours (Table 1.1). The N^2 profiles for the two stations are almost identical, but the S^2 profiles are different (cf. Figures 2.3 and A.6), with YVETTE 8 having a higher $\overline{S^2}$. This accounts for the lower ratio of $\overline{N^2}$ to $\overline{S^2}$ exhibited by YVETTE 8 than by YVETTE 9 in Figure 4.7. Hence the $\overline{N^2}$ value for a particular portion of the water column may establish, in a statistical sense, an "expected" value for $\overline{S^2}$, but whether or not the observed $\overline{S^2}$ level fulfills these expectations depends on the availability of sources of kinetic energy. The trend of increasing ratio seen in Figure 4.7 might be an artifact of arranging the stations in order of decreasing $\overline{S^2}$ which automatically incorporates the effects of decreasing availability of kinetic energy.

Section 5
SUMMARY AND CONCLUSIONS

Vertical profiles of density and horizontal velocity from a diverse range of oceanic conditions have been examined. Vertical gradients of these quantities are computed by taking simple differences over a vertical interval, Δz. The magnitudes of the vertical gradients, in particular Brunt-Väisälä frequency squared (N^2) and vertical shear squared (S^2), appear to be arranged into distinct regimes of differing stratification. The surface mixed layer (ML), sampled in some profiles, is characterized by vertically homogeneous density and weak mean vertical shear. The near-surface thermocline (ST) is characterized by a broad range of values in both N^2 and S^2. The regime below the ST (the BST regime) is characterized by uniformly small values of N^2 and S^2. Vertical profiles of Log_{10} (Ri), where $Ri = N^2/S^2$, exhibit values spanning several orders of magnitude, but show only very slight differences between the ST and BST regimes. The ML, on the other hand, exhibits very low Ri values and is therefore distinctly different than the deeper regimes. The lowest values of Ri generally occur where N^2 is low rather than where S^2 is high.

Histograms for each stratification regime reveal that the mean, mode, and variance of S^2 distributions decrease with increasing Δz. This is because the highest values of S^2 are associated with small scale fluctuations in the velocity profile. As Δz increases, the ability to resolve these small scale fluctuations is lost. The

decrease in mean S^2 ($\overline{S^2}$) with increasing Δz is consistent enough to suggest the possiblity of extrapolating to vertical scales which are not well resolved by YVETTE. This might allow direct intercomparison of $\overline{S^2}$ levels measured by sensors with different vertical resolution capabilities.

Since the S^2 distributions are sensitive to changes in Δz, the same is true for distributions of Ri. The Ri values become generally larger as Δz increases. While the S^2 distributions for the ST and BST regimes are distinctly different, the corresponding Ri distriubitons are very similar. Ri distributions are more sensitive to changes in Δz than to changes in stratification regime. This suggests that the details of the shape of the Ri distributions may depend more on the vertical resoluton capabilities of the velocity sensor than on the ocean environment.

In the North Atlantic $\overline{N^2}$ and $\overline{S^2}$ appear to be approximately proportional. If $\Delta z = 2m$, the proportionality constant is $Ri = 1$. Both $\overline{N^2}$ and $\overline{S^2}$ tend to decrease with distance from the Gulf Stream. Both appear to increase toward the center of cyclonic mesoscale eddies. A first approximation to the climatology of small scale vertical shear in the North Atlantic might be derived from the historical observations of the density field contained in the data archives. The relationship between $\overline{N^2}$ and $\overline{S^2}$ in other ocean areas needs to be established with additional YVETTE-type observations.

The correlation coefficient between N^2 and S^2 values (computed over a specified Δz) increases with increasing vertical smoothing interval (vertical filter

length). Hence the correlation between long vertical wavelength components of the profiles is better than the correlation between the short vertical wavelength components. Apparently, small scale vertical shear has an expected value which is modulated by the large scale density gradient. Since the magnitude of S^2 depends on vertical changes in either the magnitude or direction of the horizontal velocity vector, the modulation by the large scale density gradient must be associated with a modulation of either or both of these quantities. Changes in speed correspond to changes in the kinetic energy level: changes in direction might be due to internal waves. The YVETTE profiles show that changes in both speed and direction contribute to changes in S^2. The correlation coefficient exhibits no consistent trend with changes in the vertical differencing interval.

The proportionality constant between $\overline{N^2}$ and $\overline{S^2}$ increases as Δz increases. This means that the relationship used to predict $\overline{S^2}$ from measured values of $\overline{N^2}$ depends on the particular vertical differencing interval employed. Our analysis of the YVETTE data suggests that $\overline{S^2}$ over a 2m interval can be predicted with a smaller percent uncertainty than $\overline{S^2}$ over a larger vertical interval.

Although a proportionality relationship between $\overline{N^2}$ and $\overline{S^2}$ seems to be a good first approximation, $\overline{S^2}$ is clearly dependent to some extent on other factors, such as the availability of sources of kinetic energy. It is possible that temporally averaged values of S^2 would

exhibit better agreement with the local N^2 profile. The apparent difference between the ratio of $\overline{N^2}$ to $\overline{S^2}$ for the ST regime and the ratio for the BST regime may be due to the natural variation of vertical scales (of internal waves and the Osmidov length) that occurs in the stratified ocean.

Section 6
RECOMMENDATIONS FOR FURTHER WORK

Although a diverse range of dynamically different oceanic conditions has been examined in this data set, most of the stations are located in the western North Atlantic. The anomalously low levels of small scale shear observed in the Norwegian Coastal Current and the equatorial Pacific cause these stations to deviate most from the more or less consistent pattern established by the other stations. To determine the generality of the conclusions of this report, other ocean areas (e.g. North Pacific and Indian Ocean) and mesoscale features (e.g. anticyclonic eddies and fronts) need to be sampled with an YVETTE-type profiler.

Each profile examined in this report provides a single realization of a temporally varying ocean. It is to be expected that the levels of small scale shear at any location will vary in time as a result of forcing events, inertial oscillations, etc. Therefore, we also need to obtain and examine time series of profiles in several locations to (1) determine how temporal variability affects the relationship between N^2 and S^2 and (2) provide enough data to resolve the vertical wavenumber spectrum for the different stratification regimes and different ocean areas.

A climatology of large scale vertical density gradients could be derived from the historical observations of the density field which are contained in the data archives. From this characterization a first cut at a climatology of small scale shear might be derived.

Section 7
REFERENCES

Bendat, J. S., and A. G. Piersol, 1971: Random Data: Analysis and Measurement Procedures. Wiley-Interscience, New York, 407pp.

Brownlee, K. A., 1965: Statistical Theory and Methodology in Science and Engineering (2nd Edition). John Wiley and Sons, New York.

Evans, D. L., H. T. Rossby, M. Mork, and T. Gytre, 1979: YVETTE - a free-fall shear profiler. Deep-Sea Res., 26, 703-718.

Grabowski, W. J., 1980: Modeling of internal-wave induced shear-progress report. Ocean Physics Division Technical Note 80-201-01, Science Applications, Inc., McLean, Virginia, 32 pp.

Hayes, S. P., T. M. Joyce, and R. C. Millard, Jr., 1975: Measurements of vertical fine structure in the Sargasso Sea. J. Geophys. Res., 80, 314-319.

Hebenstreit, G. T., and W. J. Grabowski, 1981: Statistical modeling of shear in the upper ocean. Ocean Physics Division Technical Report, SAI-82-383-WA, Science Applications, Inc., McLean, Virginia.

Lambert, R. B., Jr., D. L. Evans, and P. J. Hendricks, 1980: Data Report - SCIMP and YVETTE, Progress Report I. Ocean Physics Division Technical Report 80-201-04, Science Applications, Inc., McLean, Virginia.

Lambert, R. B., Jr., and S. L. Patterson, 1980: Review of upper ocean vertical shear. Ocean Physics Division Technical Report 80-201-02, Science Applications, Inc., McLean, Virginia, 170 pp. (CONFIDENTIAL)

Molinelli, E. J., S. L. Patterson, and F. C. Newman, 1981: Estimates of YVETTE measurement error. Ocean Physics Division Technical Report (in preparation), Science Applications, Inc., McLean, Virginia.

Newman, F. C., S. L. Patterson, D. M. Rubenstein, and R. B. Lambert, Jr., 1981: Methods of calculating Richardson number from observed data. Ocean Physics Division Technical Report 81-201-01. Science Applications, Inc., McLean, Virginia.

Pollard, R. T., 1980: Properties of near-surface inertial oscillations. J. Phys. Oceanogr., 10, 385-398.

Richardson, P. L., 1980: Gulf Stream ring trajectories. J. Phys. Oceanogr., 10, 90-104.

Rubenstein, D. M., F. C. Newman, and R. B. Lambert, Jr., 1980: A comparison of vertical shear profilers: YVETTE and SCIMP, Progress Report II. Ocean Physics Division Technical Report 80-201-04, Science Applications, Inc., McLean, Virginia, 65pp.

Sanford, T. B., R. G. Drever, and J. H. Dunlap, 1978: A velocity profiler based on the principles of geomagnetic induction. Deep-Sea Res., 25, 183-210.

Simpson, J. H., 1975: Observations of small scale vertical shear in the ocean. Deep-Sea Res., 22, 619-627.

Sippican Corporation, 1979: An expendable current profiler (XCP), Horizon, A Technical Newsletter, Sippican Ocean Systems Division, 4, 1-2.

Appendix A
YVETTE PROFILES

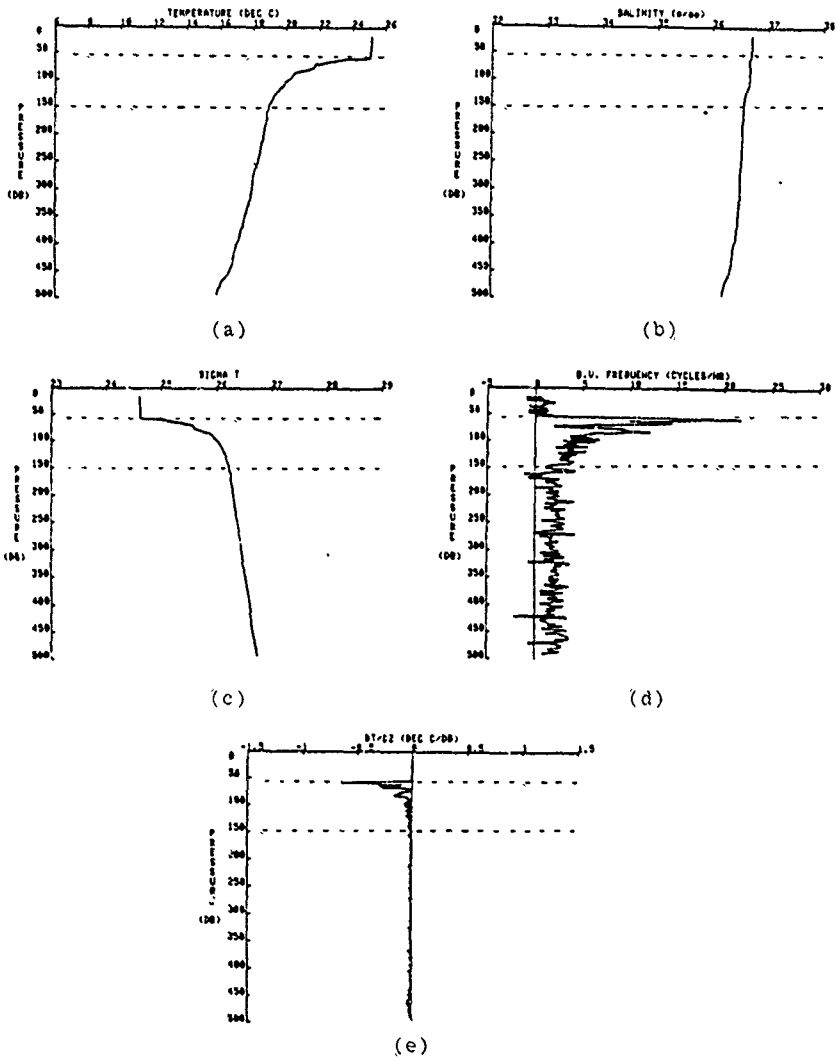

Figure A.1 Profiles of (a) temperature, (b) salinity, (c) density (sigma-t), (d) Brunt-Väisälä frequency, and (e) vertical gradient of temperature for YVETTE station 5 occupied on 5 November 1975 at 32°19'N, 64°34'W (near Bermuda). The profiles can be divided into stratification regimes as indicated by the dotted lines at 55 and 150 dbars

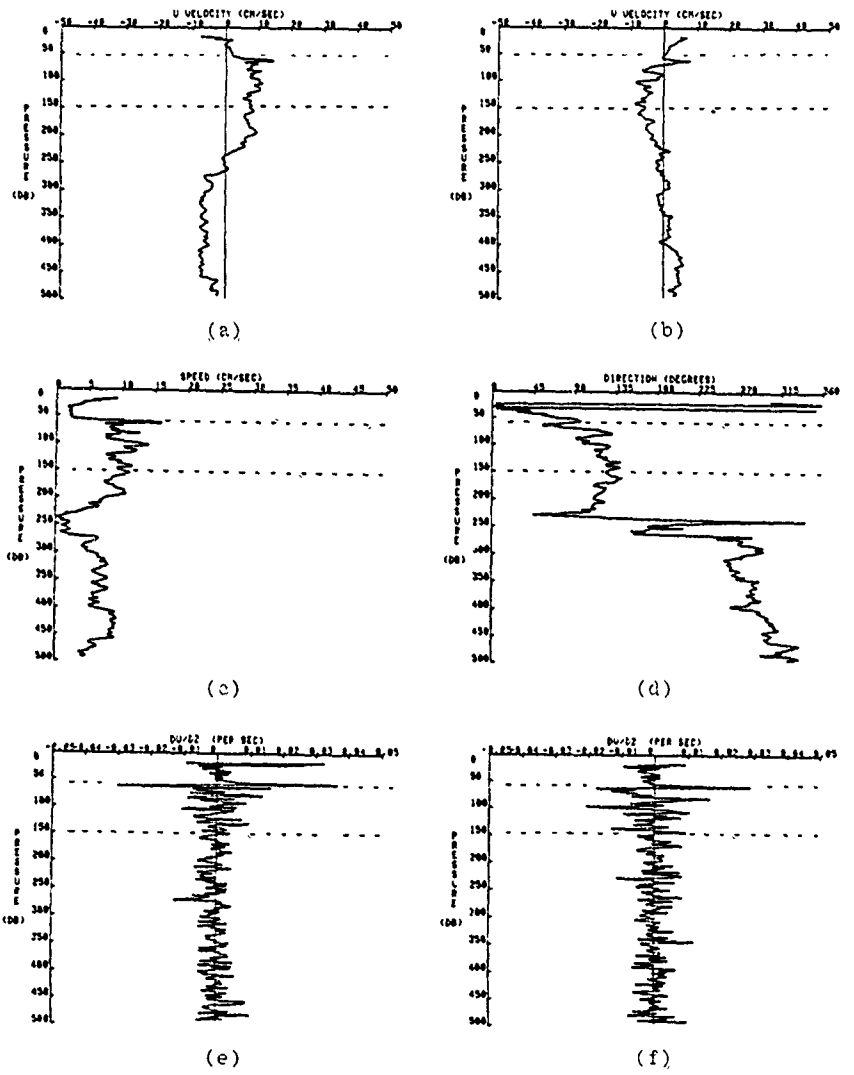

Figure A.2 Profiles of the (a) east and (b) north component of velocity, the (c) magnitude and (d) direction of the horizontal velocity vector, and the vertical gradient of the (e) east and (f) north component of velocity for YVETTE station 5 near Bermuda. The dotted lines are at 55 and 150 dbars.

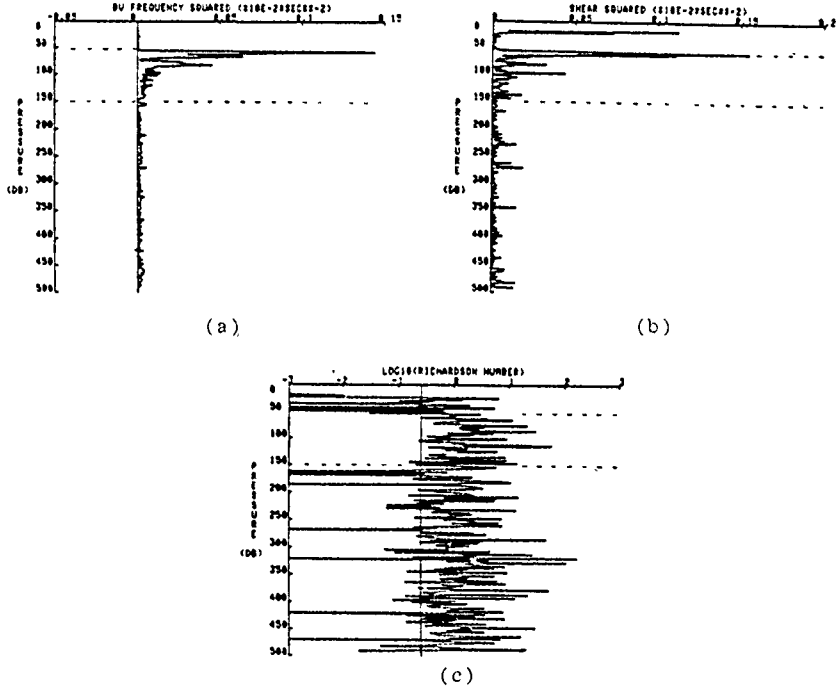

Figure A.3 Profiles of (a) Brunt-Väisälä frequency squared, (b) vertical shear squared, and (c) Log_{10} (Ri), where Ri = N^2/S^2, for YVETTE station 5 near Bermuda. The vertical line in (c) is at Ri = 0.25. The dotted lines are at 55 and 150 dbars.

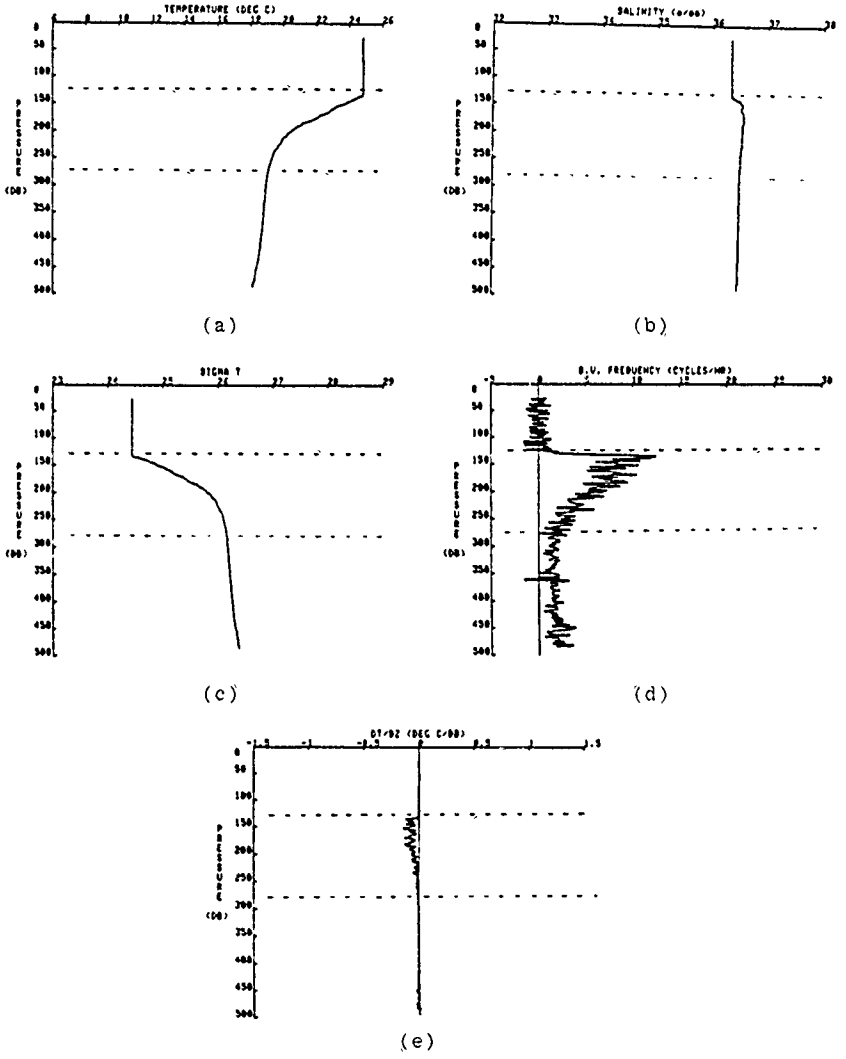

Figure A.4 As in Figure A.1 except for YVETTE station 9 occupied on 8 November 1975 at 35°00 N, 66°30'W (Sargasso Sea). The dotted lines are at 130 and 280 dbars

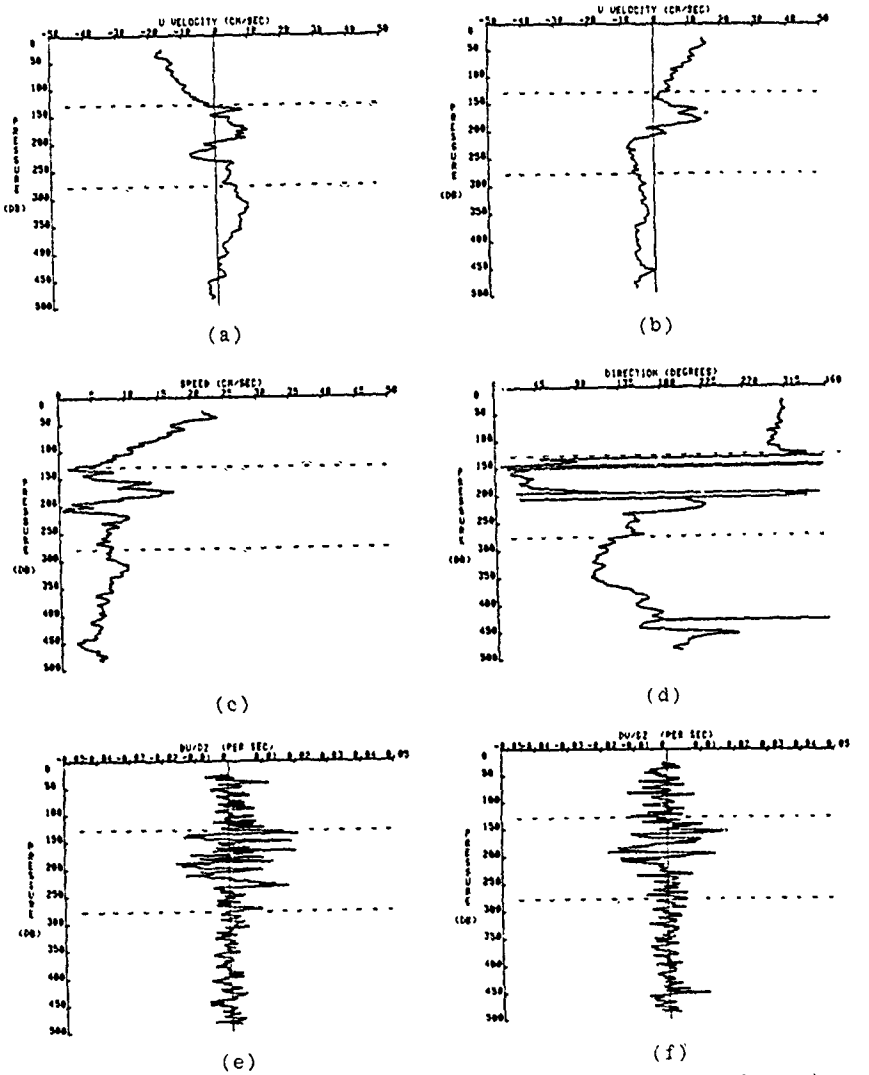

Figure A.5 As in Figure A.2 except for YVETTE station 9 in the Sargasso Sea. The dotted lines are at 130 and 280 dbars.

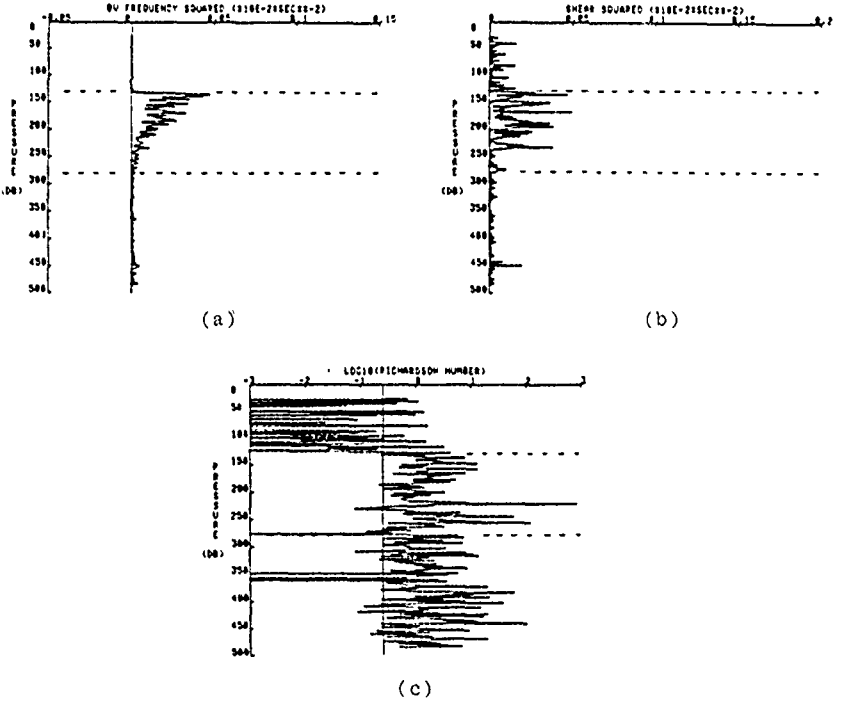

Figure A.6 As in Figure A.3 except for YVETTE station 9 in the Sargasso Sea. The dotted lines are at 130 and 280 dbars.

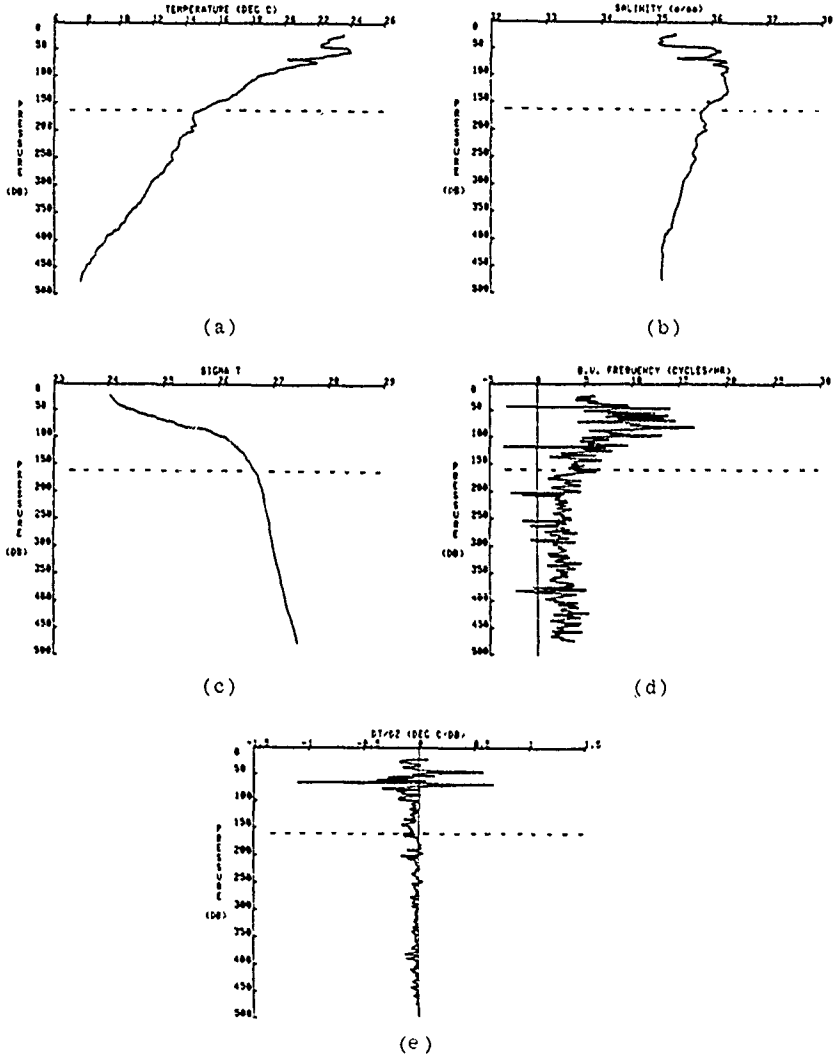

Figure A.7 As in Figure A.1 except for YVETTE station 10 occupied on 9 November 1975 at 38°09'N, 69°06'W (Gulf Stream). The dotted line is at 160 dbars.

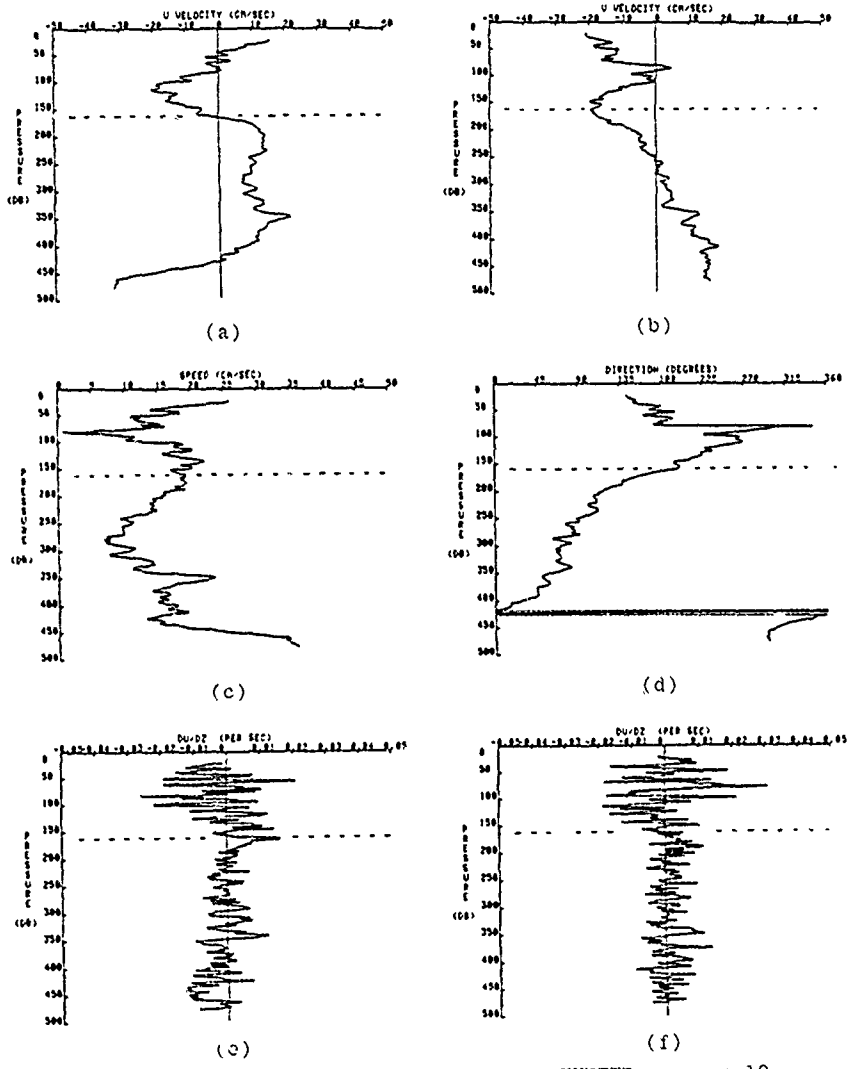

Figure A.8 As in Figure A.2 except for YVETTE station 10 in the Gulf Stream. The dotted line is at 160 dbars.

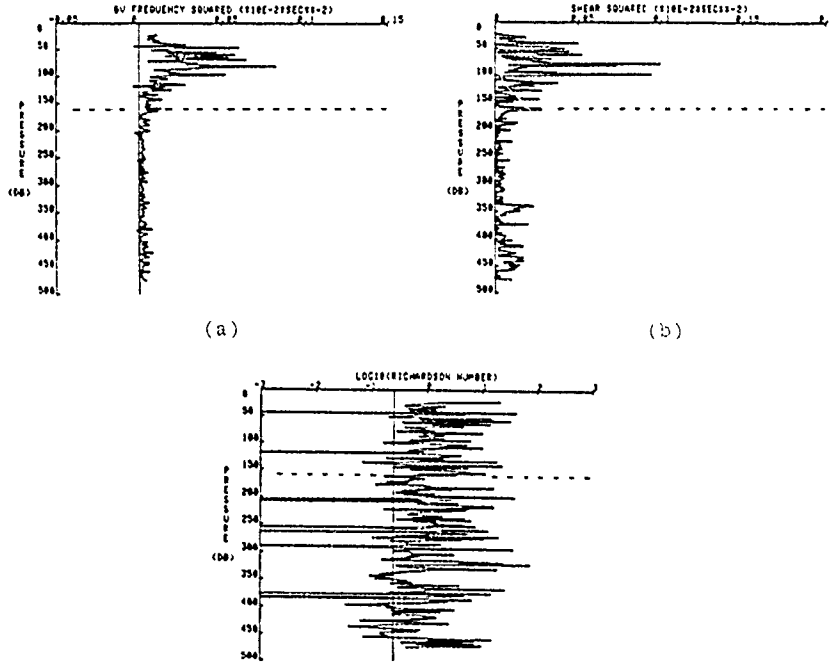

Figure A.9 As in Figure A.3 except for YVETTE station 10 in the Gulf Stream. The dotted line is at 160 dbars.

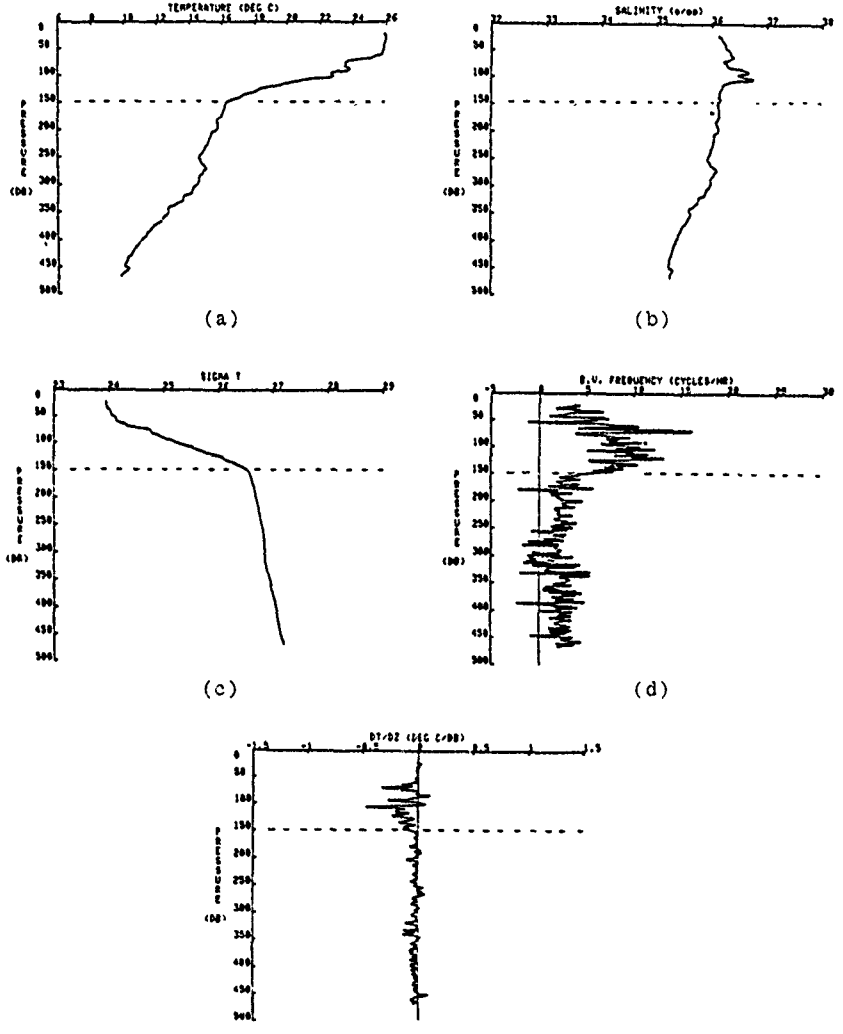

Figure A.10 As in Figure A.1 except for YVETTE station 11 occupied on 10 November 1975 at 38°05'N, 69°03'W (Gulf Stream). The dotted line is at 150 dbars.

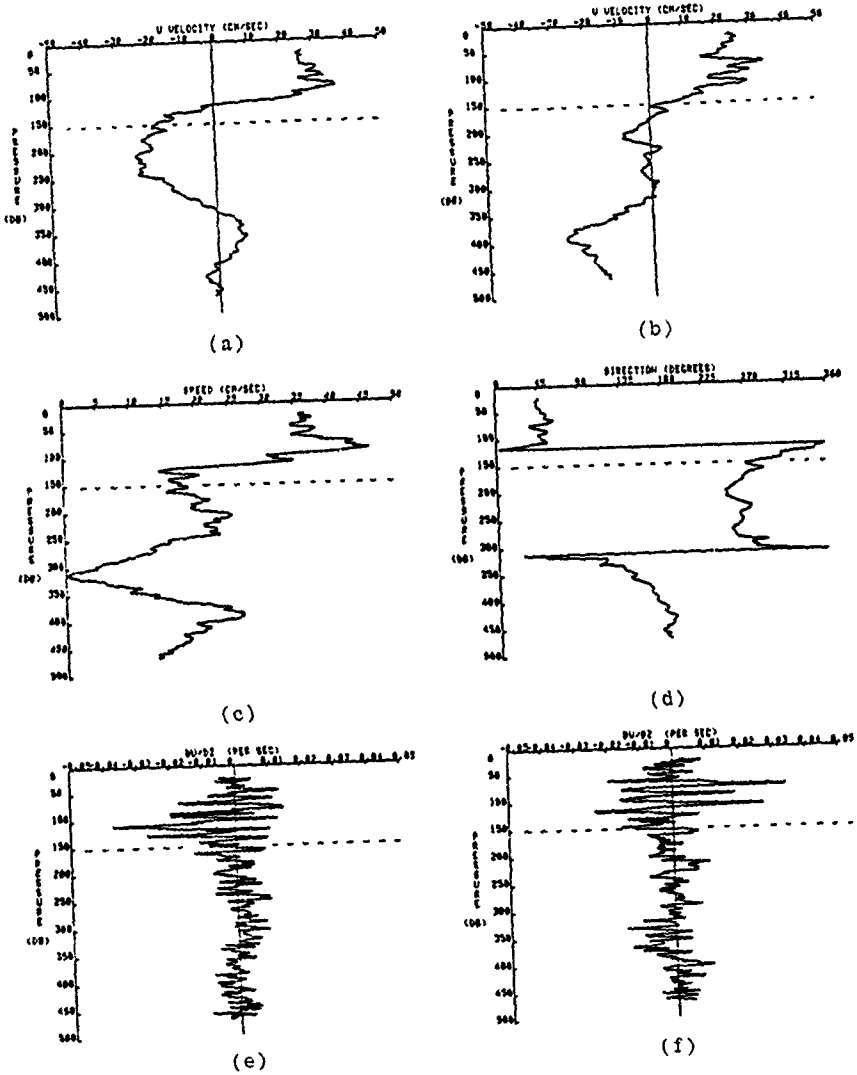

Figure A.11 As in Figure A.2 except for YVETTE station 11 in the Gulf Stream. The dotted line is at 150 dbars.

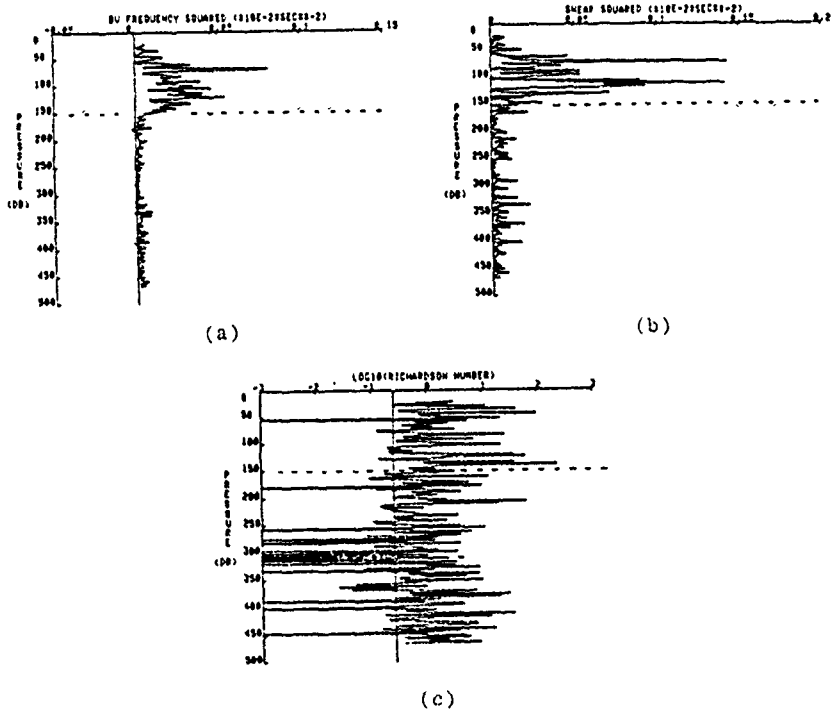

Figure A.12 As in Figure A.3 except for YVETTE station 11 in the Gulf Stream. The dotted line is at 150 dbars.

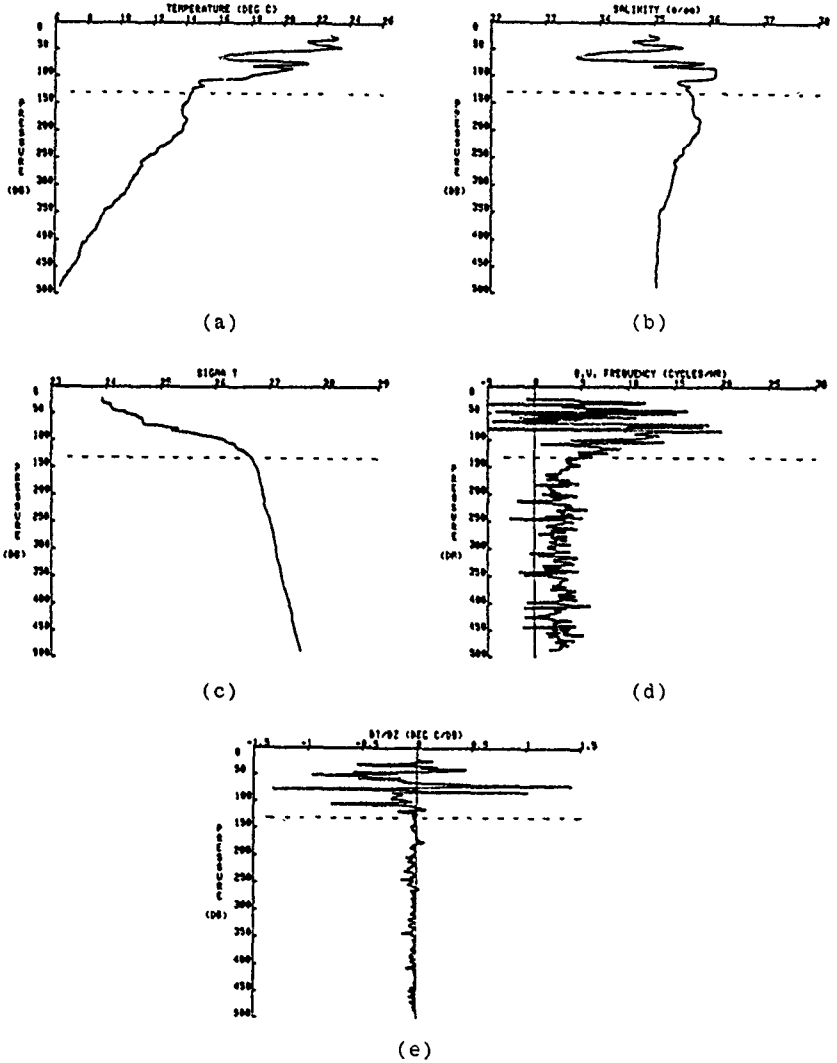

Figure A.13 As in Figure A.1 except for YVETTE station 12 occupied on 10 November 1975 at 35°15'N, 69°07'W (Gulf Stream). The dotted line is at 135 dbars.

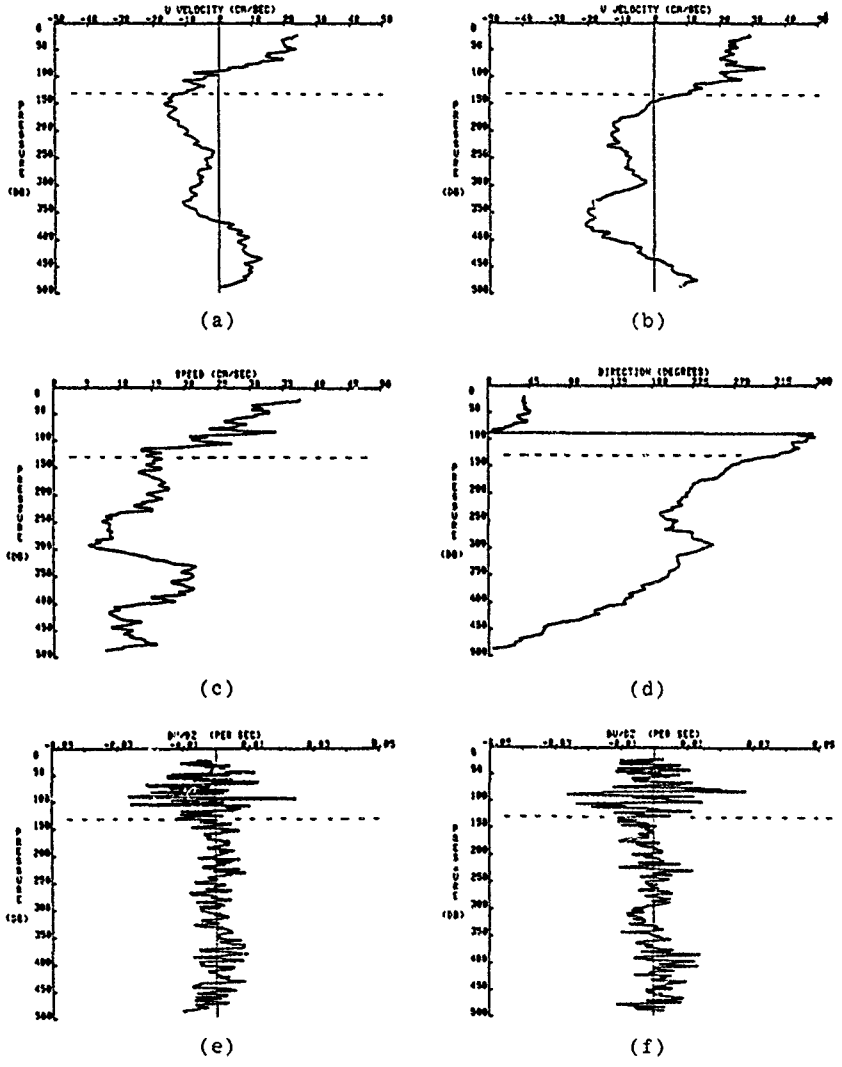

Figure A.14 As in Figure A.2 except for YVETTE station 12 in the Gulf Stream. The dotted line is at 135 dbars.

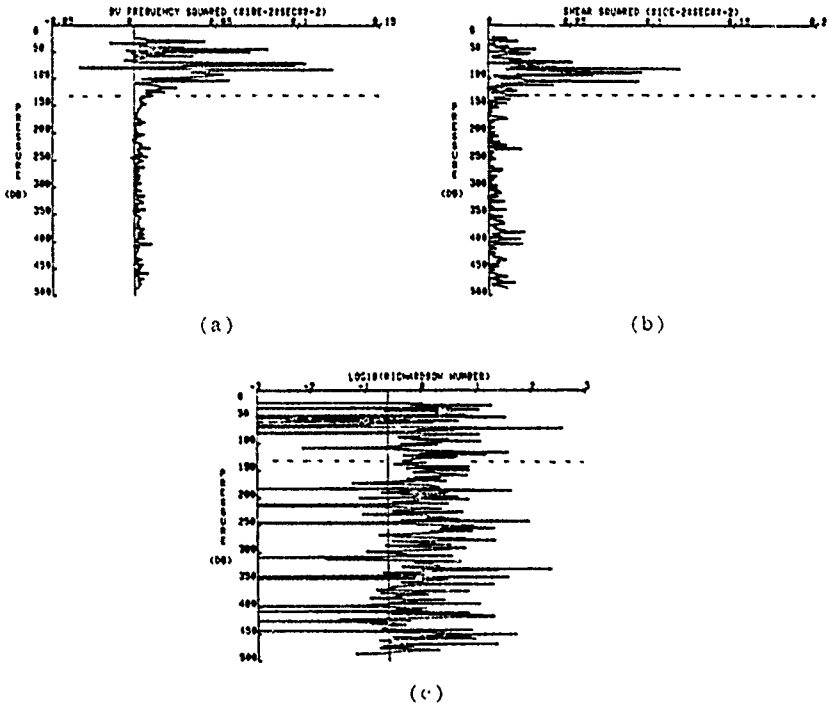

(a) (b)

(c)

Figure A.15 As in Figure A.3 except for YVETTE station 12 in the Gulf Stream. The dotted line is at 135 dbars.

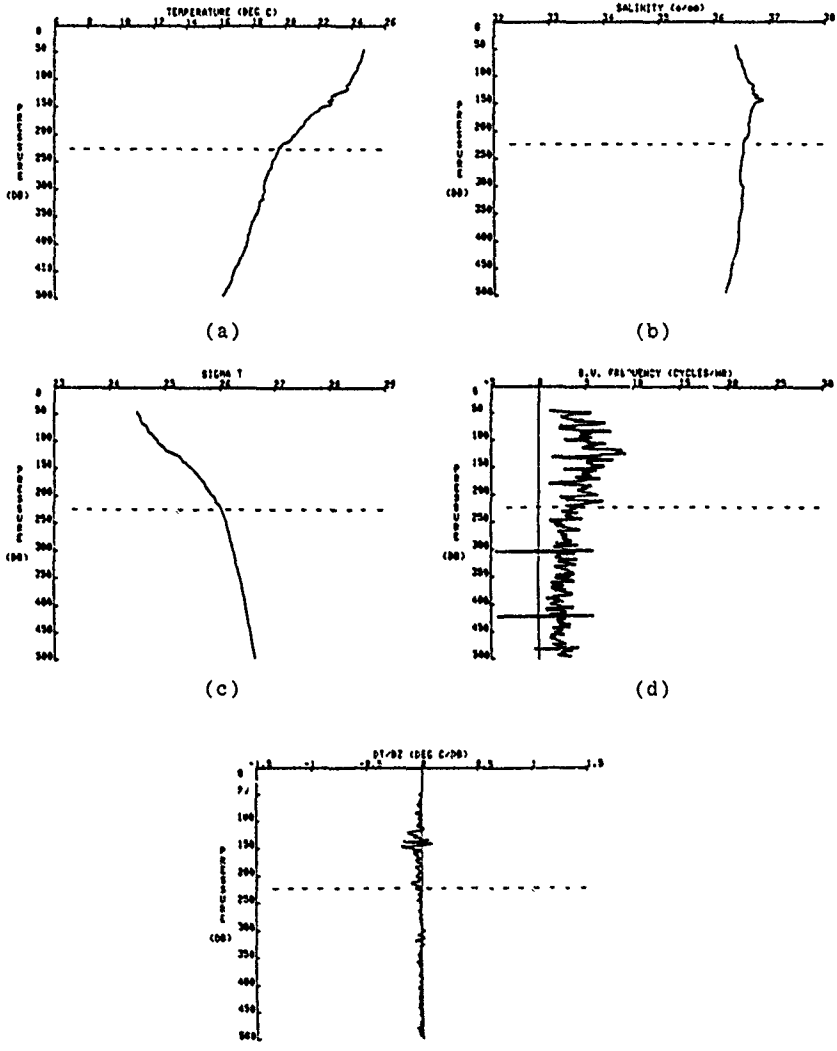

Figure A.16 As in Figure A.1 except for YVETTE station 18 occupied on 7 May 1977 at 22°47'N, 70°43'W (at the outer edge of a thermocline eddy near the Bahamas). The dotted line is at 225 dbars.

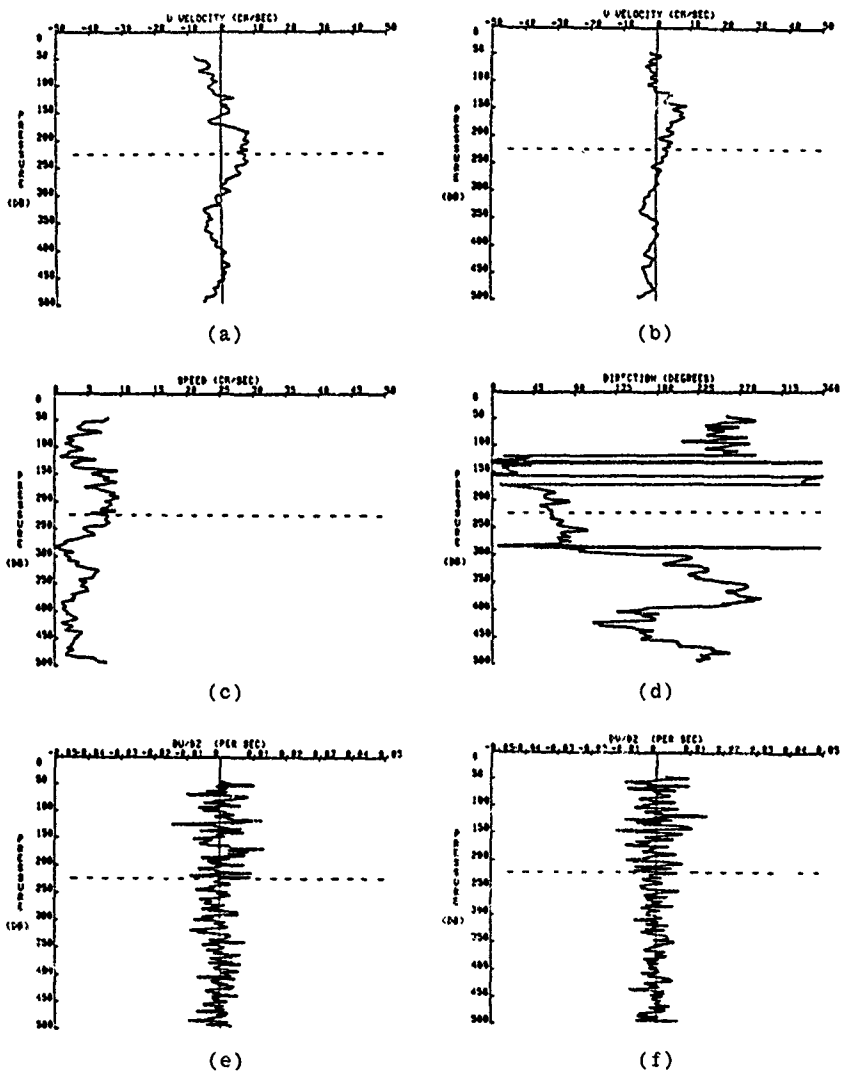

Figure A.17 As in Figure A.2 except for YVETTE station 18 near the Bahamas. The dotted line is at 225 dbars.

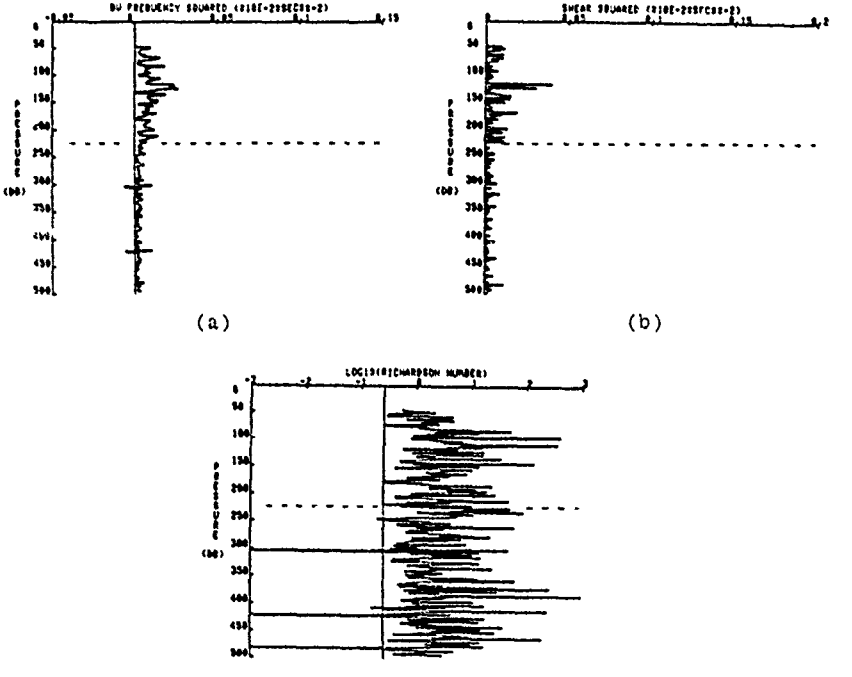

Figure A.18 As in Figure A.3 except for YVETTE station 18 near the Bahamas. The dotted line is at 225 dbars.

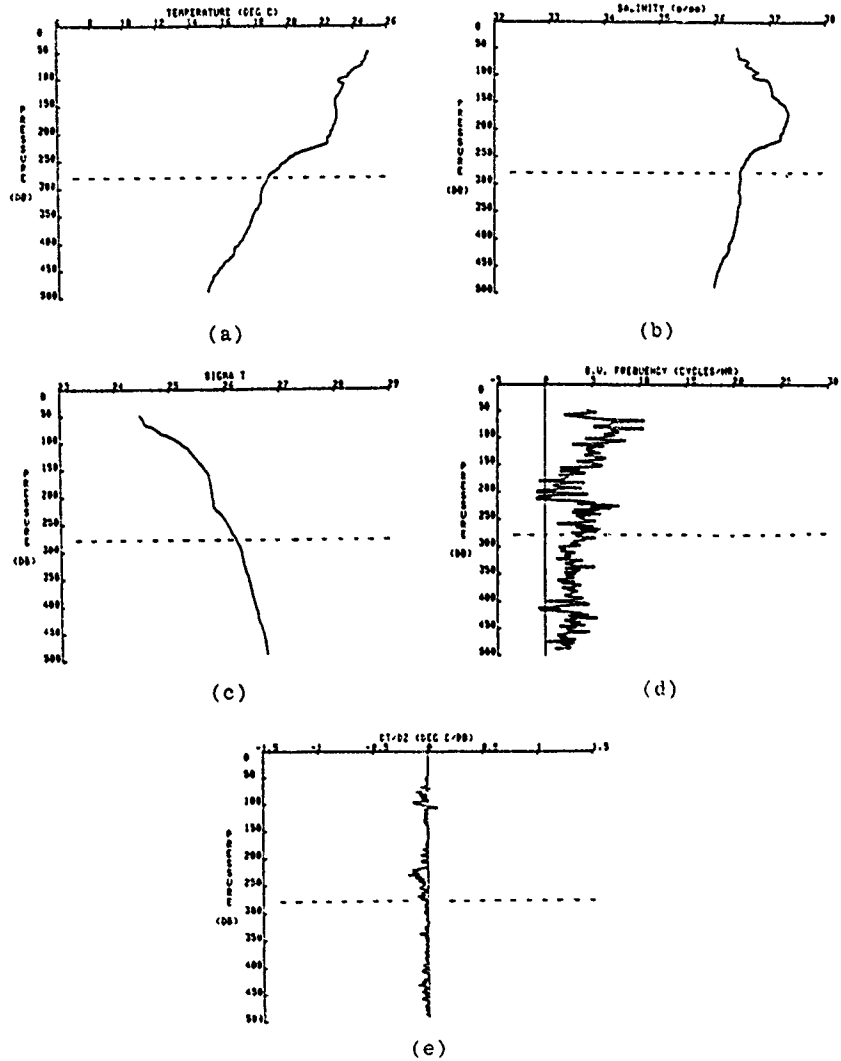

Figure A.19 As in Figure A.1 except for YVETTE station 21 occupied on 9 May 1977 at 22°27'N, 70°57'W (at center of thermocline eddy near the Bahamas). The dotted line is at 280 dbars.

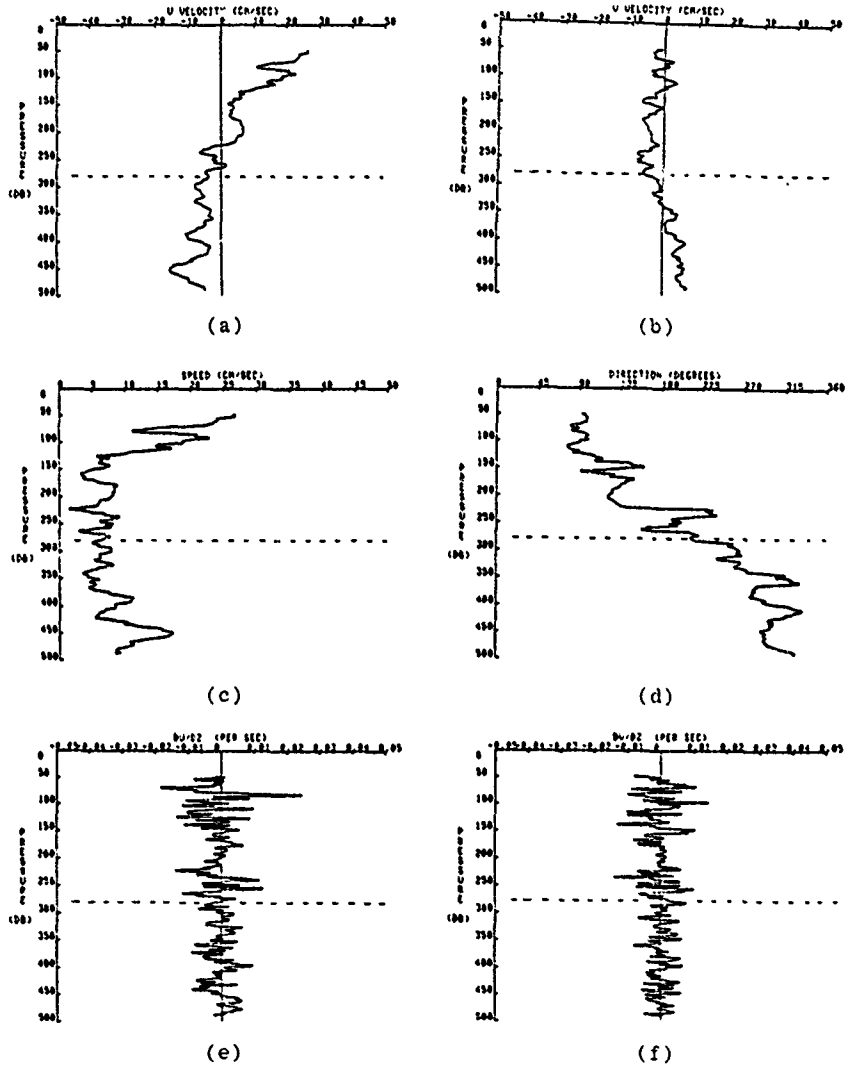

Figure A.20 As in Figure A.2 except for YVETTE station 21 near the Bahamas. The dotted line is at 280 dbars.

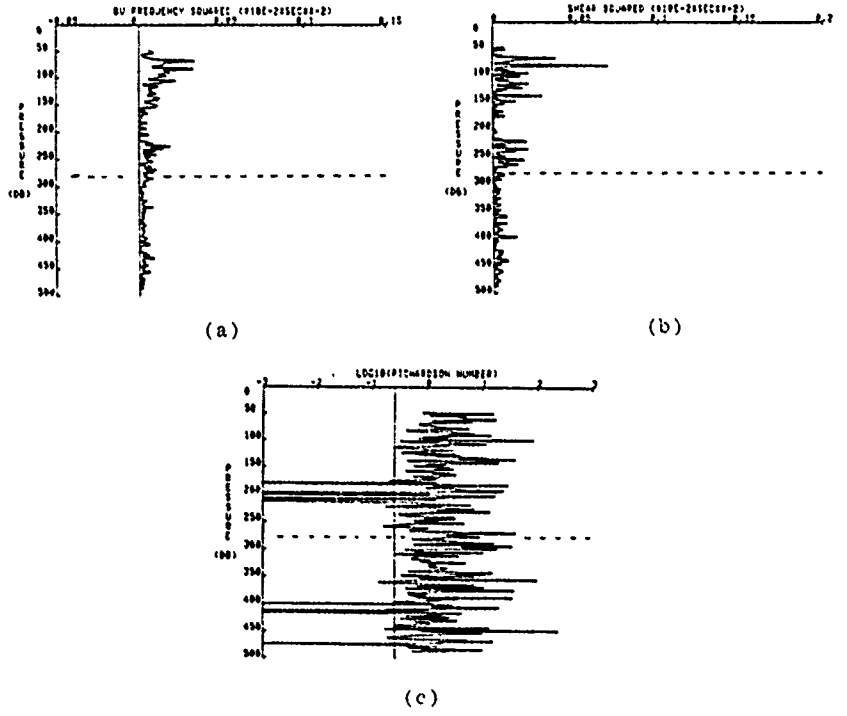

Figure A.21 As in Figure A.3 except for YVETTE station 21 near the Bahamas. The dotted line is at 280 dbars.

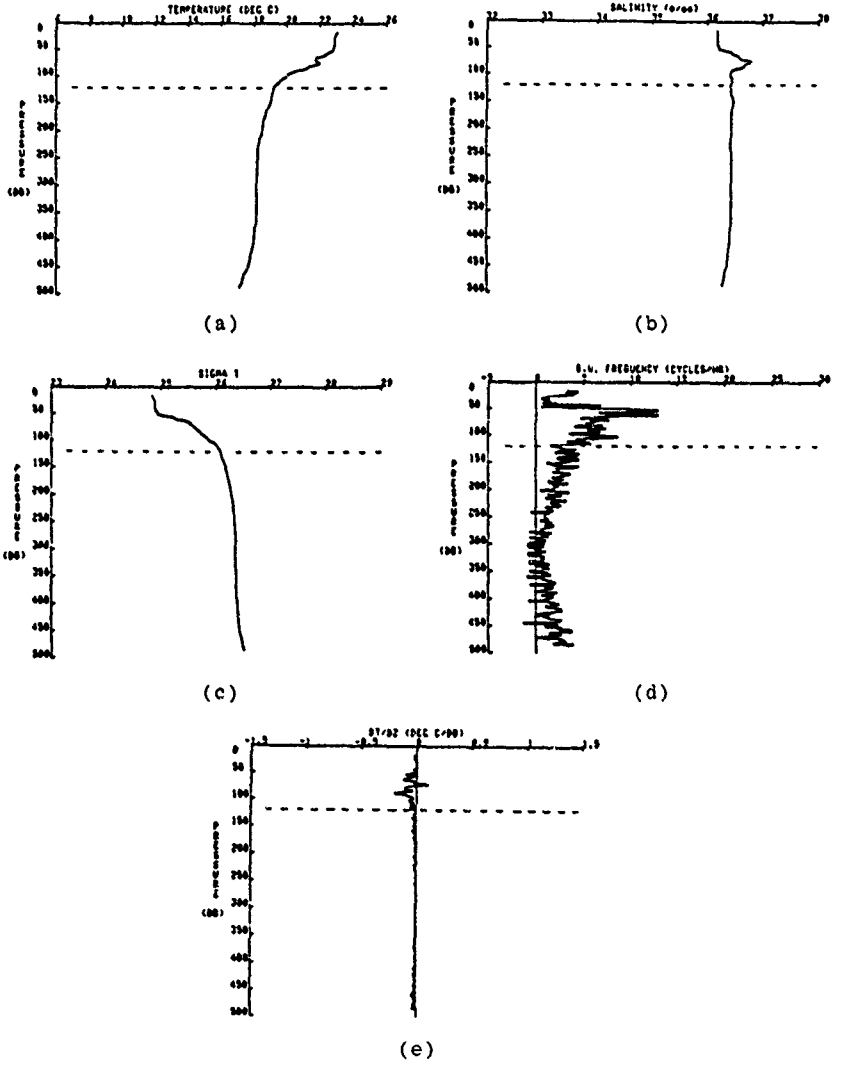

Figure A.22 As in Figure A.1 except for YVETTE station 23 occupied on 16 May 1977 at 36°24'N, 67°36'W (on the outer edge of a Gulf Stream ring). The dotted line is at 120 dbars.

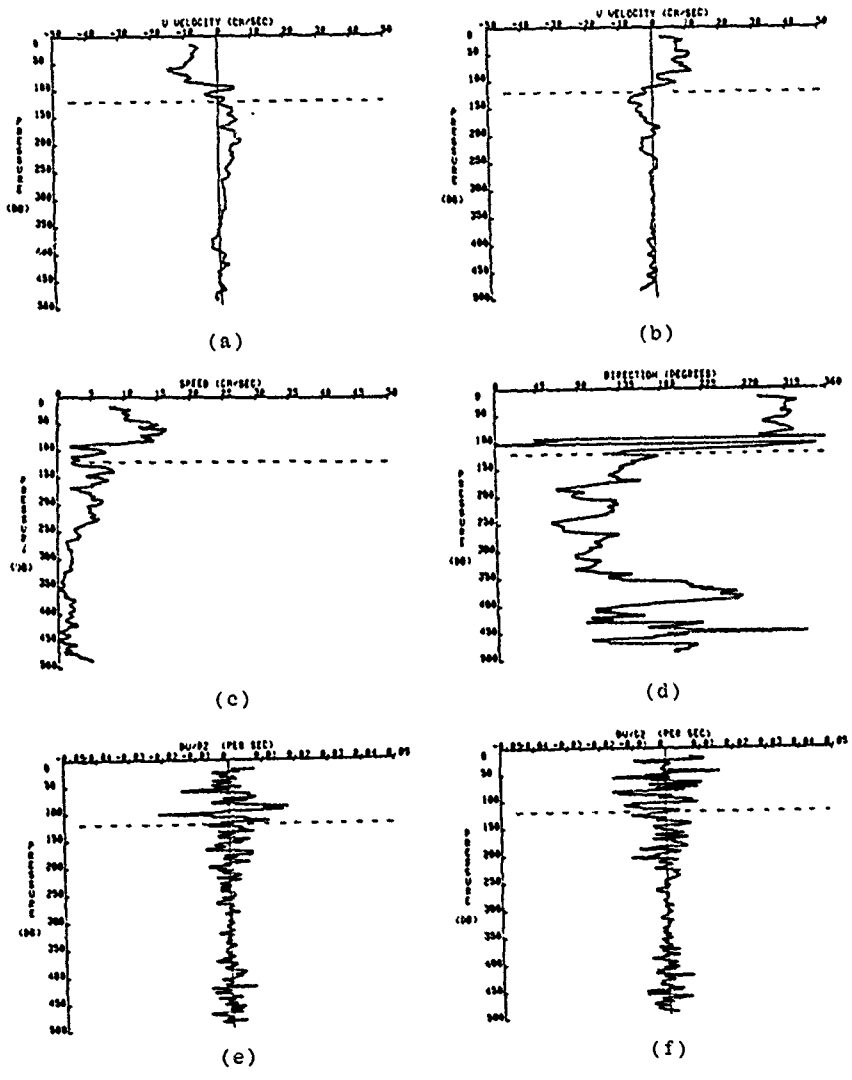

Figure A.23 As in Figure A.2 except for YVETTE station 23 on the outer edge of a Gulf Stream ring. The dotted line is at 120 dbars.

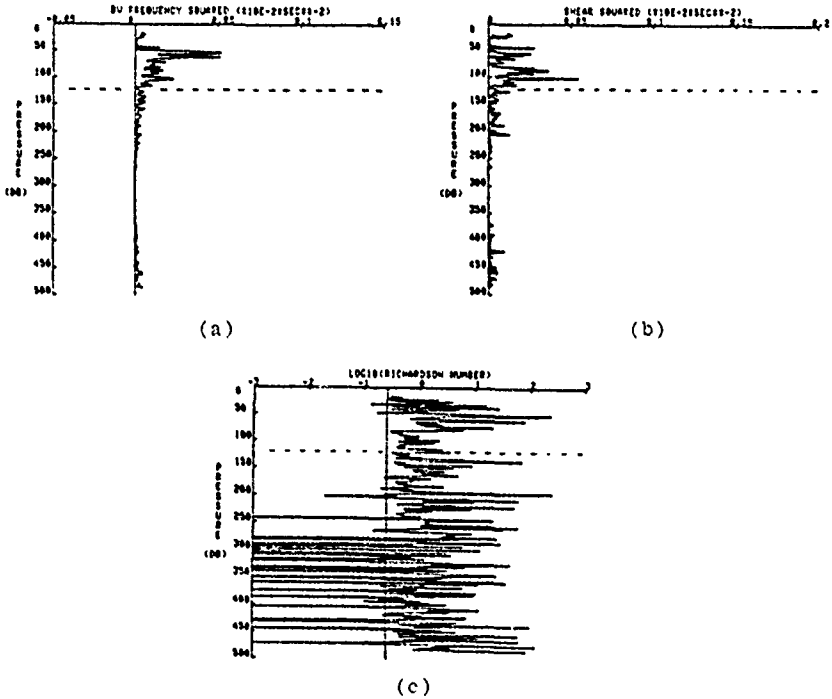

Figure A.24 As in Figure A.3 except for YVETTE station 23 at the outer edge of a Gulf Stream ring. The dotted line is at 120 dbars.

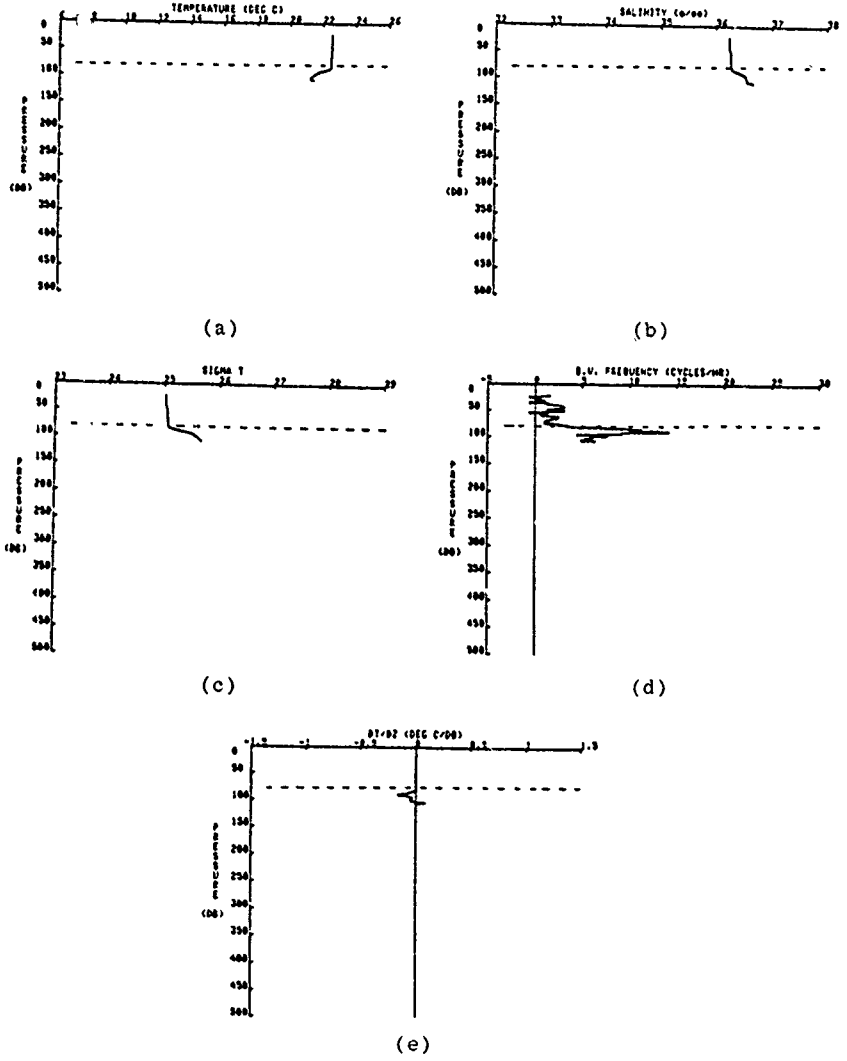

Figure A.25 As in Figure A.1 except for YVETTE station 24 occupied on 16 May 1977 at 36°20'N, 67°44'W (midway along radius of Gulf Stream ring). The dotted line is at 82 dbars.

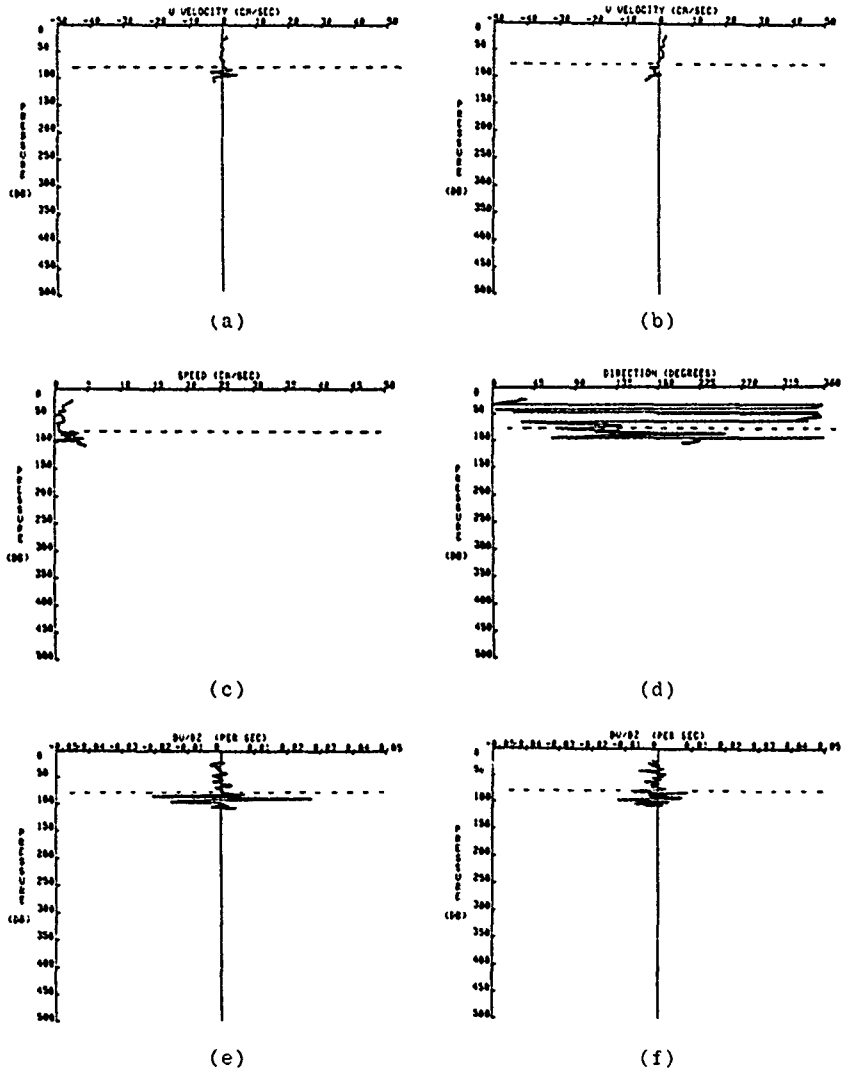

Figure A.26 As in Figure A 2 except for YVETTE station 24 midway along the radius of a Gulf Stream ring. The dotted line is at 82 dbars.

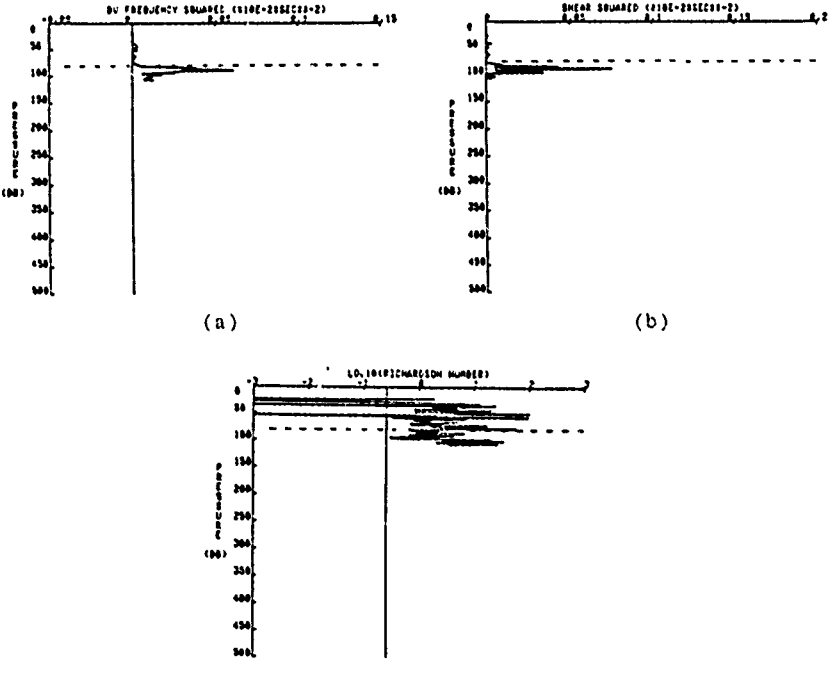

Figure A.27 As in Figure A.3 except for YVETTE station 24 midway along the radius of a Gulf Stream ring. The dotted line is at 82 dbars.

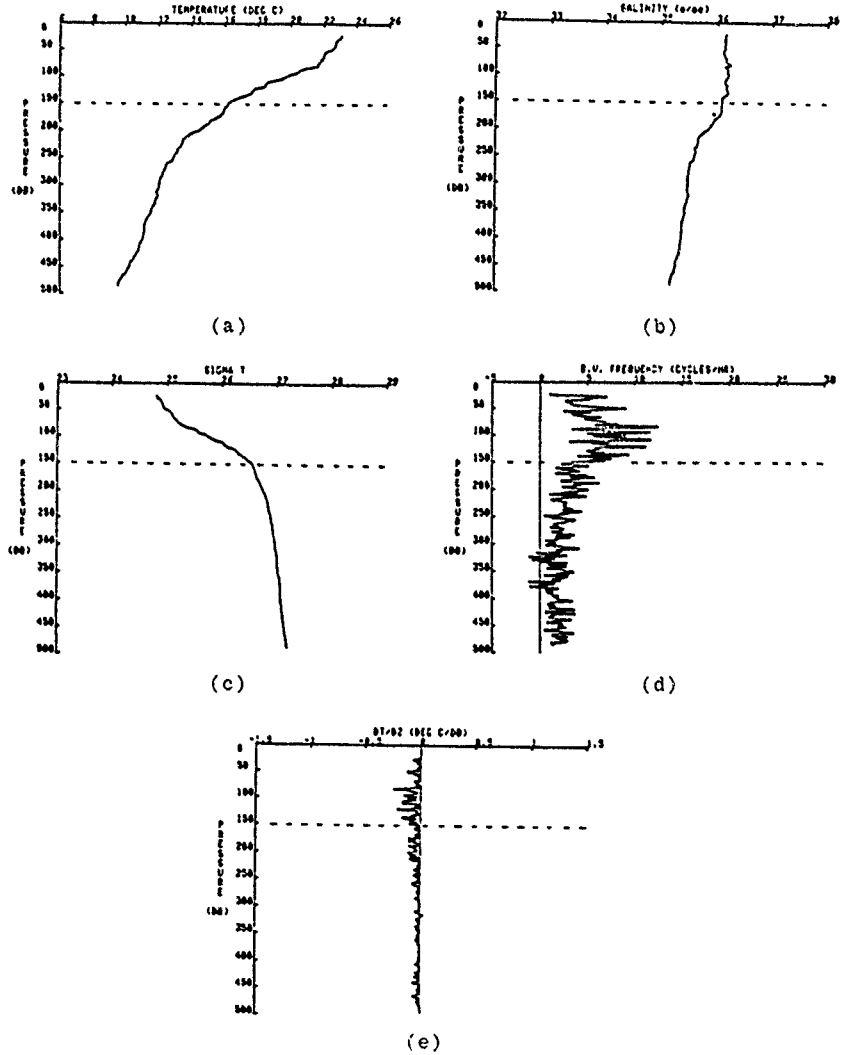

Figure A.28 As in Figure A.1 except for YVETTE station 25 occupied on 17 May 1977 at 36°09'N, 67°53'W (near the center of a Gulf Stream ring). The dotted line is at 150 dbars.

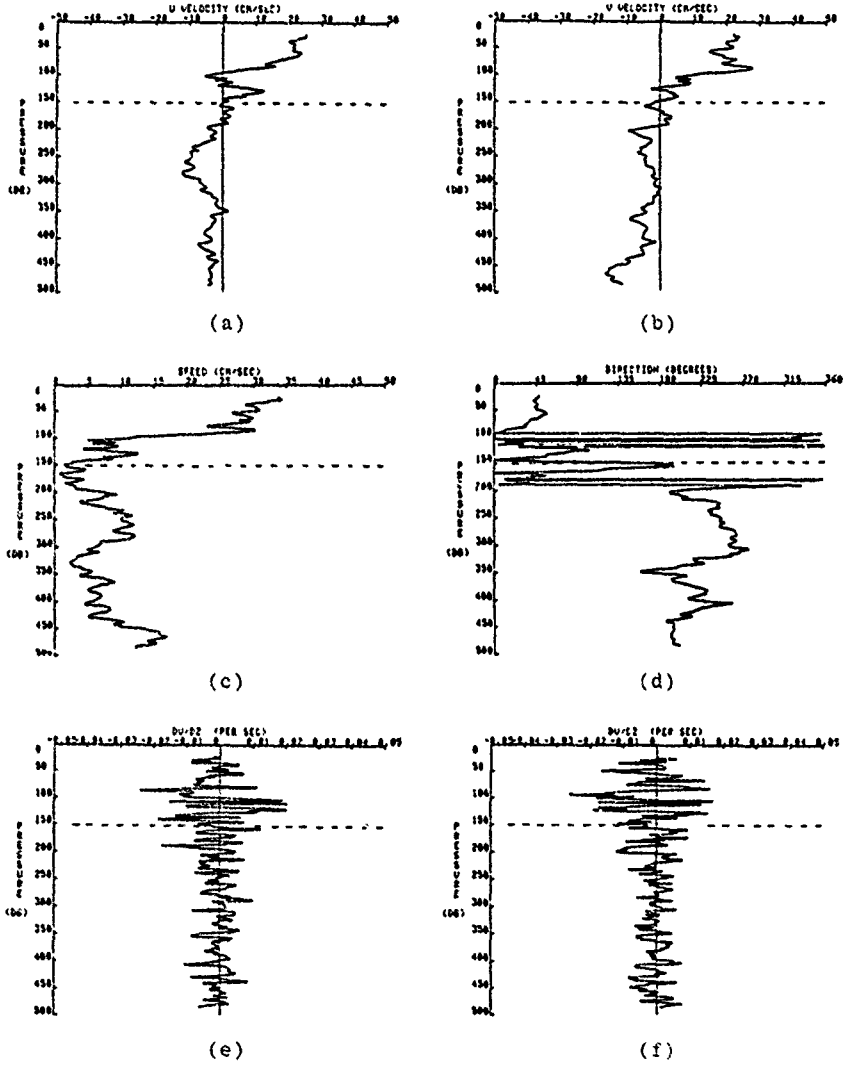

Figure A.29 As in Figure A.2 except for YVETTE station 25 near the center of a Gulf Stream ring. The dotted line is at 150 dbars.

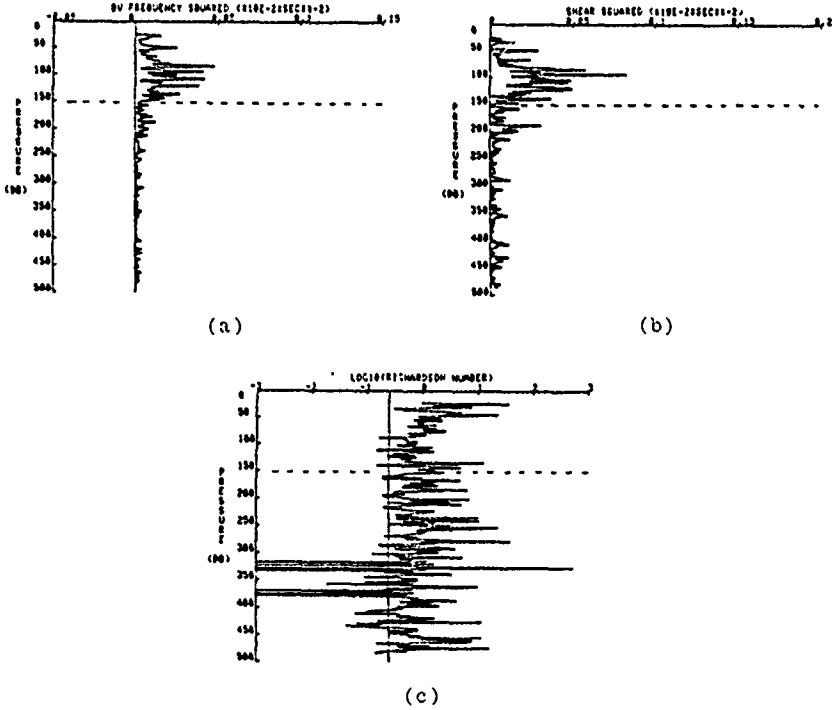

Figure A.30 As in Figure A.3 except for YVETTE station 25 near the center of a Gulf Stream ring. The dotted line is at 150 dbars.

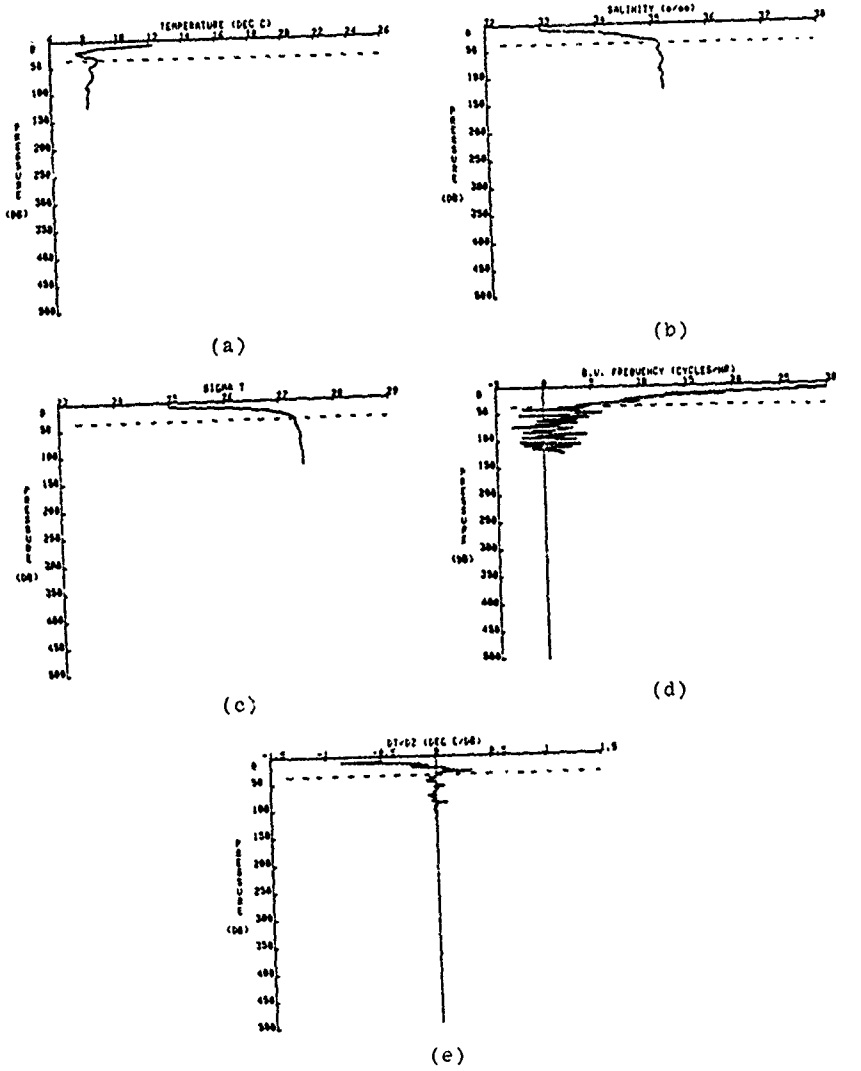

Figure A.31 As in Figure A.1 except for YVETTE station N1 occupied during 1973 in a Norwegian fjord. The dotted line is at 34 dbars.

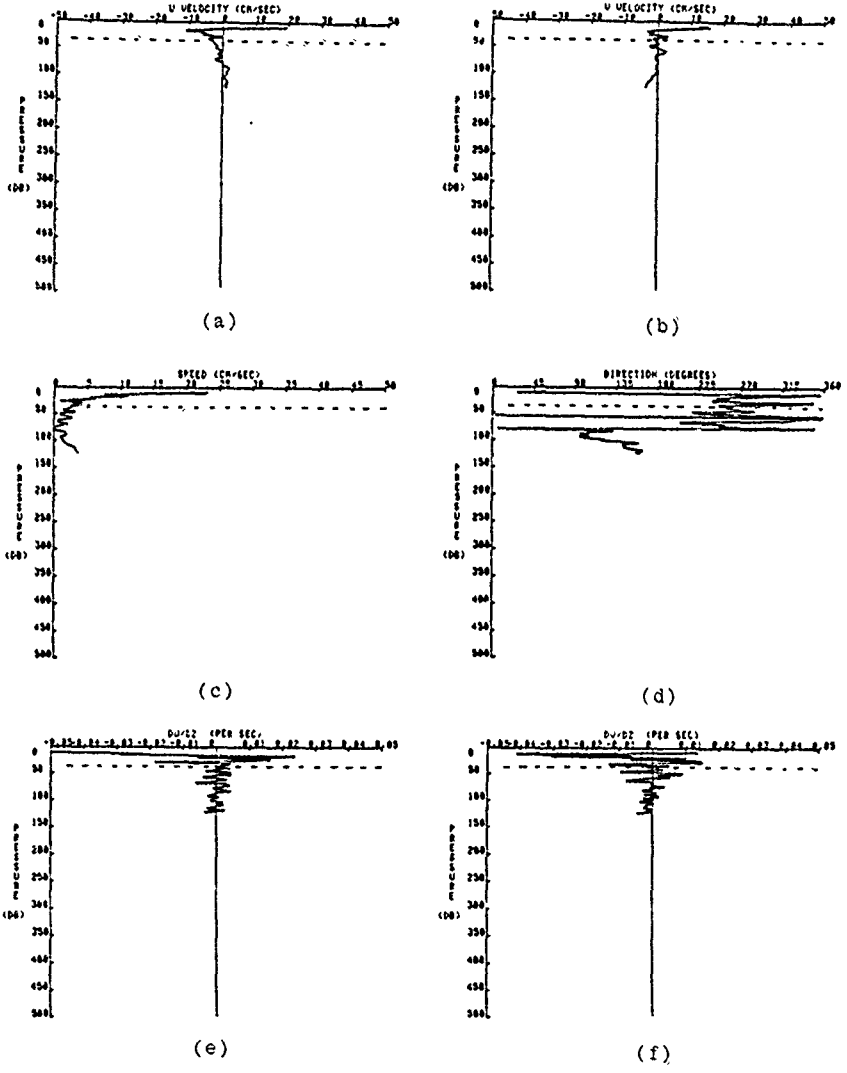

Figure A.32 As in Figure A.2 except for YVETTE station N1 in a Norwegian fjord. The dotted line is at 34 dbars.

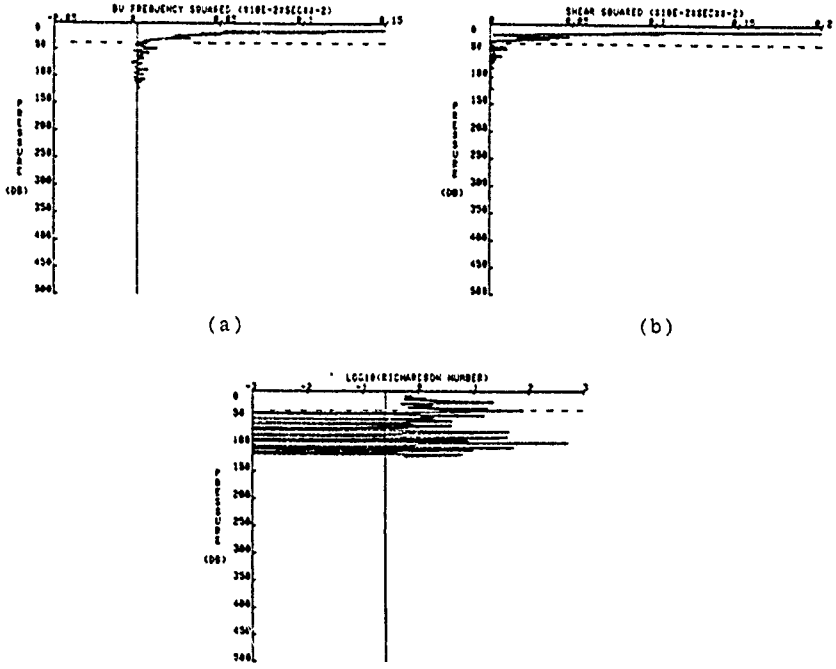

Figure A.33 As in Figure A.3 except for YVETTE station N1 in a Norwegian fjord. The dotted line is at 34 dbars.

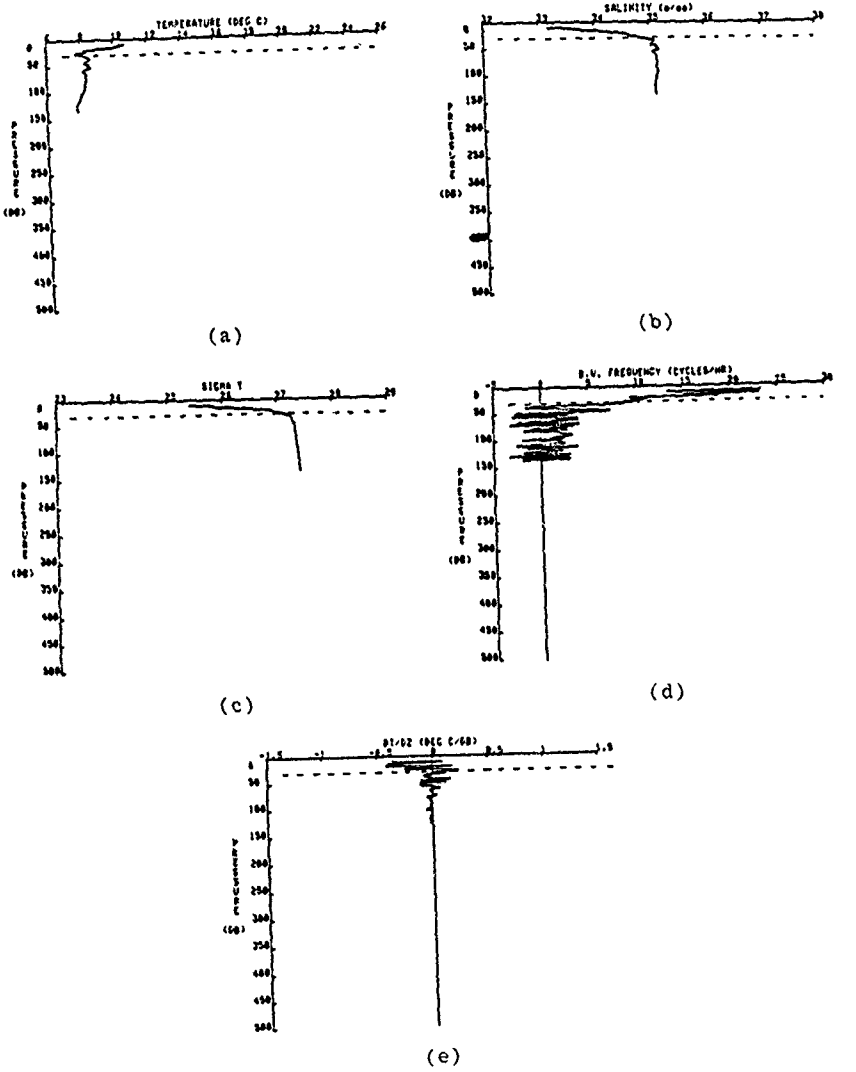

Figure A.34 As in Figure A.1 except for YVETTE station N4 occupied during 1973 in a Norwegian fjord. The dotted line is at 30 dbars.

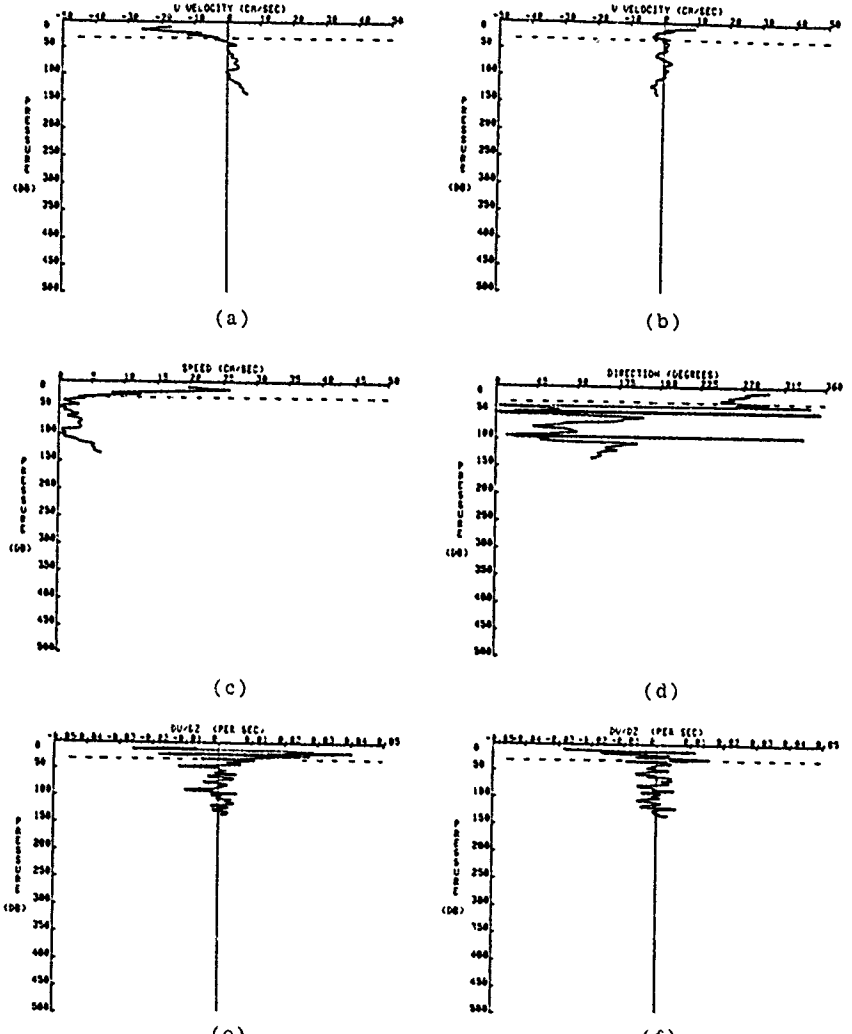

Figure A.35 As in Figure A.2 except for YVETTE station N4 in a Norwegian fjord. The dotted line is at 30 dbars.

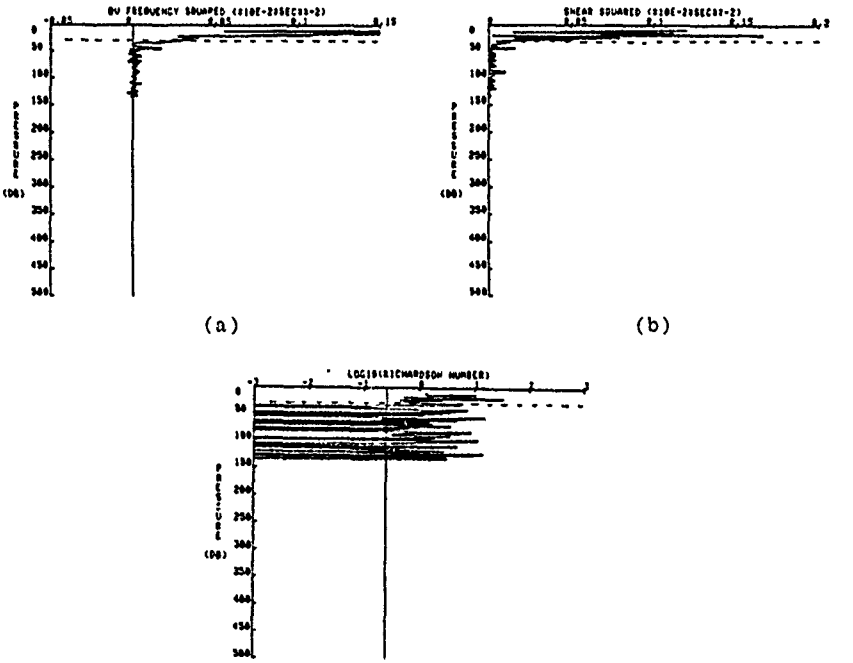

Figure A.36 As in Figure A.3 except for YVETTE station N4 in a Norwegian fjord. The dotted line is at 30 dbars.

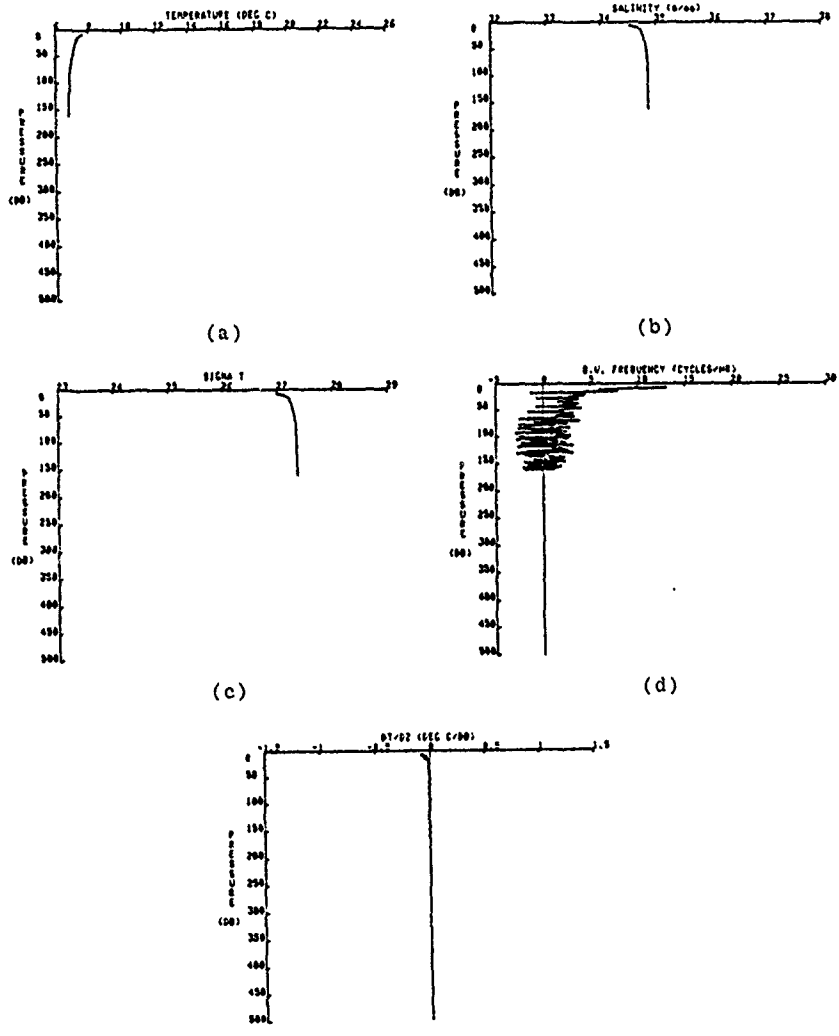

Figure A.37 As in Figure A.1 except for YVETTE station N6 occupied during 1973 in the Norwegian Coastal Current.

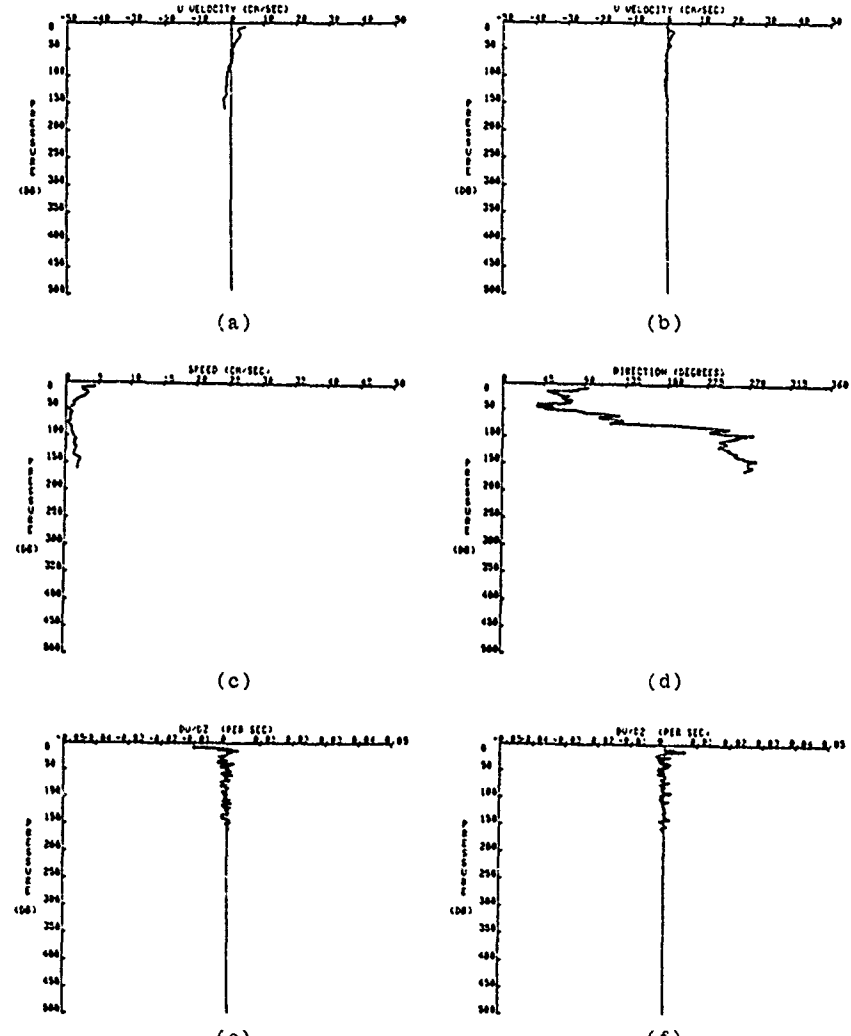

Figure A.38 As in Figure A.2 except for YVETTE station N6 in the Norwegian Coastal Current.

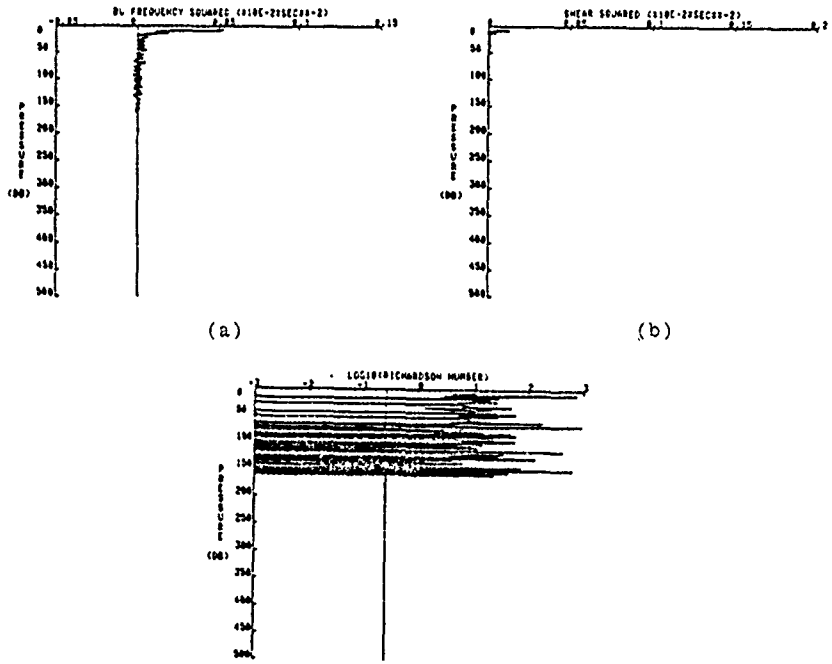

Figure A.39 As in Figure A.3 except for YVETTE station N6 in the Norwegian Coastal Current.

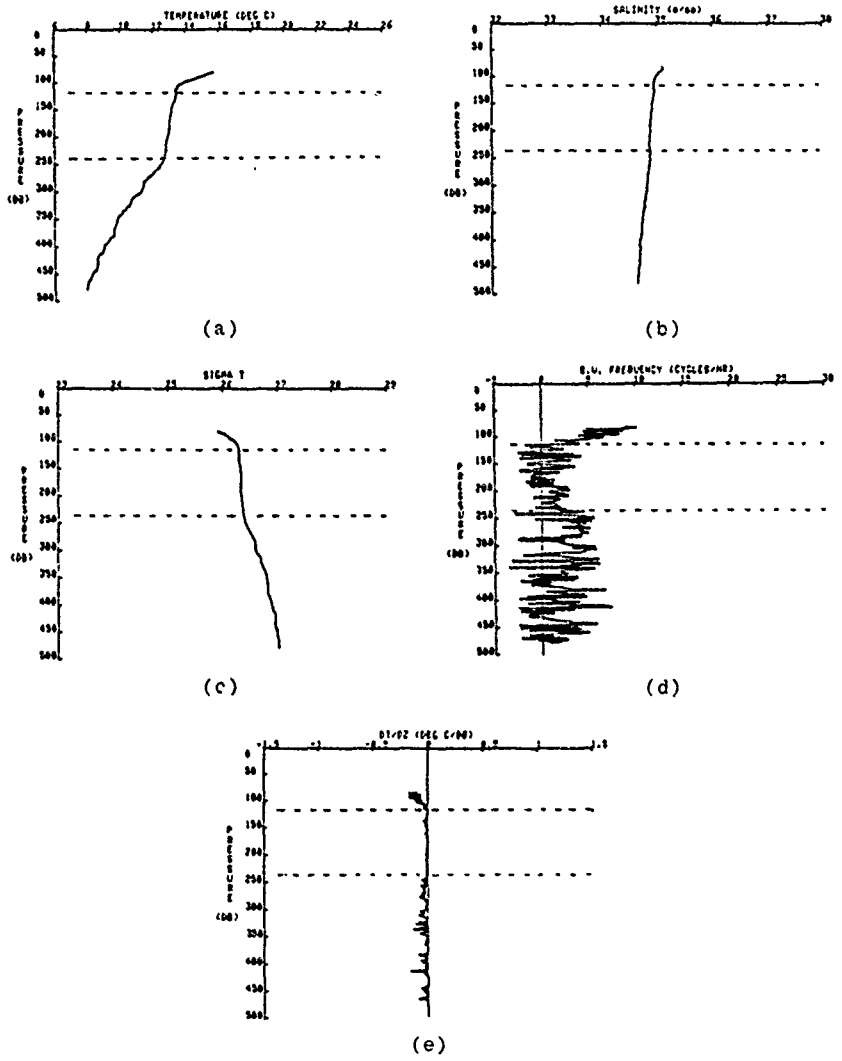

Figure A.40 As in Figure A.1 except for YVETTE station E6 occupied in July 1979 at 0°03'N, 109°57'W (equatorial Pacific). The dotted lines are at 115 and 240 dbars. In this case the upper regime is referred to as the near-surface thermocline (ST), the central regime is a subsurface pycnostad (P), and the lower regime is below the pycnostad (BP).

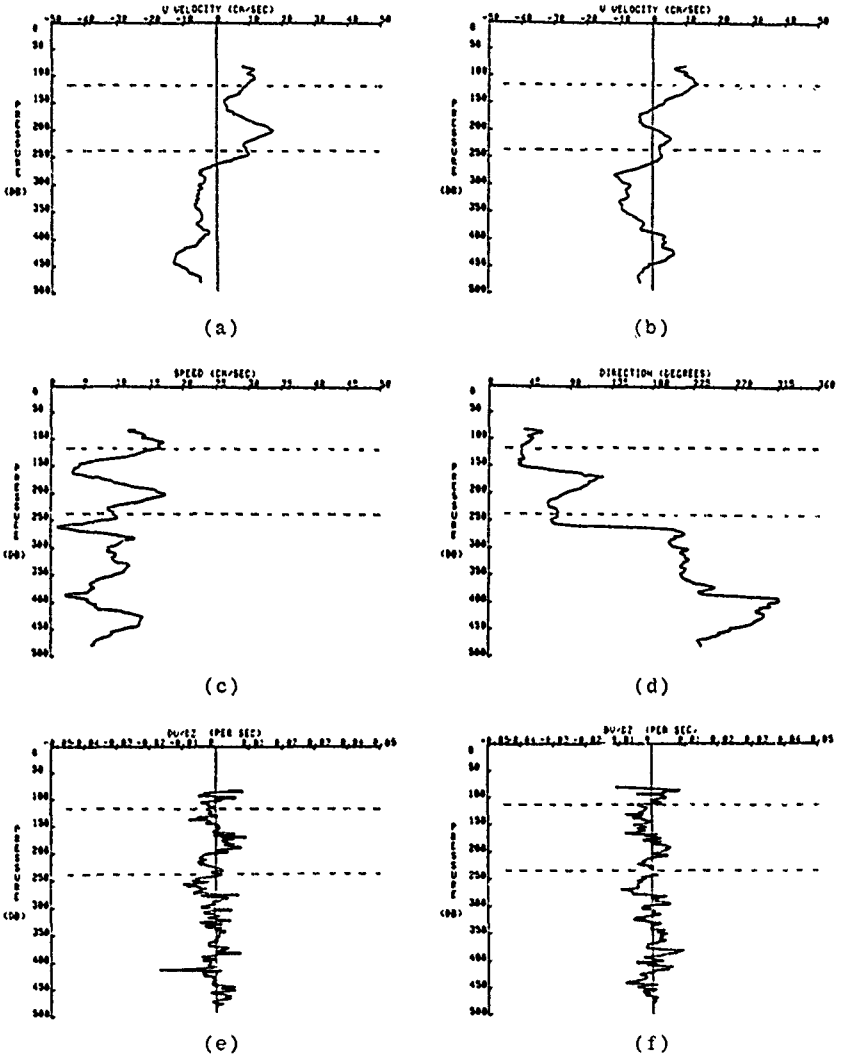

Figure A.41 As in Figure A.2 except for YVETTE station E6 in the equatorial Pacific. The dotted lines are at 115 and 240 dbars.

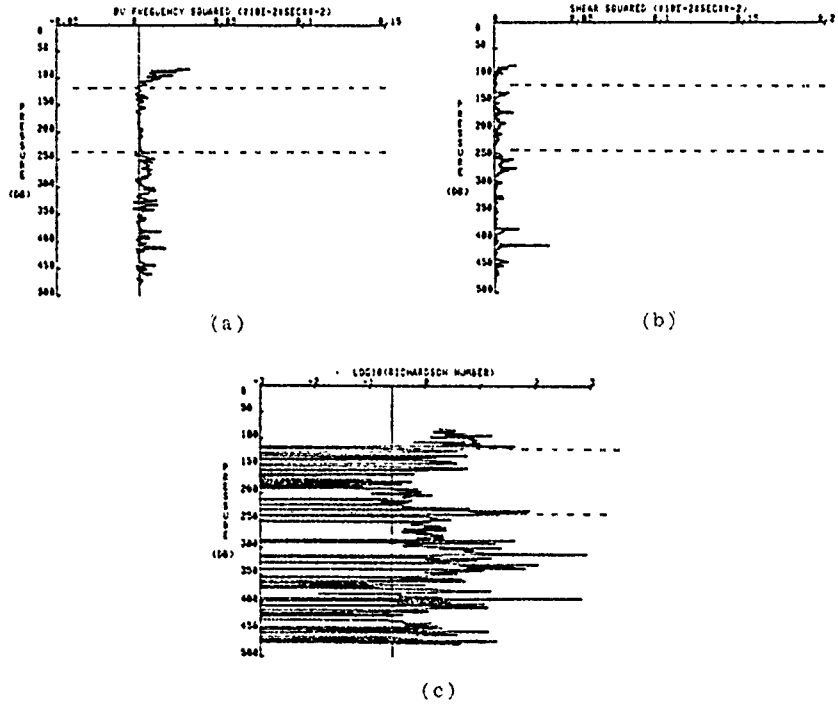

Figure A.42 As in Figure A.3 except for YVETTE station E6 in the equatorial Pacific. The dotted lines are at 115 and 240 dbars.

Appendix B
YVETTE HISTOGRAMS

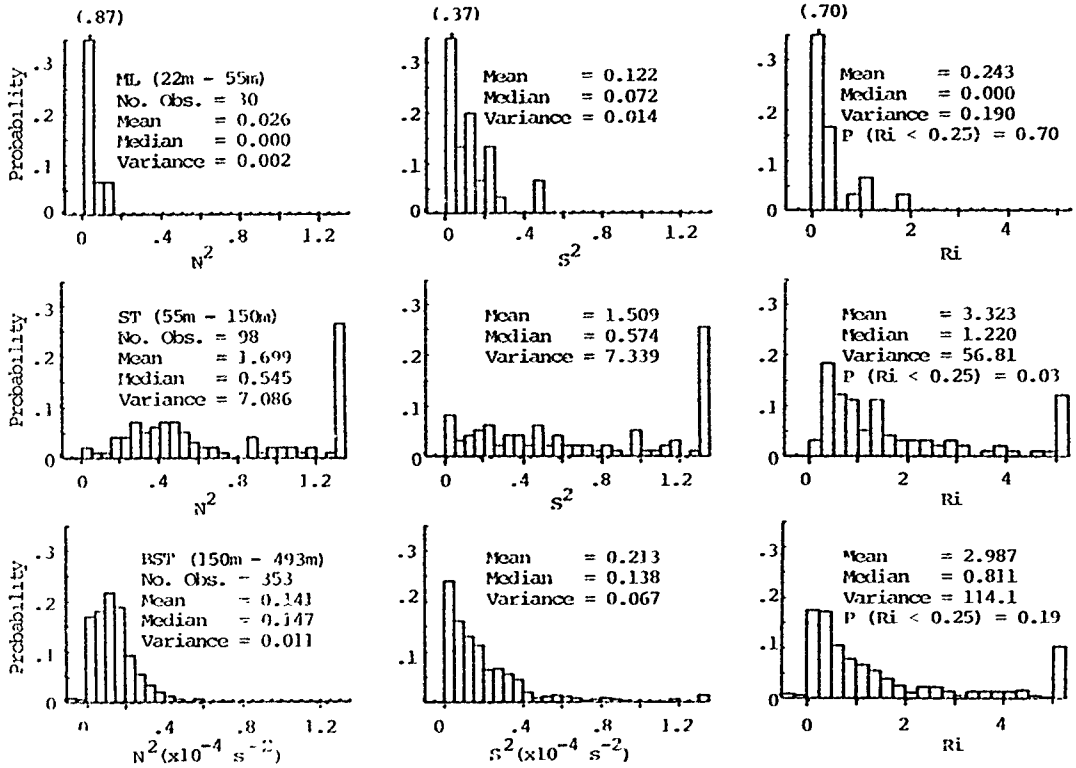

Figure B.1 Histograms of Brunt-Väisälä frequency squared (N^2), vertical shear squared (S^2), and Richardson number (Ri) for YVETTE station 5 near Bermuda. Gradients were computed using a vertical differencing interval of 2m. Histograms for the surface mixed layer (ML), the near-surface thermocline (ST), and the regime below the thermocline (BST) are displayed in the top, center, and bottom rows, respectively. (Cf. Figure A.3.)

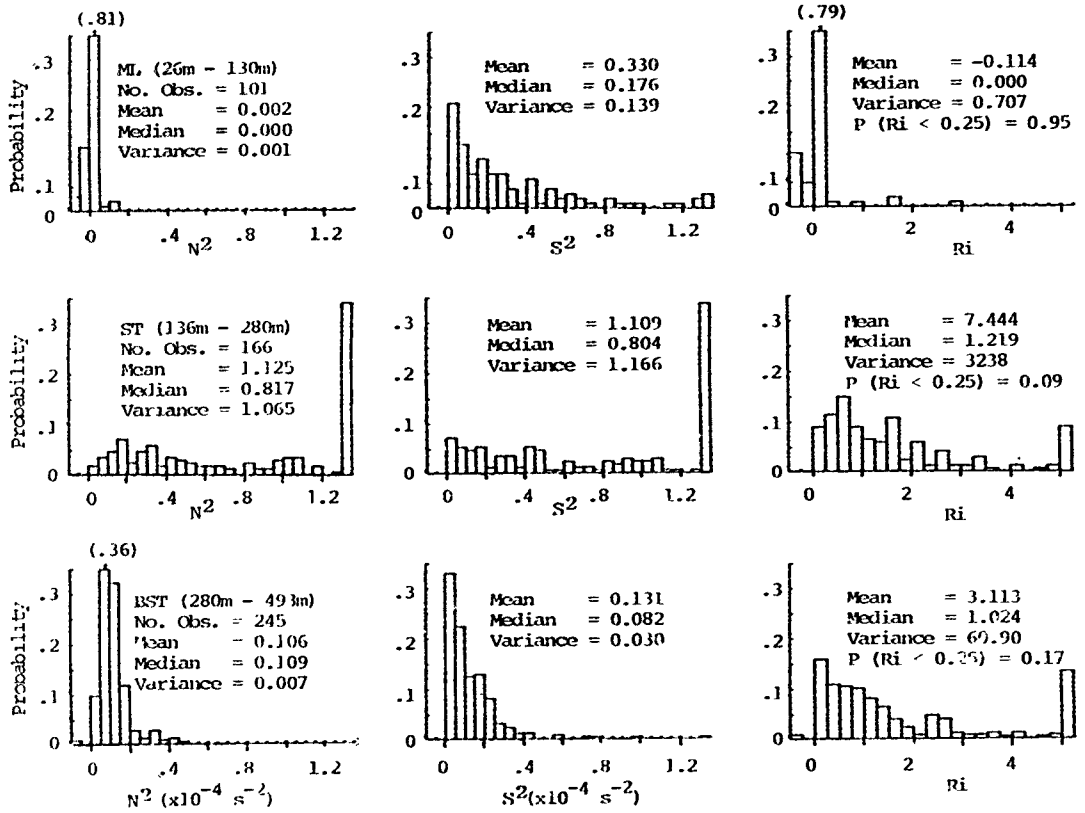

Figure B.2 As in Figure B.1 except for YVETTE Station 9 in the Sargasso Sea. (Cf. Figure A.6.)

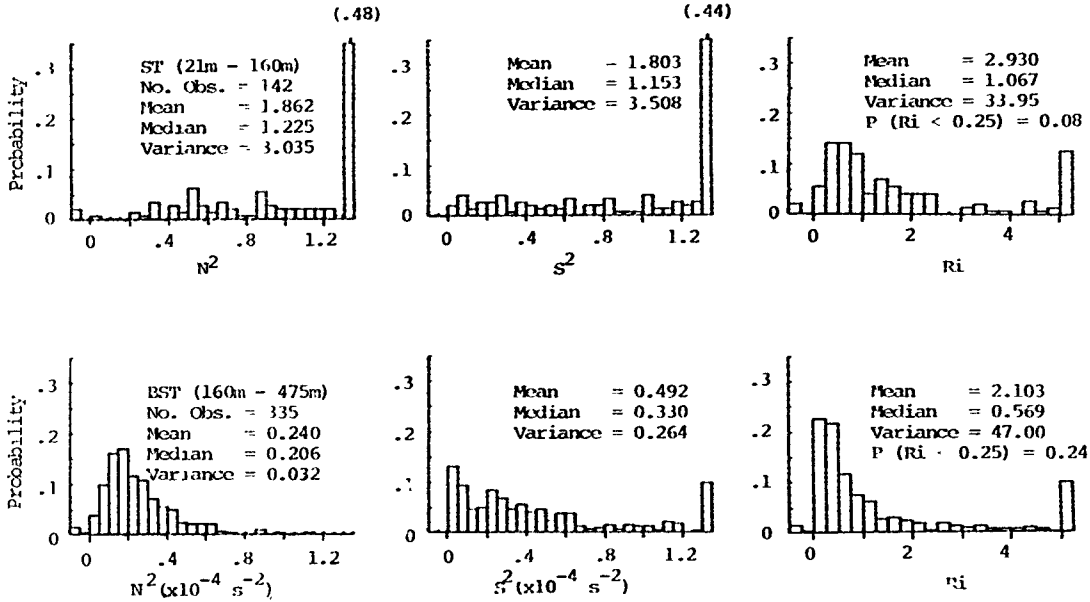

Figure B.3 Histograms of Brunt-Väisälä frequency squared (N^2), vertical shear squared (S^2), and Richardson number (Ri) for YVETTE station 10 in the Gulf Stream. Gradients were computed using a vertical differencing interval of 2m. Histograms from the near-surface thermocline (ST) and the regime below the thermocline (BST) are displayed in the top and bottom rows, respectively. (Cf. Figure A.9.)

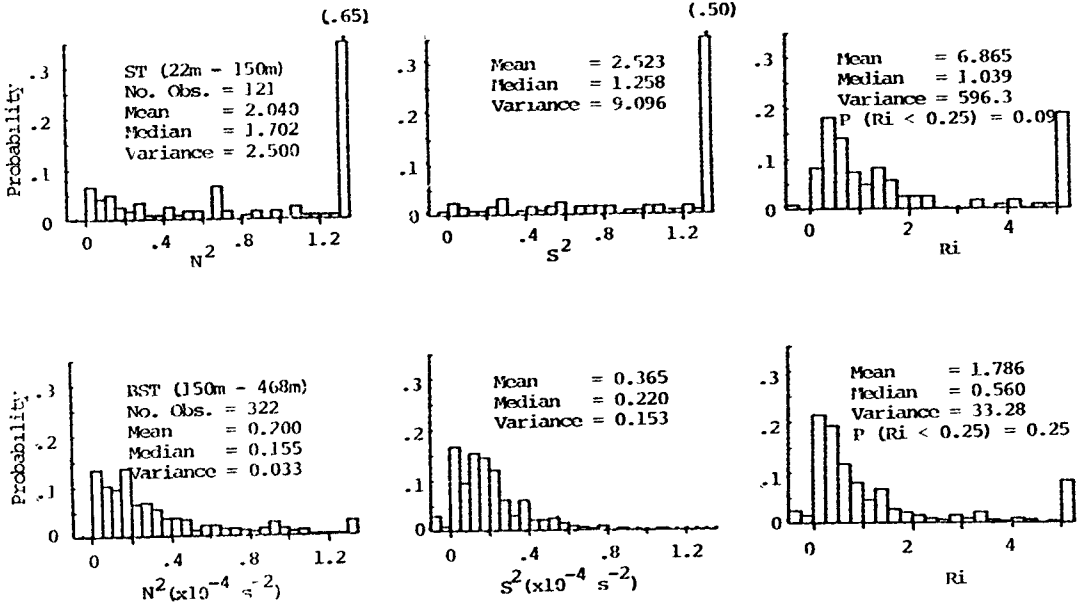

Figure B.4 As in Figure B.3 except for YVETTE Station 11 in the Gulf Stream. (Cf. Figure A.12.)

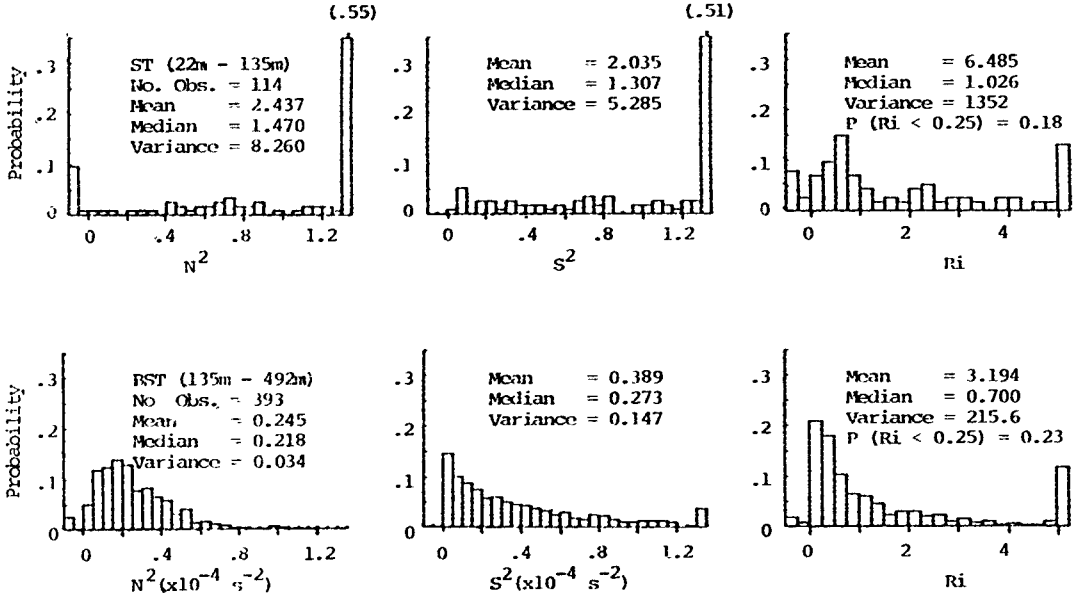

Figure B.5 As in Figure B.3 except for YVETTE station 12 in the Gulf Stream. (Cf. Figure A.15.)

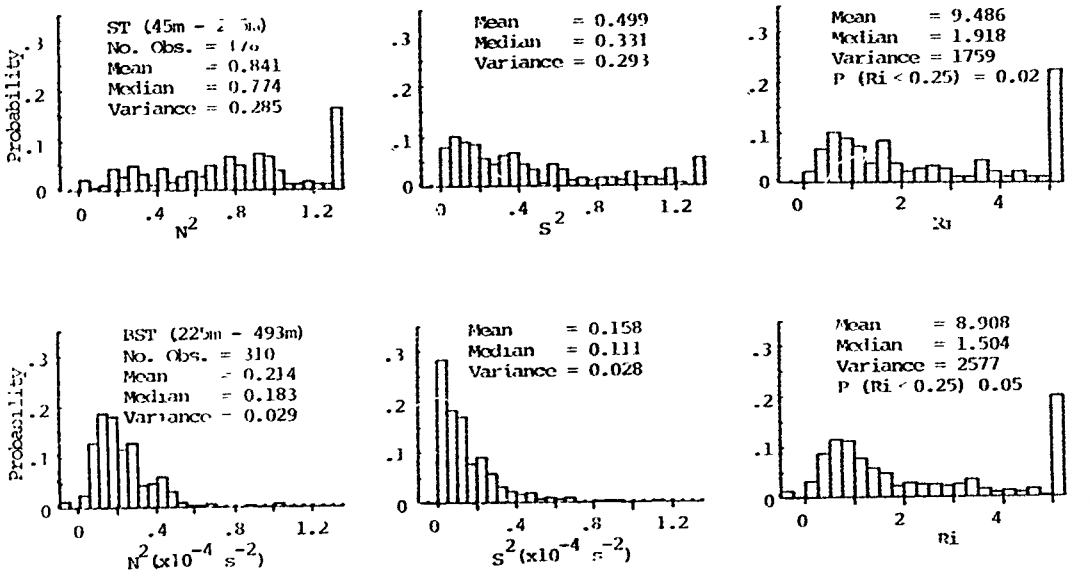

Figure B.6 As in Figure B.3 except for YVETTE station 18 near the Bahamas. (Cf. Figure A.18.)

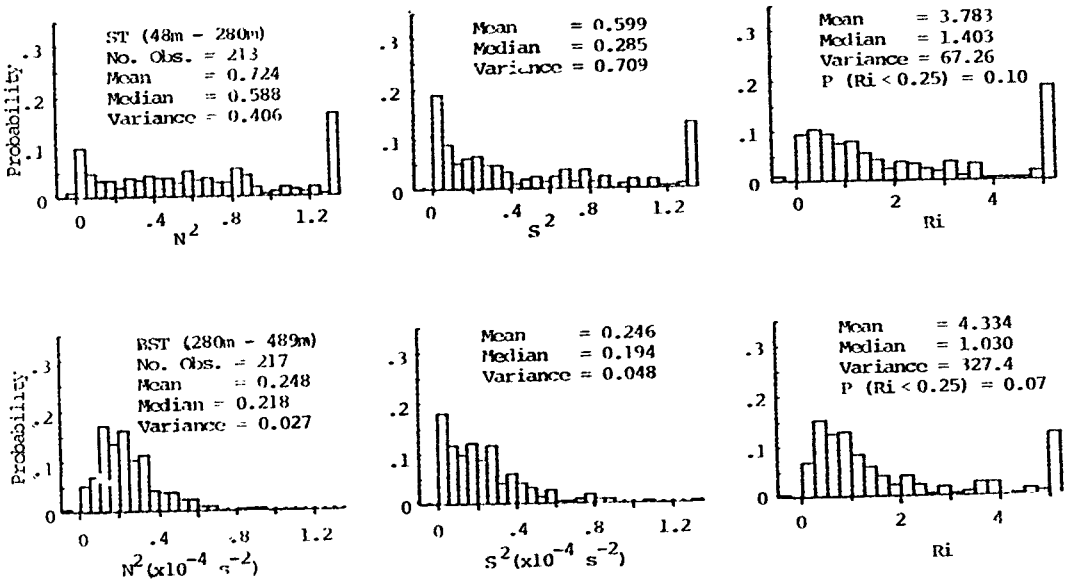

Figure B.7 As in Figure B.3 except for YVETTE Station 21 near the Bahamas. (Cf. Figure A.21.)

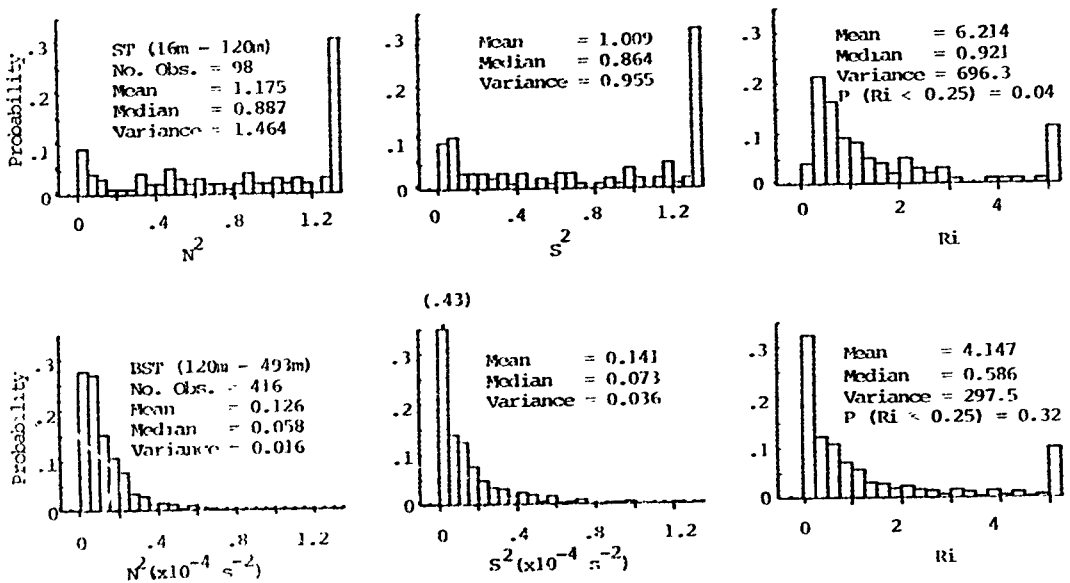

Figure B.8 As in Figure B.3 except for YVETTE station 23 at the outer edge of the Gulf Stream ring. (Cf. Figure A.24.)

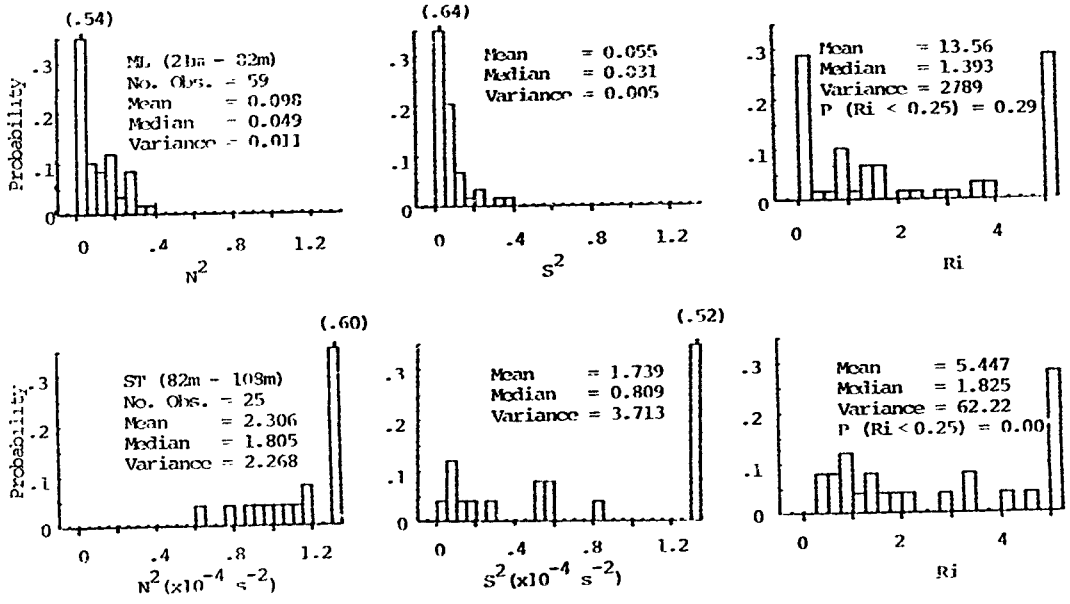

Figure B.9 As in Figure B.3 except for YVETTE station 24 midway along the radius of a Gulf Stream ring. (Cf. Figure A.27.)

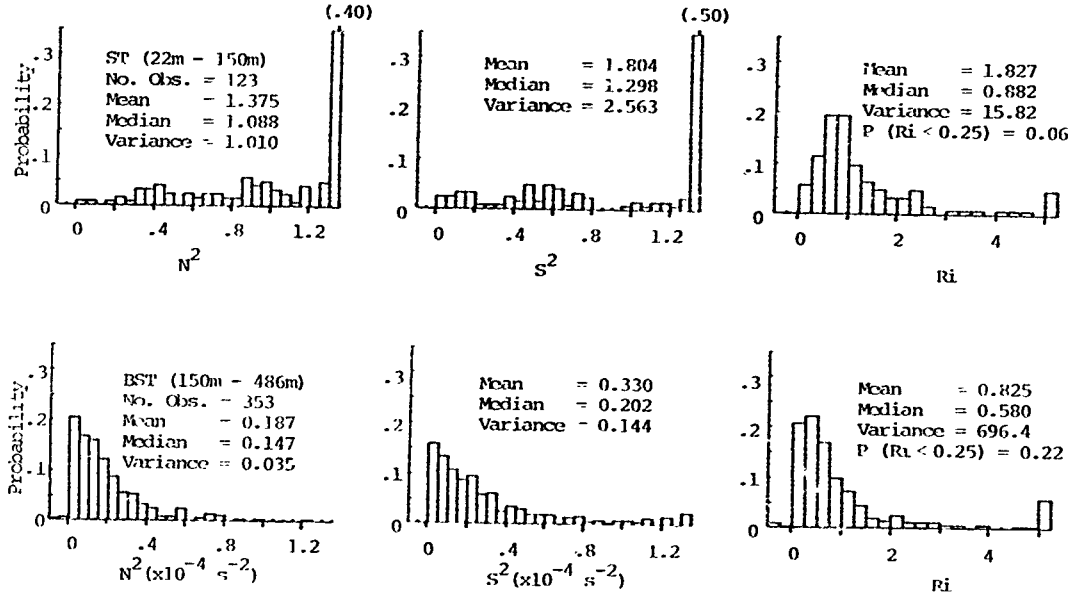

Figure B.10 As in Figure B.3 except for YVETTE station 25 near the center of the Gulf Stream ring. (Cf. Figure A.30.)

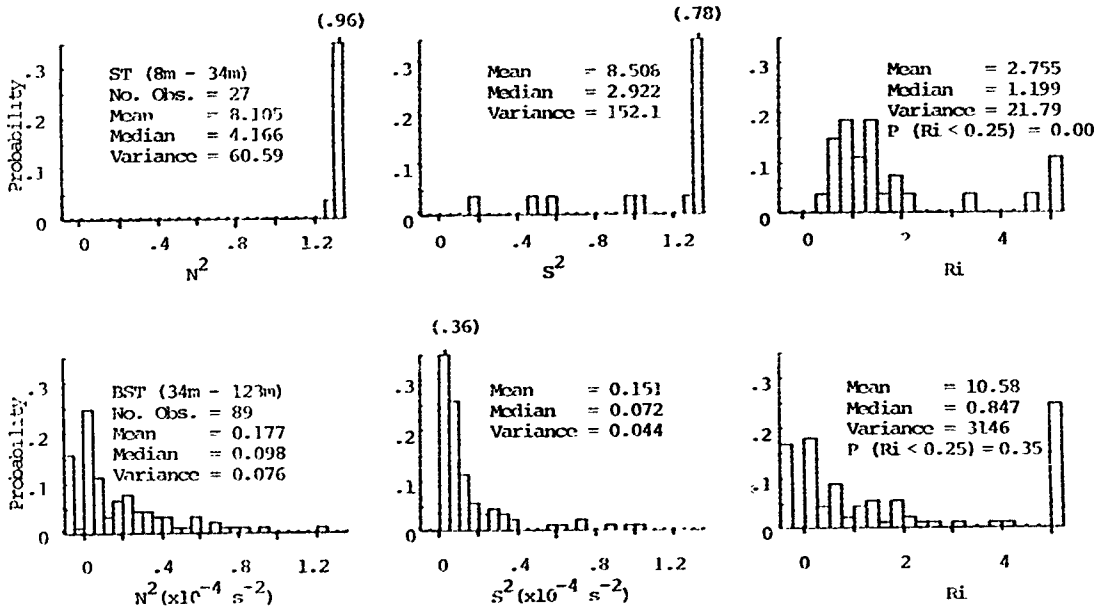

Figure B.11 As in Figure B.3 except at YVETTE station N1 in a Norwegian Fjord. (Cf. Figure A.33.)

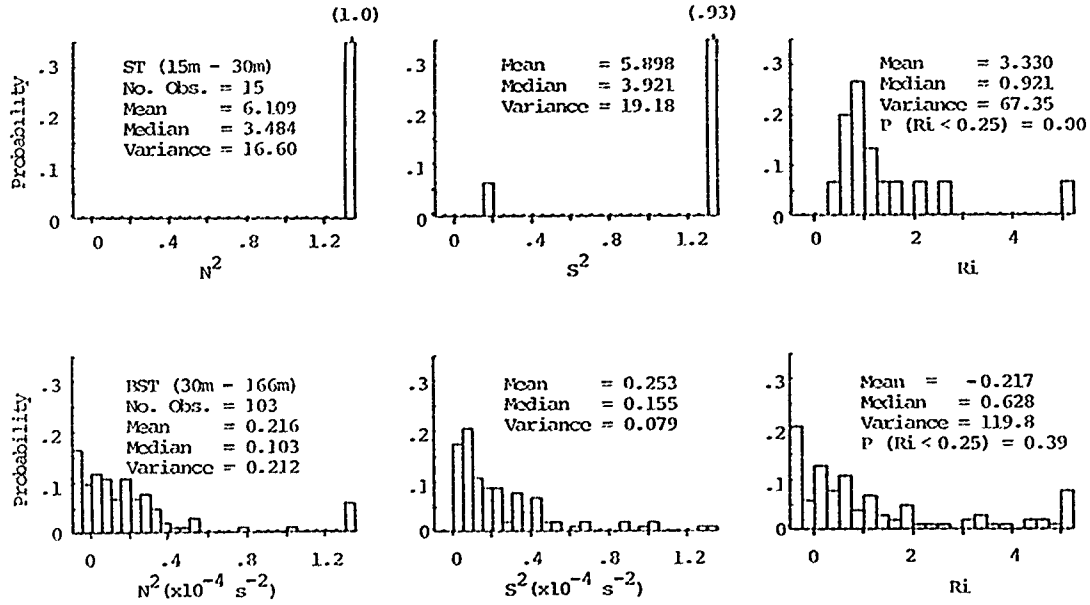

Figure B.12 As in Figure B.3 except for YVETTE station N4 in a Norwegian Fjord. (Cf. Figure A.36.)

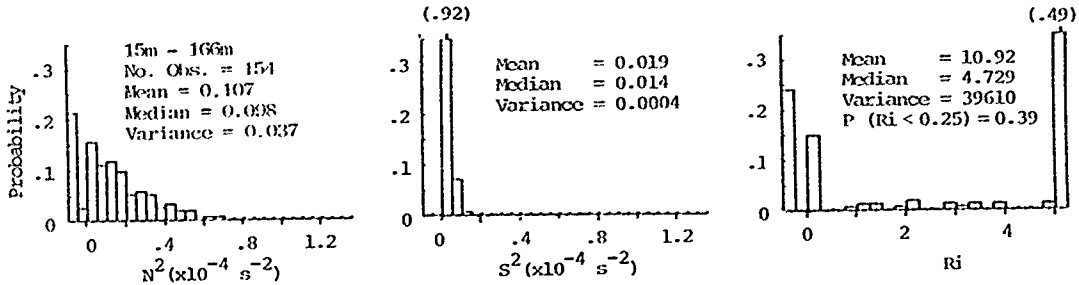

Figure B.13 Histograms of Brunt-Väisälä frequency squared (N^2), vertical shear squared (S^2), and Richardson number (Ri) for YVETTE station N6 in the Norwegian Coastal Current. (Cf. Figure A.39.)

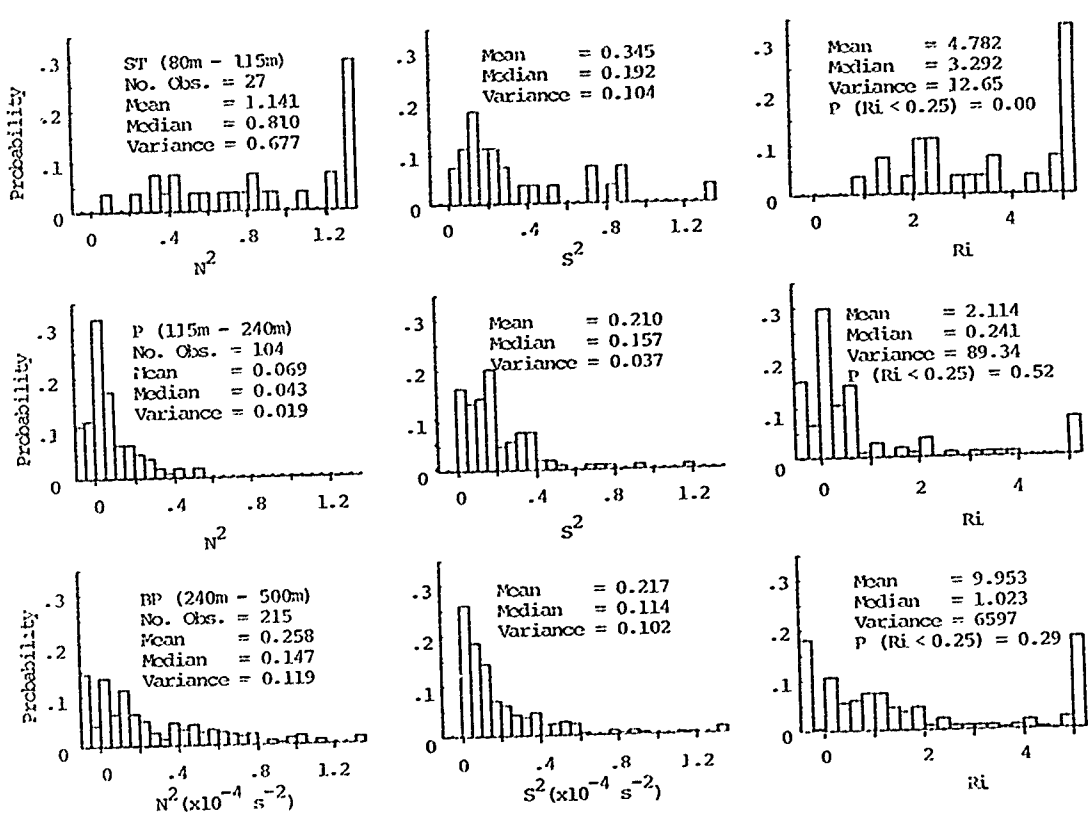

Figure B.14 As in Figure B.13 except for YVETTE station E6 in the equatorial Pacific. Histograms from the near-surface thermocline (ST), the subsurface pycnostad (P), and the regime below the pycnostad (BP) are displayed in the top, center, and bottom rows, respectively. (Cf. Figure A.42.)